FORCE AND PRESSURE TESTS OF THE GA(W)-1 AIRFOIL WITH A 20% AILERON AND PRESSURE TESTS WITH A 30% FOWLER FLAP

W. H. Wentz, Jr., H. C. Seetharam, and K. A. Fiscko
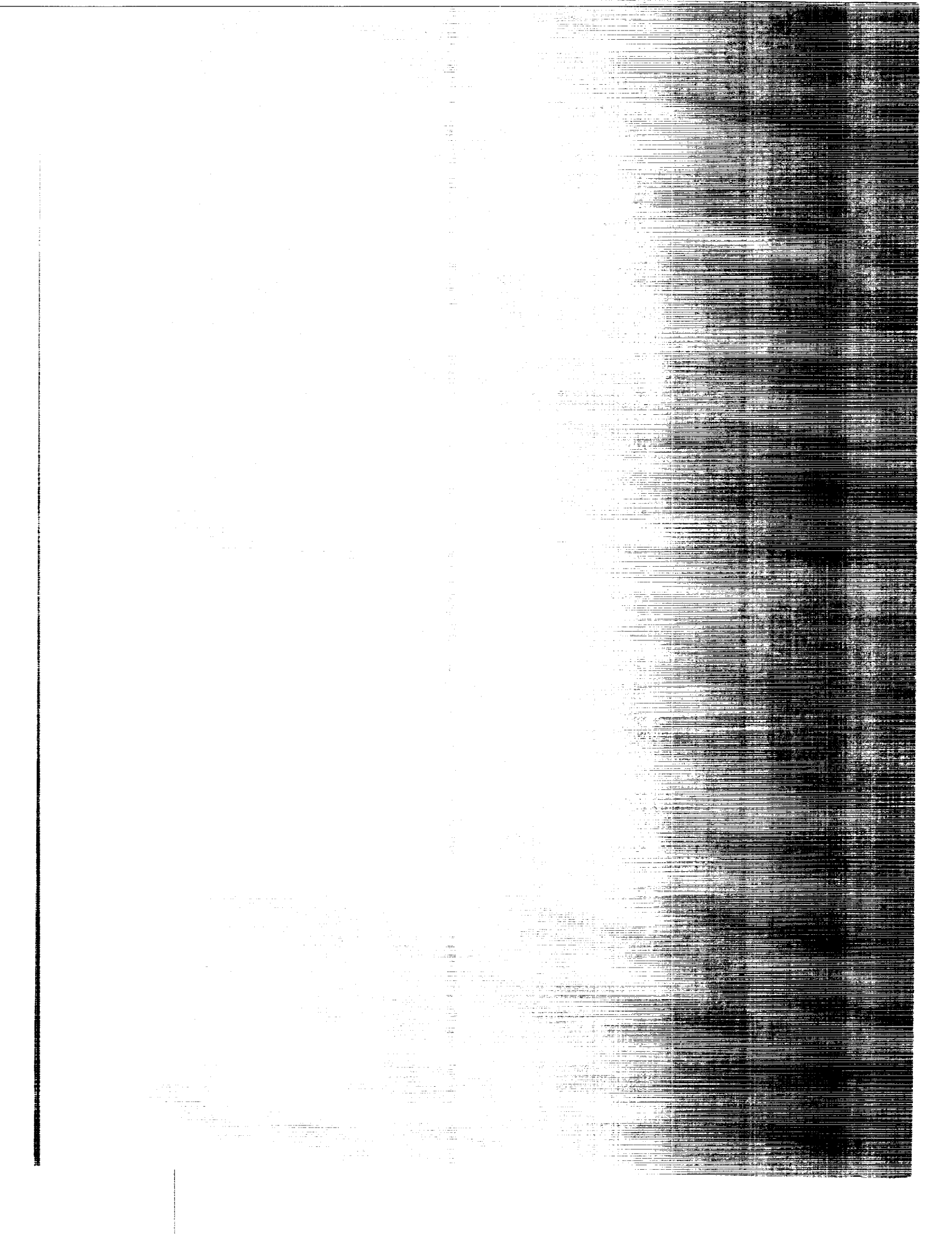
Prepared by
WICHITA STATE UNIVERSITY
Wichita, Kans. 67208
for Langley Research Center

1. Report No. NASA CR-2833	2. Government Accession No.	3. Recipient's Catalog No.
4. Title and Subtitle FORCE AND PRESSURE TESTS OF THE GA(W)-1 AIRFOIL WITH A 20% AILERON AND PRESSURE TESTS WITH A 30% FOWLER FLAP		5. Report Date June 1977
		6. Performing Organization Code
7. Author(s) W. H. Wentz, Jr , H. C. Seetharam, and K. A. Fiscko		8. Performing Organization Report No. WSU AR 76-1
9. Performing Organization Name and Address Wichita State University Wichita, KS 67208		10. Work Unit No. 505-06-33-10
		11. Contract or Grant No. NSG-1165
12. Sponsoring Agency Name and Address National Aeronautics & Space Administration Washington, DC 20546		13. Type of Report and Period Covered Contractor Report
		14. Sponsoring Agency Code

15. Supplementary Notes
Topical report
Langley technical monitor: Robert J. McGhee

16. Abstract

Wind-tunnel force and pressure tests have been conducted for the GA(W)-1 airfoil equipped with a 20% aileron, and pressure tests have been conducted with a 30% Fowler flap. All tests were conducted at a Reynolds number of 2.2×10^6 and a Mach number of 0.13. The aileron provides control effectiveness similar to ailerons applied to more conventional airfoils. Effects of aileron gaps from 0% to 2% chord were evaluated, as well as hinge moment characteristics. The aft camber of the GA(W)-1 section results in a substantial up-aileron moment, but the hinge moments associated with aileron deflection are similar to other configurations.

Fowler flap pressure distributions indicate that unseparated flow is achieved for flap settings up to $40°$, over a limited angle-of-attack range. Theoretical pressure distributions compare favorable with experiment for low flap deflections, but show substantial errors at large deflections.

17. Key Words (Suggested by Author(s)) Airfoil Flap Aileron Pressure distributions	18. Distribution Statement Unclassified - Unlimited Subject Category 02		
19. Security Classif. (of this report) Unclassified	20. Security Classif. (of this page) Unclassified	21. No. of Pages 94	22. Price* $5.00

SUMMARY

Wind tunnel force and pressure tests have been conducted
for the GA(W)-1 airfoil equipped with a 20% aileron, and pres-
sure tests have been conducted with a 30% Fowler flap. All
tests were conducted at a Reynolds number of 2.2 x 10^6 and a
Mach number of 0.13. The aileron provides control effective-
ness similar to ailerons applied to more conventional airfoils.
Effects of aileron gaps from 0% to 2% chord were evaluated, as
well as hinge moment characteristics. The aft camber of the
GA(W)-1 section results in a substantial up-aileron moment,
but the hinge moments associated with aileron deflection are
similar to other configurations.

Fowler flap pressure distributions indicate that unsepa-
rated flow is achieved for flap settings up to 40°, over a
limited angle of attack range   Theoretical pressure distri-
butions compare favorably with experiment for low flap deflec-
tions, but show substantial errors at large deflections.

INTRODUCTION

The high performance possible with the new GA(W)-1 airfoil and airfoil-flap combinations has been reported earlier (Refs. 1,2,3). The present report documents force and pressure tests of the airfoil fitted with a 20% aileron, and pressure studies of the airfoil with a 30% Fowler flap.

All experimental tests reported herein were conducted in the Walter Beech Memorial Wind Tunnel at Wichita State University.

SYMBOLS

The force and moment data have been referred to the .25c location on the flap-nested airfoil. Dimensional quantities are given in both International (SI) Units and U.S. Customary Units. Measurements were made in U.S. Customary Units. Conversion factors between the various units may be found in reference 4. The symbols used in the present report are defined as follows:

c Airfoil reference chord (flap-nested)

c_d Airfoil section drag coefficient, section drag/ (dynamic pressure x chord)

c_f Flap chord

c_h Control surface hinge moment coefficient, section moment/ (dynamic pressure x control surface reference chord^2)

c_ℓ Airfoil section lift coefficient, section lift/(dynamic pressure x chord)

c_m Airfoil section pitching moment coefficient with respect to the .25c location, section moment/(dynamic pressure x chord^2)

c_n Airfoil or flap normal force coefficient, section normal force/(dynamic pressure x chord)

c_p Coefficient of pressure, $(p-p_\infty)$/dynamic pressure

ℓ_c Cove length

p Static pressure

x Coordinate parallel to airfoil chord

z Coordinate normal to airfoil chord

α Angle of attack, degrees

Δ Increment

δ Rotation of surface from nested position, degrees

1

Subscripts:

a   Aileron

f   Flap

p   Pivot

∞   Remote free-stream value

APPARATUS AND TEST METHODS
Model Description

The GA(W)-1 airfoil is a 17% maximum thickness section developed at the NASA Langley Research Center (Ref. 1). For tests in the WSU two-dimensional facility, models are sized with a 91.4 cm (36 inch) span and 61.0 cm (24 inch) chord. The forward section of the model was fabricated from laminated mahogany bonded to a 2.5 cm x 34.8 cm (1 inch x 13.7 inch) aluminum spar. Wing trailing sections to match each flap and aileron were fabricated from solid aluminum as were the flaps and ailerons. Airfoil and flap or aileron are mounted on 107 cm (42 inch) diameter end plates. A set of external brackets permit positioning of flap or aileron without disturbing the flow over the model. Models are fitted with flush tubes for static pressure surveys. Geometric contour details are given in figure 1.

As shown, the 20% aileron model has inserts to permit tests with leading edge gaps of 2%, 1%, and 0.5% chord. Tests were made with zero gap by sealing the slot with cloth-backed adhesive tape applied to the airfoil lower surface.

The Fowler flap has 30% chord with full Fowler action possible as shown in figure 1(b). The force characteristics and optimization of this airfoil-flap combination have been reported in reference 2. Performance with spoilers has been reported in references 3 and 5. The purpose of the present research is to provide surface pressure distribution and flap loads information for optimum flap settings.

All tests were conducted with transition fixed by 2.5 mm (0.10 inch) wide strips of #80 carborundum grit located at 5% chord on upper and lower surfaces.

Instrumentation

Pressure studies are conducted by multiplexing as many as 96 pressure ports through four pressure transducers by means of a set

of pressure scanning switches. The tunnel is equipped with a
semi-automated data system which converts analog force and pres-
sure output signals to digital form, and records the data on
punch cards. Computational analysis and computer graphics are
done through the University Digital Computing Center.

Test Procedure

All tests were conducted at a Reynolds number of 2.2×10^6
and Mach number of 0.13. Lift, drag and pitching moment data
are obtained by direct load cell measurements from the tunnel
main balance. Drag data are corrected for end plate tare drag
based upon wake survey drag measurements conducted with the un-
flapped airfoil.

Wind Tunnel

The WSU Walter Beech Tunnel is a closed return tunnel with
atmospheric test section static pressure. The test section with
two-dimensional inserts is 0.91 m x 2.13 m (3 feet x 7 feet).
Complete description of the insert and calibration details are
given in reference 6.

TEST RESULTS

Force Tests with 20% Aileron

Results of three-component force measurements are shown in
figures 2 through 4 for 0%, 0.5%, 1% and 2% aileron gaps. Cross-
plots of important incremental effects of aileron deflection are
shown in figures 5 through 7.

These data show that the aileron provides positive control
response for deflections from -60° to +60° throughout the angle
of attack range prior to stall.

From the c_ℓ vs. alpha curves, it is observed that down aile-
ron results in early stalling, and conversely for up aileron. This
means that control reversal occurs at post-stall angles of attack.
While this is not a desirable characteristic, it is typical aileron
behavior, and is not peculiar to the GA(W)-1 airfoil.

Pitching moment data reflect a nose-down tendency for downward
aileron deflections. Drag data reflect a tendency toward greater

3

drag increase for down aileron than for up aileron. This drag difference will produce adverse yawing moments on a finite span wing. It must be remembered, however, that the principal contribution to aileron adverse yaw is _induced_ drag.

Effects of aileron slot gap opening are illustrated by comparing the various figures. Figures 5(a) through 5(d) show that opening the gap from 0% to 2.0% results in only very slight degradation of control authority. Close examination of figures 3(a) through 3(d) shows that the most significant effect of gap opening is to increase the basic section drag with zero aileron deflection. This effect becomes more pronounced as lift coefficient is increased. Gaps of 0.5% and 1% actually increase $c_{\ell max}$ slightly, evidently as a result of the boundary layer energization provided. A gap of 0.5% would seem to be a good compromise, providing adequate clearance with minimal penalty.

Pressure Tests with 20% Aileron

Pressure surveys were conducted for -10° to +10° aileron with zero gap to determine whether gap sealing had any significant influence (figure 8). Because of the extensive time required to obtain pressure data, complete pressure surveys were conducted only for the 0.5% gap configuration (figure 9). Comparison of figures 8 and 9 shows that the gap has little effect on overall pressure distributions.

Aileron hinge moment data with respect to the 80% chord hingeline location were obtained by numerical integration of the surface pressure data. Results of this analysis are shown in figure 10. The data show that the hinge moment variation is nearly linear with aileron deflection. The 0.5% gap has negligible effect on hinge moment. The aileron is subjected to large up-aileron moments with zero deflection at high angles of attack. This is attributed to the relatively large camber near the trailing edge which characterizes the GA(W)-1 airfoil section.

Pressure Tests with 30% Fowler Flap

Optimum settings for the 30% Fowler flap were determined from force tests reported earlier (Ref. 2). Subsequent to those tests,

a slightly modified 40° flap setting was developed to simplify
flap track design. The c_ℓ vs. α performance with original and
modified flap settings is essentially the same, as shown in fig-
ure 11. The pressure data presented here were obtained with the
modified setting for 40° flap, and original settings for all
other flap deflections. Experimental pressure distributions are
presented in figure 12.

The flap cove on this model has a fairly abrupt entry. Theo-
retical analysis of the airfoil-flap combination (using the method
of reference 7) with the true cove shape invariably results in a
computer prediction of flow separation at the cove entry. It was
experimentally observed that the flow does separate in the region,
but reattachment occurs ahead of the slot exit. Since the present
theoretical techniques do not account for flow reattachment, it was
decided that the effective airfoil contour should be modified in
the cove region to approximate the separation and reattachment.
Figure 13 compares results of analyses using three cove contours
with an experimental pressure distribution for 30° flap at 10.3°
angle of attack.

Based upon these results, a decision was made to approximate
the effective shape of the free streamline within the cove by a
straight line from the cove entrance to the 75% assumed reattach-
ment location. It is seen that this modification results in con-
siderable improvement in the prediction of pressures near the air-
foil trailing edge. Two additional difficulties arise in utiliz-
ing the theoretical computing routine. First, the computational
program may indicate flow separation. If separation is present
at 0.95c or further aft, little change in pressure distribution is
expected, and the program results are probably valid. However, if
a substantial region of separation is present, large changes in
pressures are expected. Calculation of separated flow cases is
beyond the capability of the present computer program, and there-
fore computer-predicted pressure distributions are probably in-
valid for these cases.

The second computational difficulty involves analysis of the
confluence of the flap and airfoil boundary layers. In a number

5

of cases the program prints a "confluent boundary layer error" message, indicating that slot flow velocity and outer flow velocity are not within limits specified in the program. No means for obtaining proper convergence for these cases are presently provided by the program.

Figures 14 through 17 compare theoretical pressure distributions with experimental distributions for a number of cases. Normal force coefficients for airfoil and flap obtained from integration of surface pressures are also compared with theory in these figures. The agreement is generally quite good for flap deflections up to 30° and angles of attack below stall. For 40° flap, the theory consistently over-predicts the flap upper surface pressures, indicating that the flap boundary layer is thicker than the theoretical prediction.

Unfortunately predictions of separation are inconsistent, and frequent confluent boundary layer errors were encountered.

CONCLUSIONS

1. Force and pressure tests have shown that aileron characteristics for the GA(W)-1 airfoil are not unlike airfoils with more conventional camber and thickness distributions. The airfoil provides excellent aileron control effectiveness.

2. Hinge moment characteristics of an aileron applied to the GA(W)-1 airfoil are reasonably linear and of expected magnitudes. The airfoil aft camber inherent to this section does result in rather large up-aileron moments, particularly at large angles of attack.

3. Pressure distributions for a 30% Fowler flap applied to the GA(W)-1 airfoil indicate that with proper gap and overlap, attached flow can be provided for flap deflections up to 40°, at least for a limited angle of attack range. Present viscous flow computational modeling is inadequate for many practical flap cove designs in which flow separation and reattachment occur.

Aeronautical Engineering Department
Wichita State University
Wichita, Kansas 67208
August 1976

REFERENCES

1. McGhee, R.J. and Beasley, W.D.: Low-Speed Aerodynamic Characteristics of a 17-Percent Thick Airfoil Section Designed for General Aviation Applications. NASA TN D-7428, 1973.

2. Wentz, W.H. and Seetharam, H.C.: Development of a Fowler Flap System for a High Performance General Aviation Airfoil. NASA CR-2443, 1974.

3. Wentz, W.H.: Effectiveness of Spoilers on the GA(W)-1 Airfoil with a High-Performance Fowler Flap. NASA CR-2538, 1975.

4. Mechtly, E.A.: The International System of Units - Physical Constants and Conversion Factors (Revised) NASA SP-7012, 1969.

5. Wentz, W.H. and Volk, C.G.: Reflection-Plane Tests of Spoilers on an Advanced Technology Wing with a Large Fowler Flap. NASA CR-2696, 1976.

6. Siew, R.: Calibration of a Two-Dimensional Insert for the WSU 7' x 10' Wind Tunnel. WSU AR 73-2, 1973.

7. Stevens, W.A., Goradia, S.H. and Braden, J.A.: Mathematical Model for Two-Dimensional Multi-Component Airfoils in Viscous Flow. NASA CR-1843, 1971.
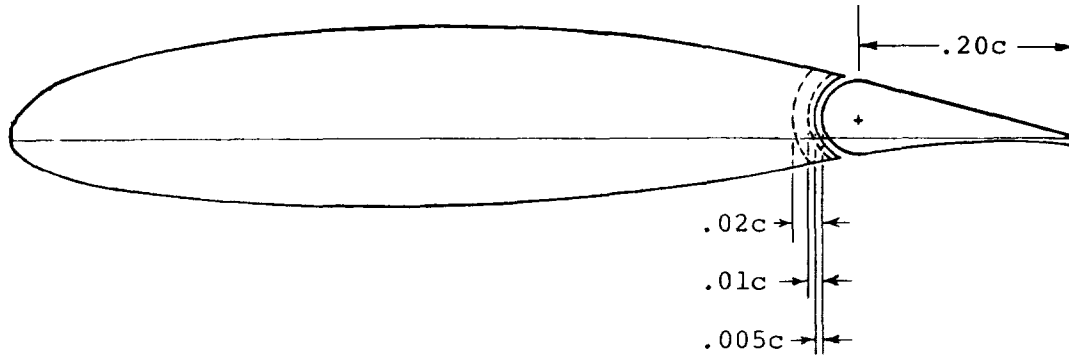
20%c Aileron Coordinates

Upper Surface			Lower Surface	
x_a/c	z_a/c		x_a/c	z_a/c
.000	.01960		.000	.01960
.005	.03750		.005	.00375
.017	.05000		.017	-.01040
.035	.05286		.035	-.01600
.060	.04646		.060	-.01200
.085	.03988		.085	-.00860
.110	.03315		.110	-.00580
.135	.02639		.135	-.00360
.160	.01961		.160	-.00250
.185	.01287		.185	-.00260
.210	.00609		.210	-.00400
.235	-.00070		.235	-.00800

L.E. Radius = 0.03443c

(a) 20% Aileron.

Figure 1 - Model Geometry.

8
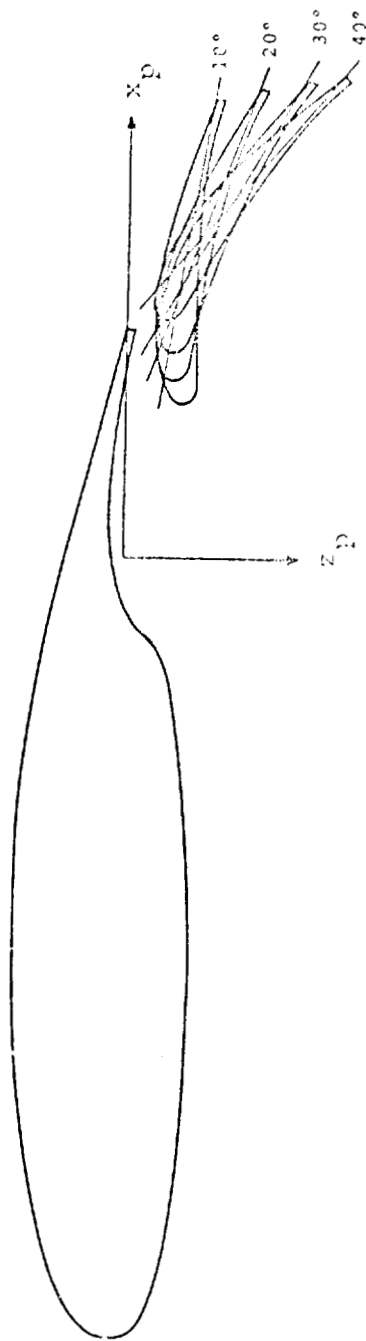
30% Fowler Flap Coordinates

Upper Surface		Lower Surface	
x_f/c	z_u/c	x_f/c	z_f/c
.000	-.01920	.000	-.01920
.025	.00250	.025	-.02940
.050	.01100	.050	-.02490
.075	.01630	.075	-.02040
.100	.01900	.100	-.01600
.125	.01950	.125	-.01200
.150	.01820	.150	-.00860
.175	.01670	.175	-.00580
.200	.01330	.200	-.00360
.225	.00950	.225	-.00250
.250	.00530	.250	-.00260
.275	.00100	.275	-.00400
.300	-.00435	.300	-.00800

L.E. Radius = 0.0122c

Flap Pivot Point Locations

δ_f	x_p/c	z_p/c	gap/c	overlap/c
0°	0.0	0.0	0.0	0.300
10°	.232	.046	.025	.071
20°	.256	.050	.025	.047
30°	.280	.058	.025	.022
40°	.306	.062	.030	.000

Note: Pivot point is at $0.25c_f$ on the wing chord line.

(b) 30% Fowler Flap.
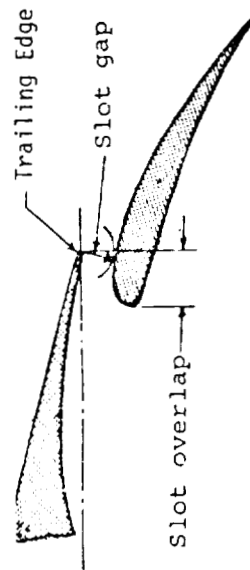
Figure 1 - Concluded.

Definitions of gap and overlap.

(a) 0% Gap.
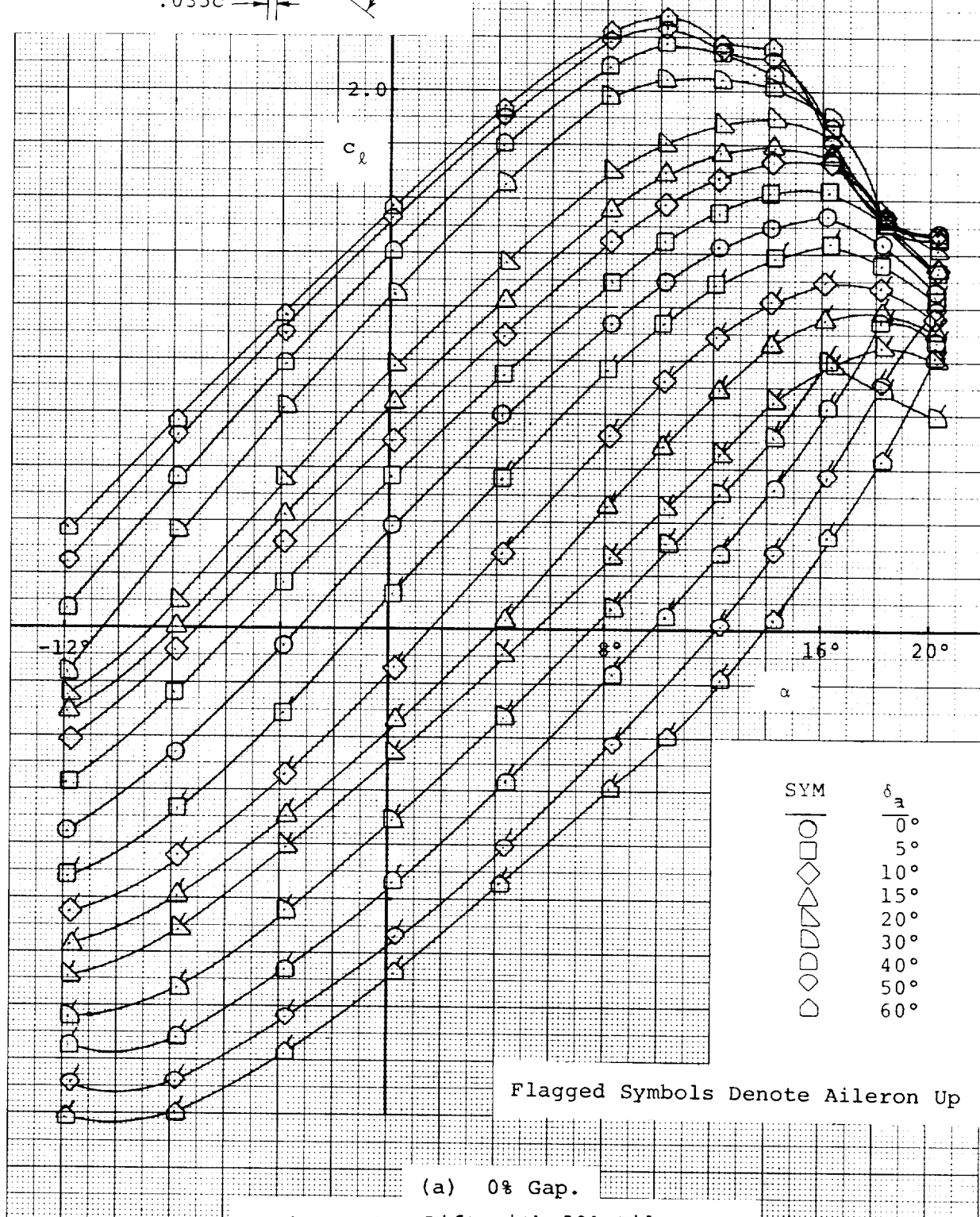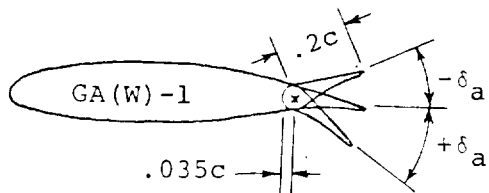
Figure 2 - Lift with 20% Aileron.

10

(b) 0.5% Gap.

Figure 2 - Continued.

11

(c) 1% Gap.

Figure 2 - Continued.

12

(d) 2% Gap.

Figure 2 - Concluded.

13

Figure 3 - Drag with 20% Aileron.

14

(b) 0.5% Gap.

Figure 3 - Continued.

15

GA(W)-1

.2c

.035c

.01c Gap

$-\delta_a$
$+\delta_a$

c_d

Aileron Up

-1.0

0

1.0

c_ℓ

SYM	δ_a
◯	0°
◇	10°
◁	20°
⬠	40°
⬠	60°

c_d

-1.0

0

1.0

2.0

Aileron Down

c_ℓ

(c) 1% Gap.

Figure 3 - Continued.

16

GA(W)-1

SYM   δₐ
────────
○   0°
◇   10°
◁ ▷   20°
□   40°
⬠   60°

Aileron Up

Aileron Down

(d)   2% Gap.

Figure 3 - Concluded.

17

Figure 4 – Moment with 20% Aileron.

(a)   0% Gap.

18

(b) 0.5% Gap.

Figure 4 - Continued.

SYM	δ_a
$\bigcirc$	$0°$
$\diamondsuit$	$10°$
$\triangle$	$20°$
$\square$	$40°$
$\pentagon$	$60°$

(c) 1% Gap.

Figure 4 - Continued.

GA(W)-1

SYM δ_a
○ ◇ ◇ ◯ 0°
         10°
         20°
△ △ 40°
     60°

Aileron Up

c_m

c_ℓ

c_ℓ

-1.0   0   1.0   2.0

c_m

Aileron Down

(d)   2% Gap.

Figure 4 - Concluded.

21

(a) 0% Gap.

Figure 5 - Aileron Effectiveness.

22
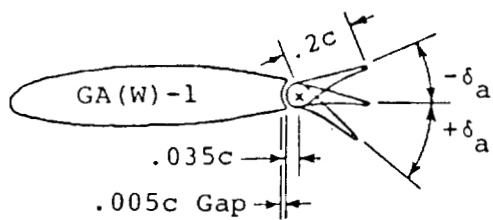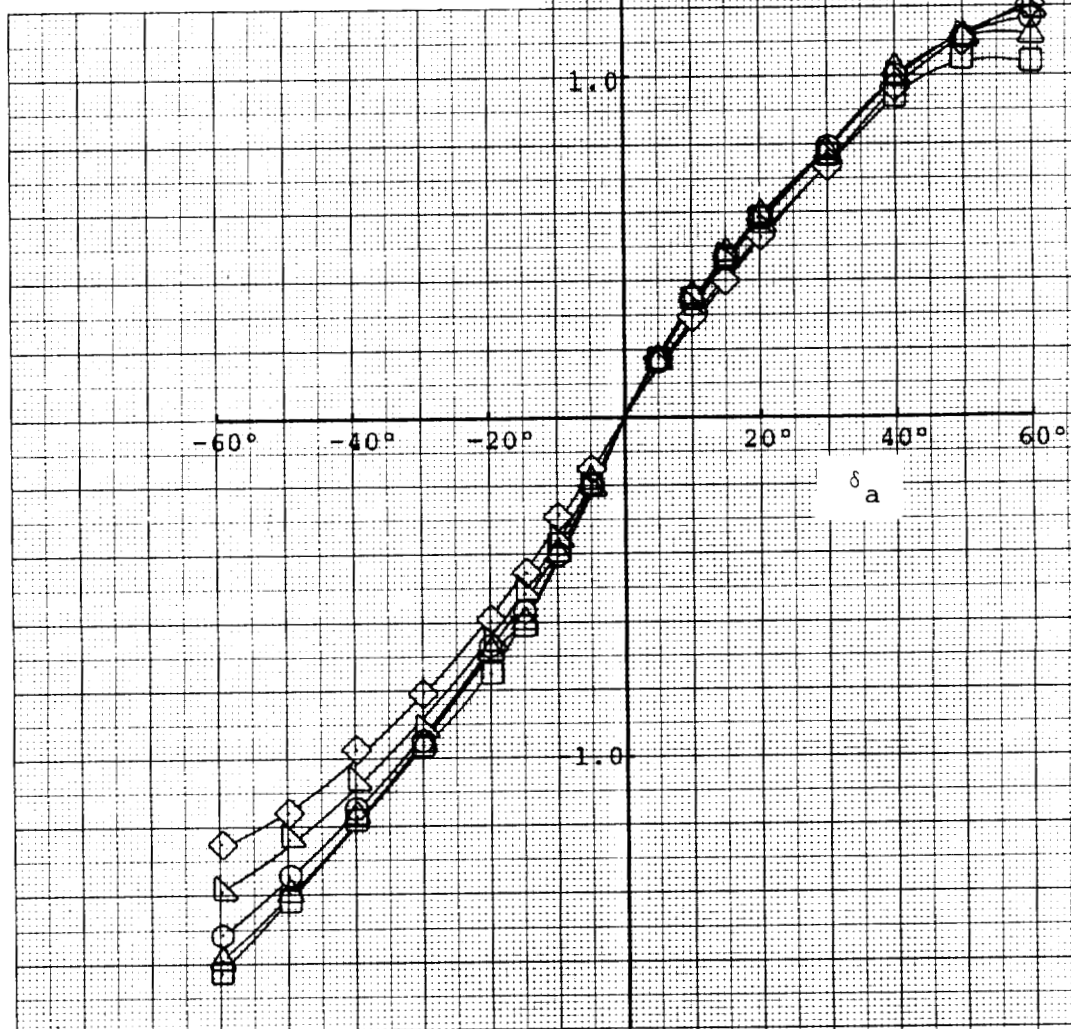
(b) 0.5% Gap.

Figure 5 - Continued.

23

(c) 1% Gap.

Figure 5 - Continued.

24
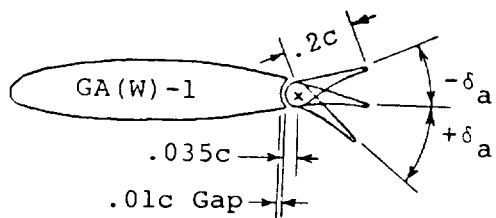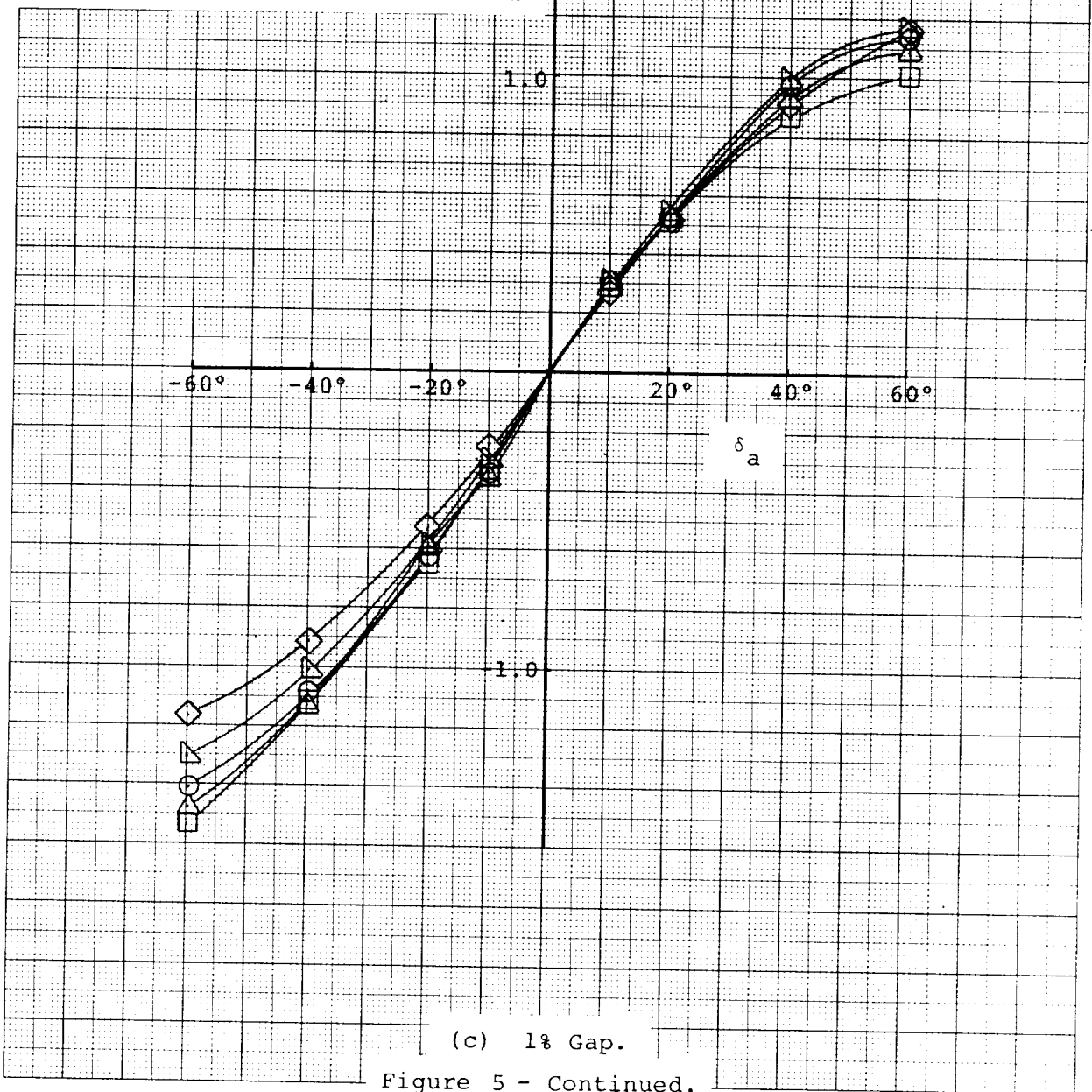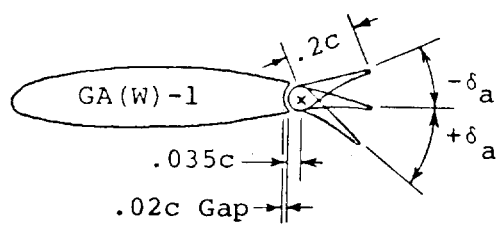
SYM	α
$\diamondsuit$	$-8°$
$\triangle$	$-4°$
$\bigcirc$	$0°$
$\triangle$	$4°$
$\square$	$8°$
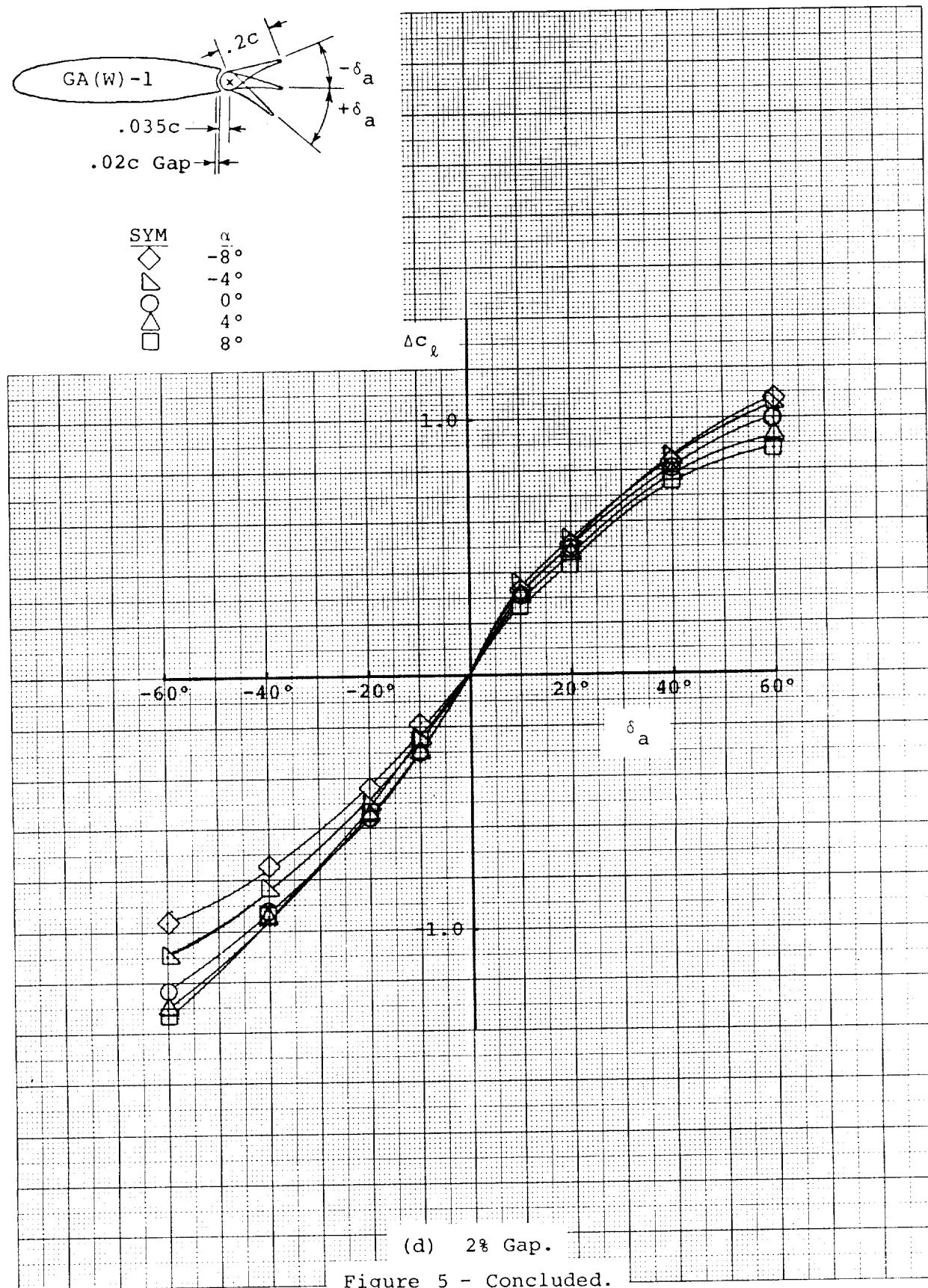
(d) 2% Gap.

Figure 5 - Concluded.

25
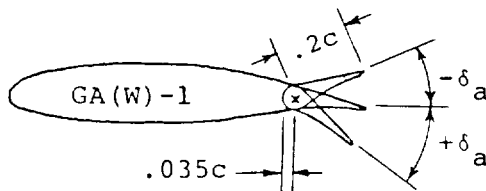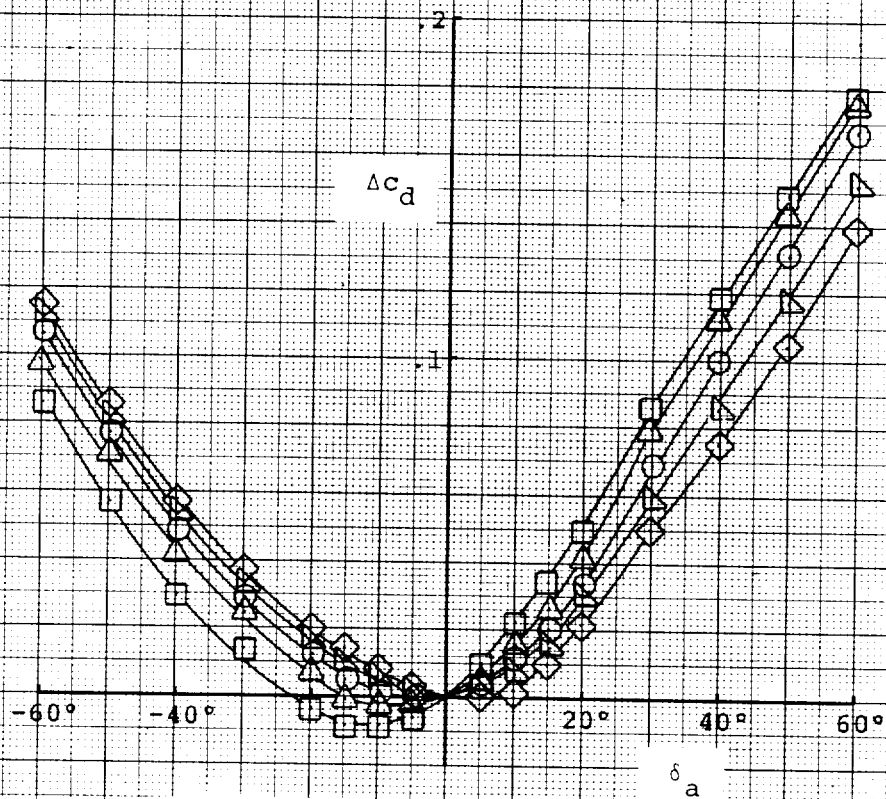
(a) 0% Gap.

Figure 6 - Aileron Effects on Drag.

Δc_d

$-60°$　$-40°$　$20°$　$40°$　$60°$

δ_a

GA(W)-1

.2c

$-\delta_a$

$+\delta_a$

.035c

.005c Gap
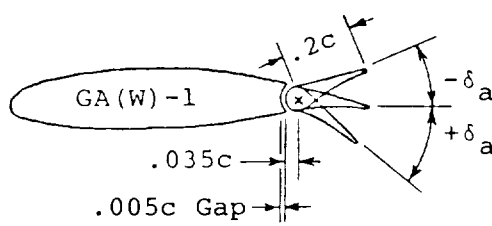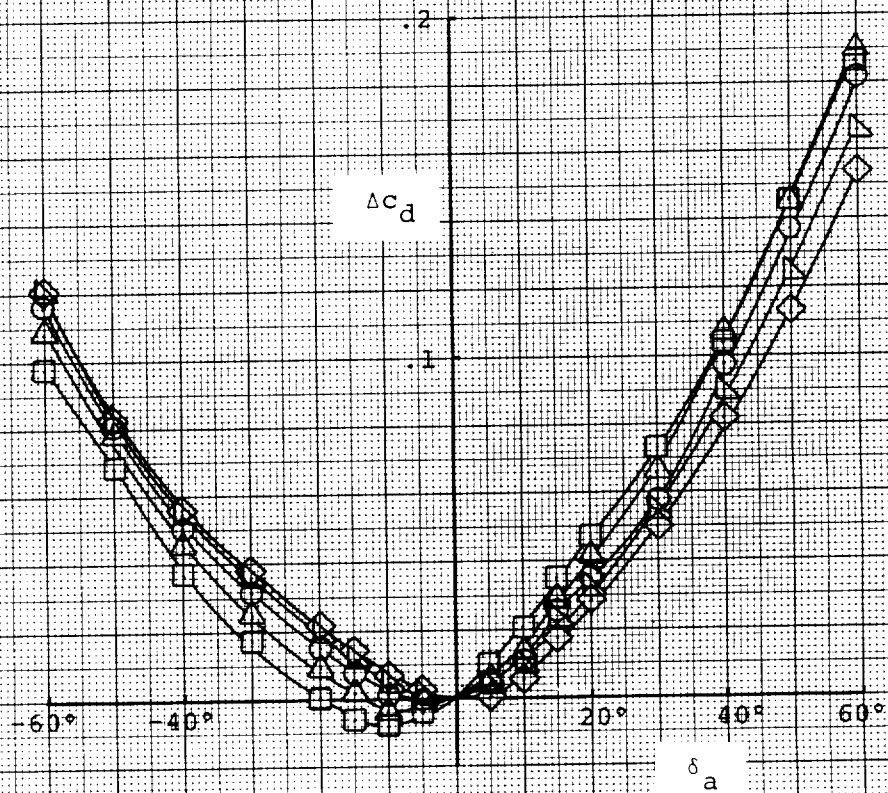
SYM	α
◇	$-8°$
△	$-4°$
○	$0°$
△	$4°$
□	$8°$

(b) 0.5% Gap.

Figure 6 - Continued.

27
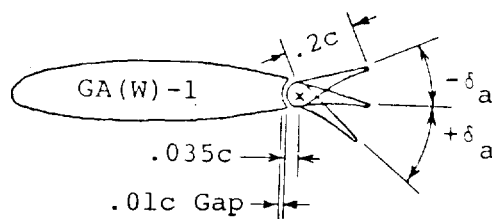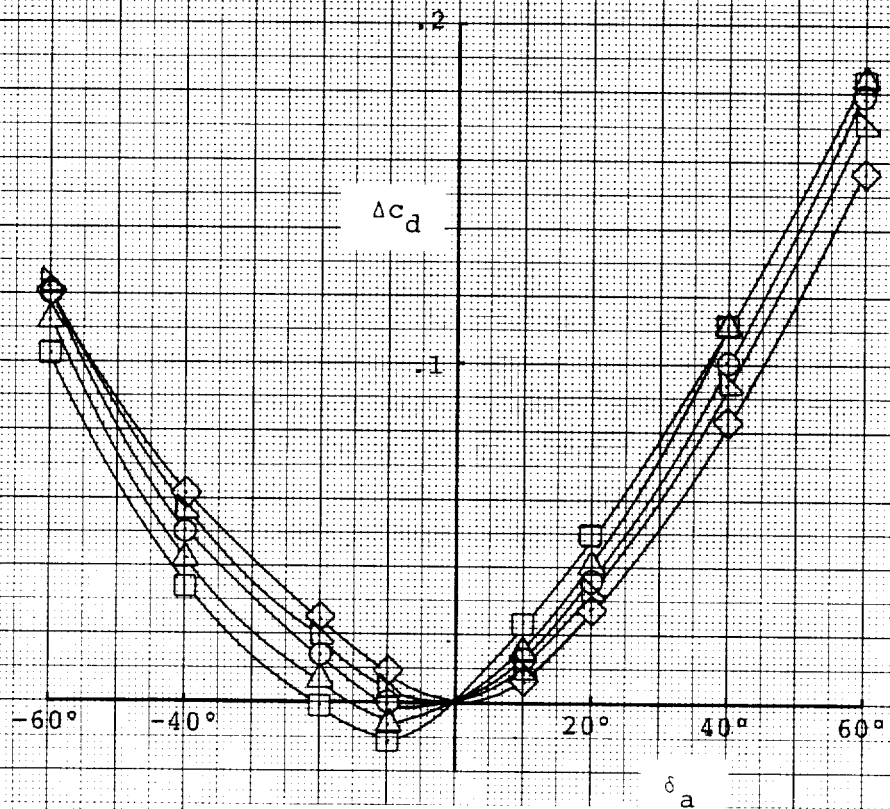
SYM	α
◇	-8°
◁	-4°
○	0°
△	4°
□	8°

(c) 1% Gap.

Figure 6 - Continued.
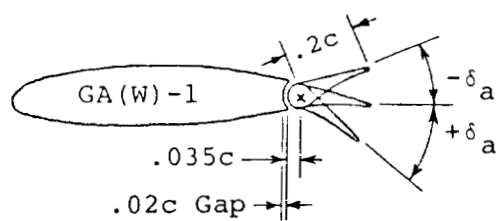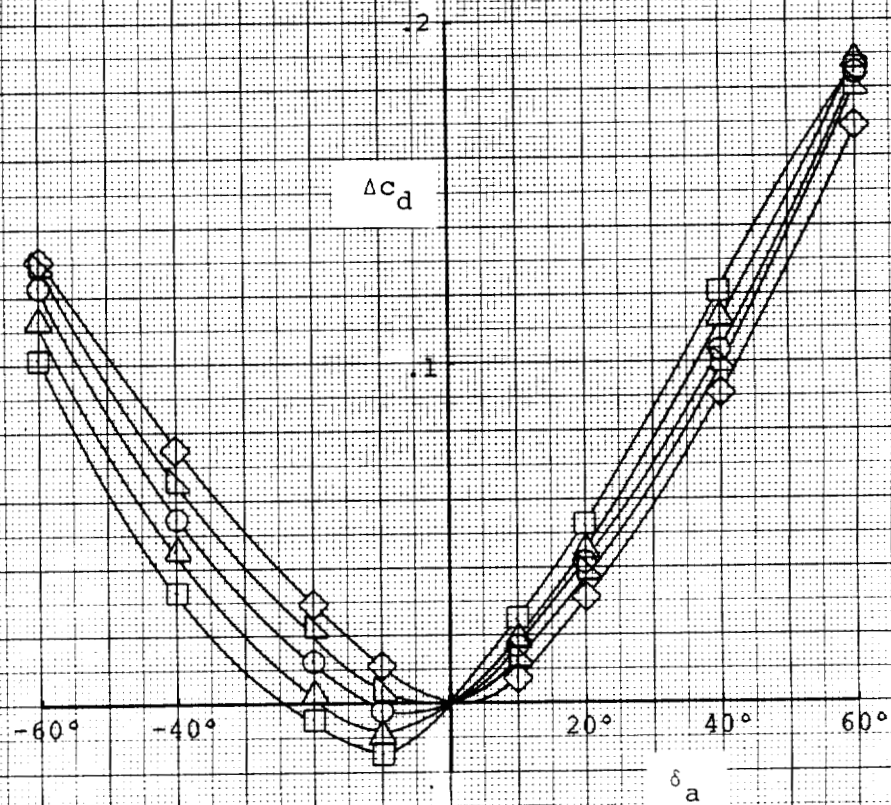
28

(d) 2% Gap.

Figure 6 - Concluded.

29

(a) 0% Gap.
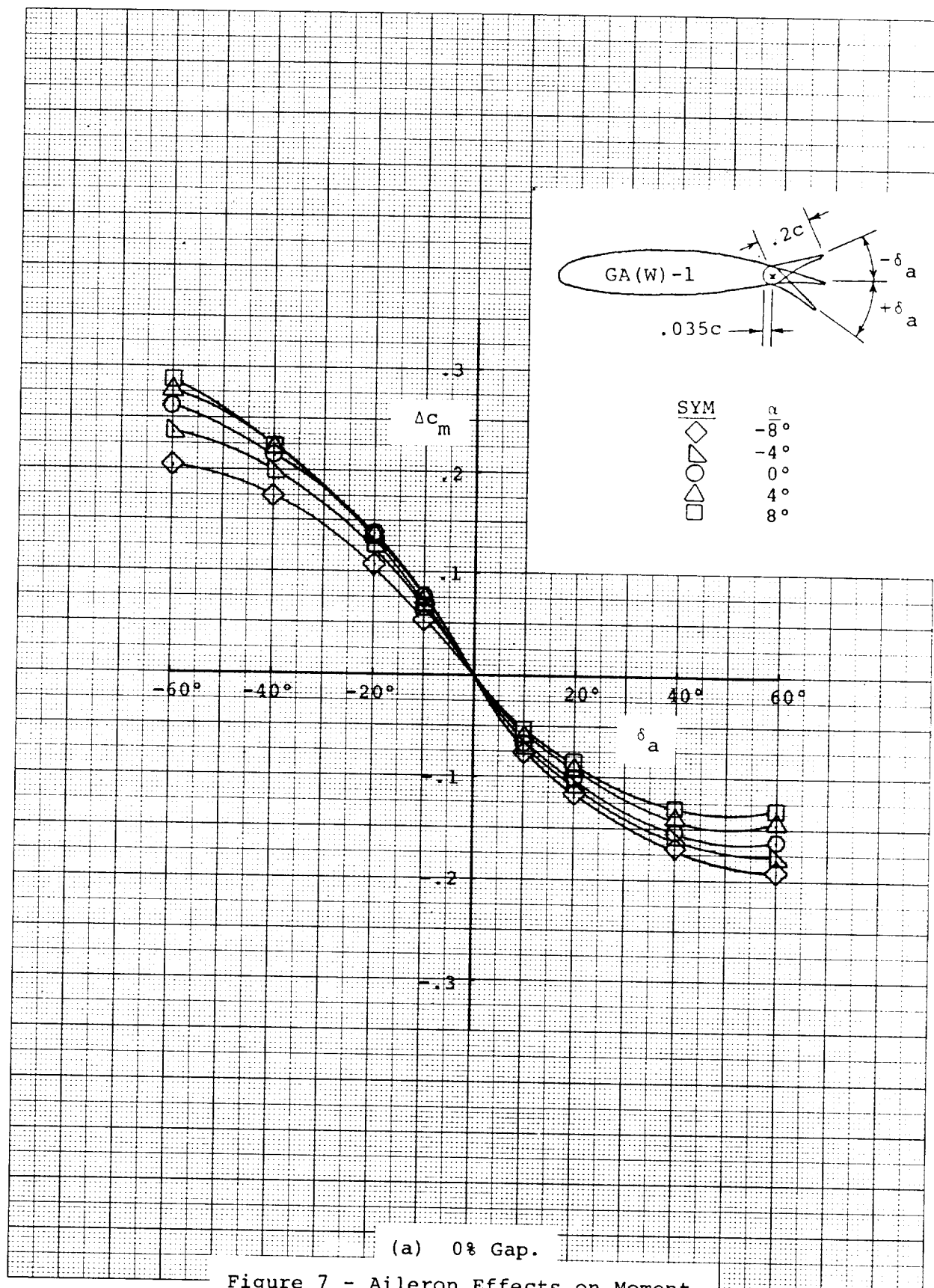
Figure 7 - Aileron Effects on Moment.

30

(b) 0.5% Gap.

Figure 7 - Continued.

31

GA(W)-1

.2c

.035c

.01c Gap

$-\delta_a$

$+\delta_a$

Δc_m

SYM	$\frac{\alpha}{}$
◇	$-8°$
△	$-4°$
○	$0°$
△	$4°$
□	$8°$

$-60°$ $-40°$ $-20°$ $20°$ $40°$ $60°$

δ_a

.3

.2

.1

-.1

-.2

-.3

(c) 1% Gap.

Figure 7 - Continued.

GA(W)-1

.2c

$-\delta_a$
$+\delta_a$

.035c

.02c Gap

Δc_m

SYM	$\frac{\alpha}{8}°$
◇	$-8°$
◁	$-4°$
○	$0°$
△	$4°$
□	$8°$

.3

.2

.1

$-60°$ $-40°$ $-20°$ $20°$ $40°$ $60°$

δ_a

$-.1$

$-.2$

$-.3$

(d)   2% Gap.

Figure 7 - Concluded.

33

AILERON DEFLECTION = -10·00 DEGREES

MACH NO· = 0·13

REYNOLDS NO· = 2·2 E 06

SYMBOL   ALPHA

+   -8°
×   0°
▷   16°
▼   20°

Flagged Symbols Denote Lower Surface Pressures
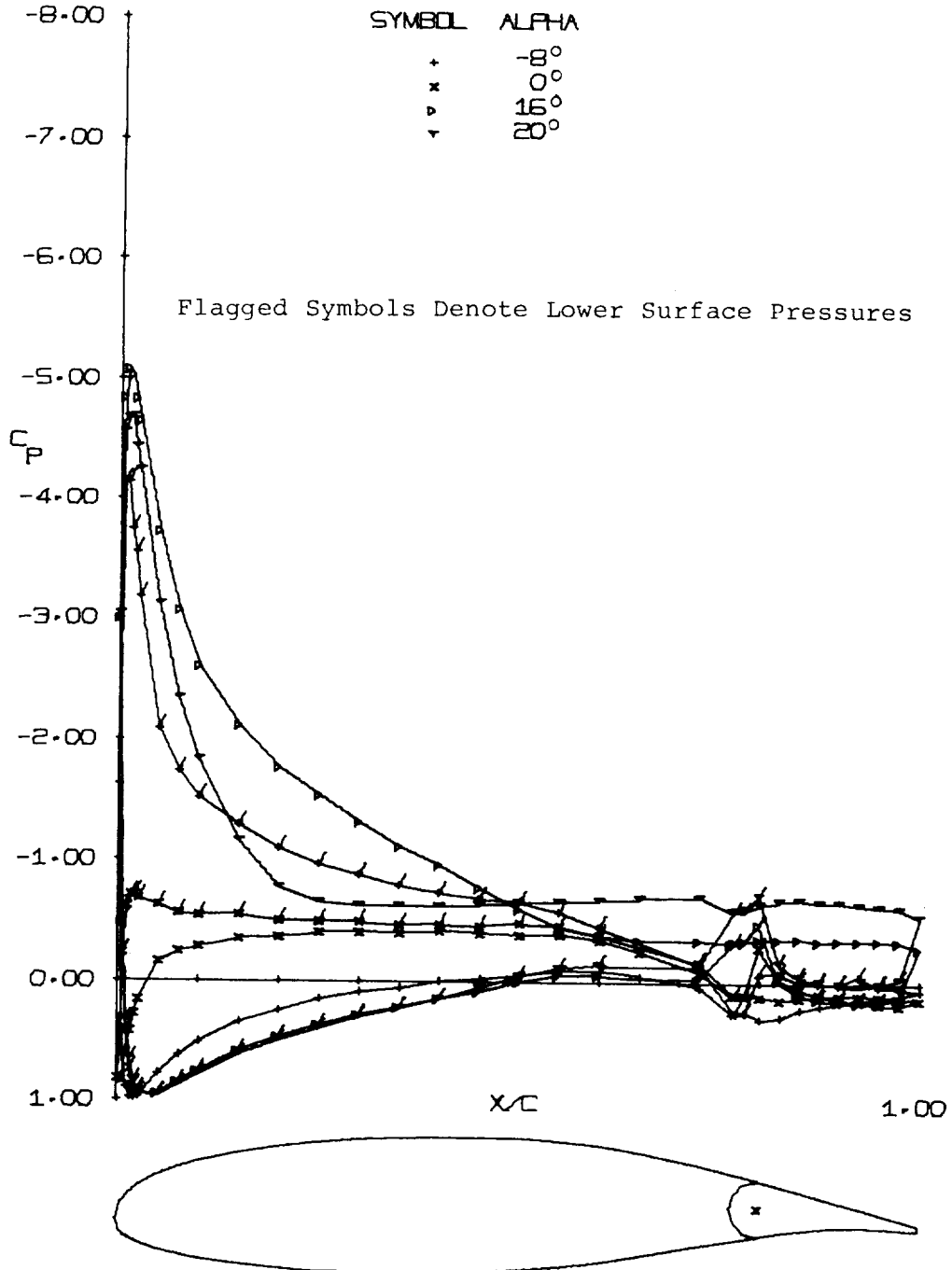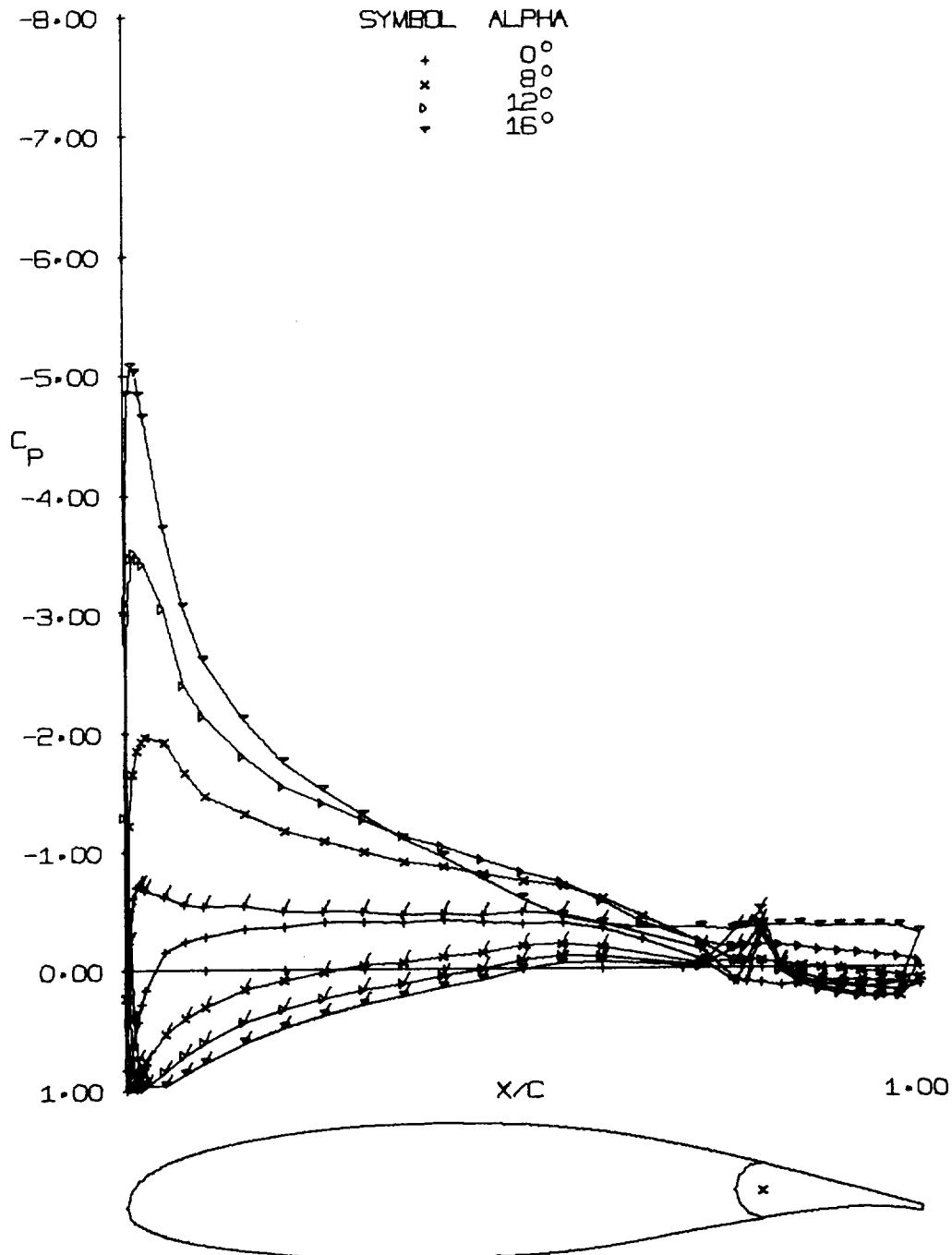

(a)   -10° Aileron, Large α's.
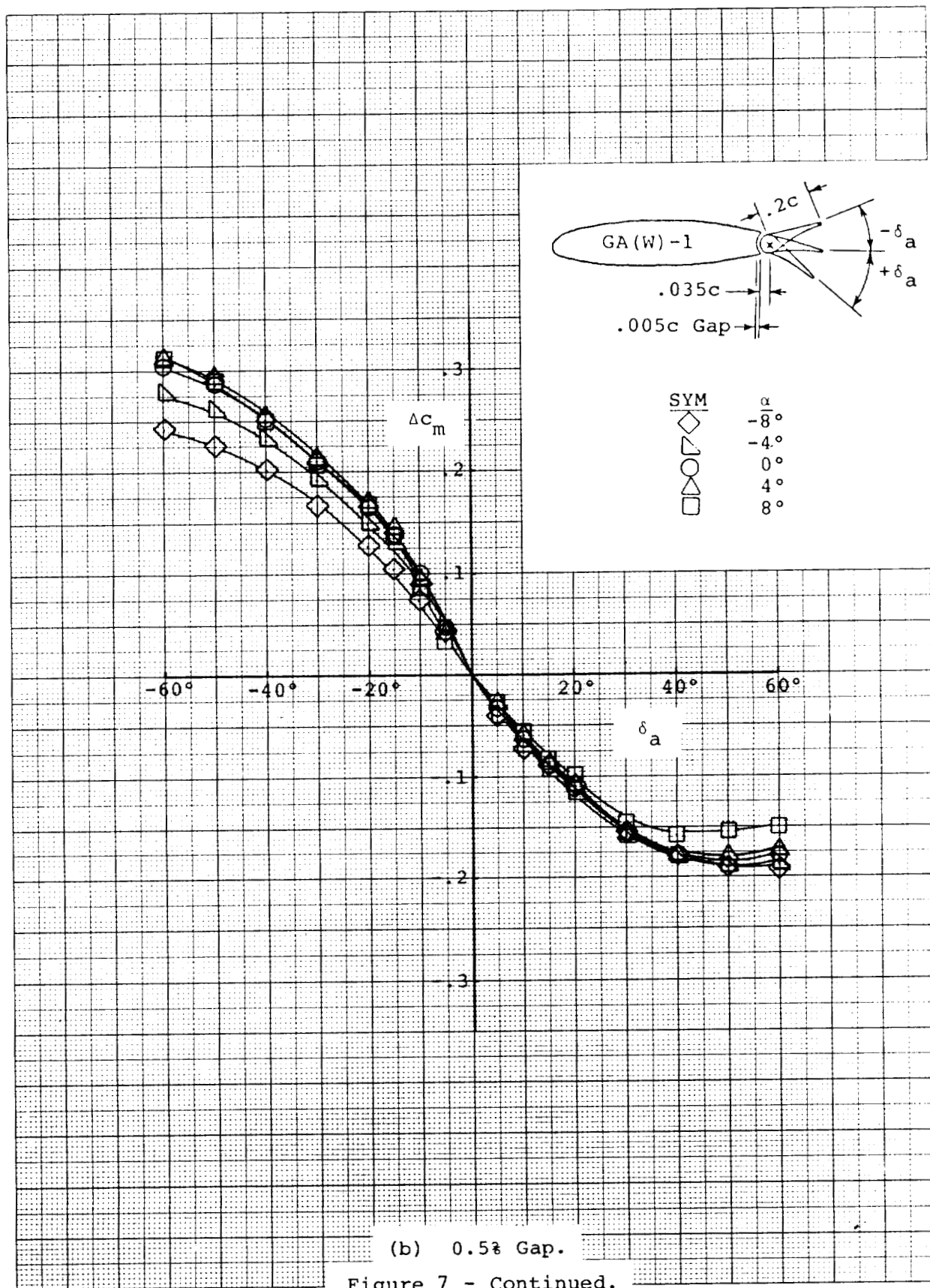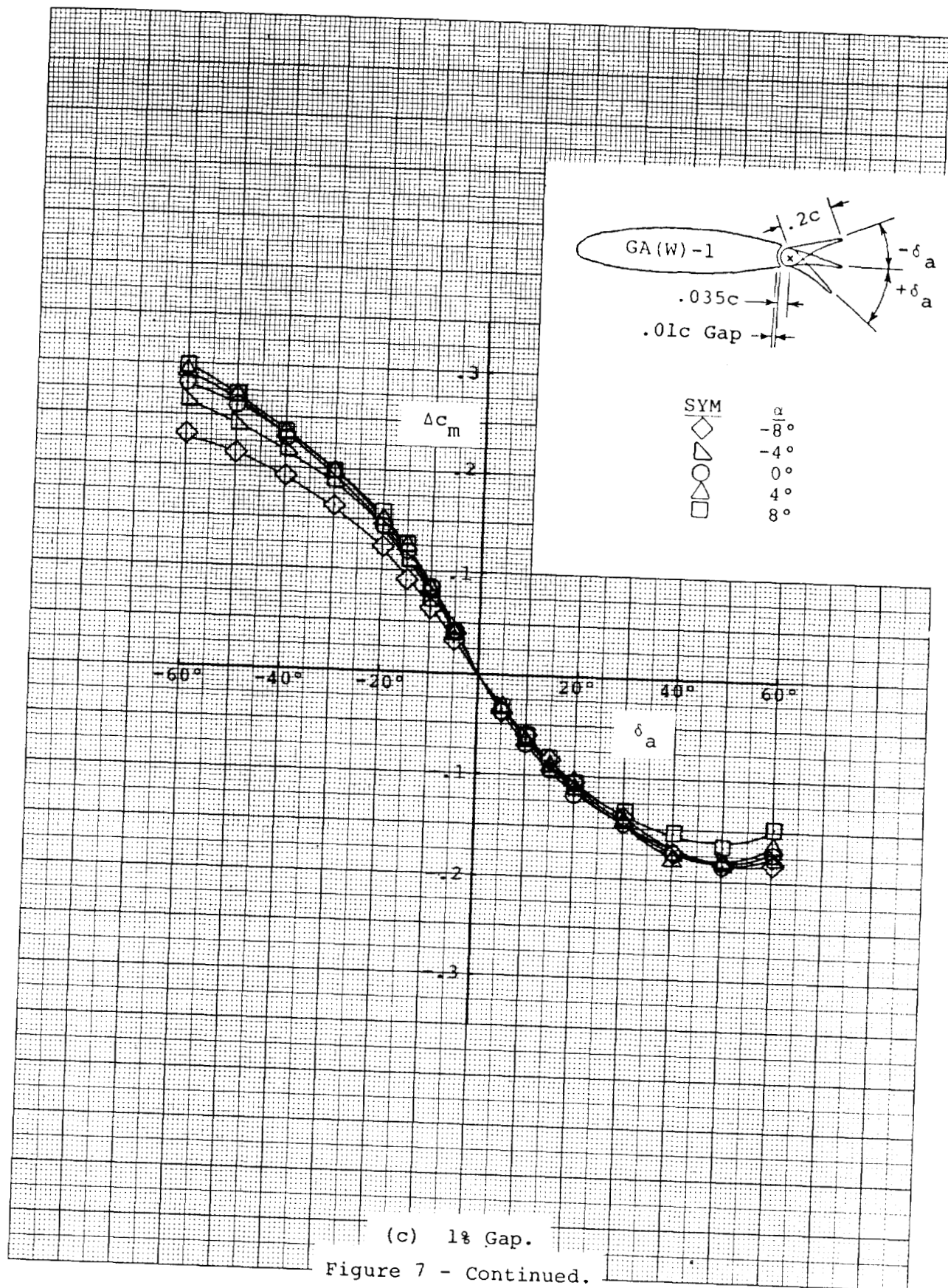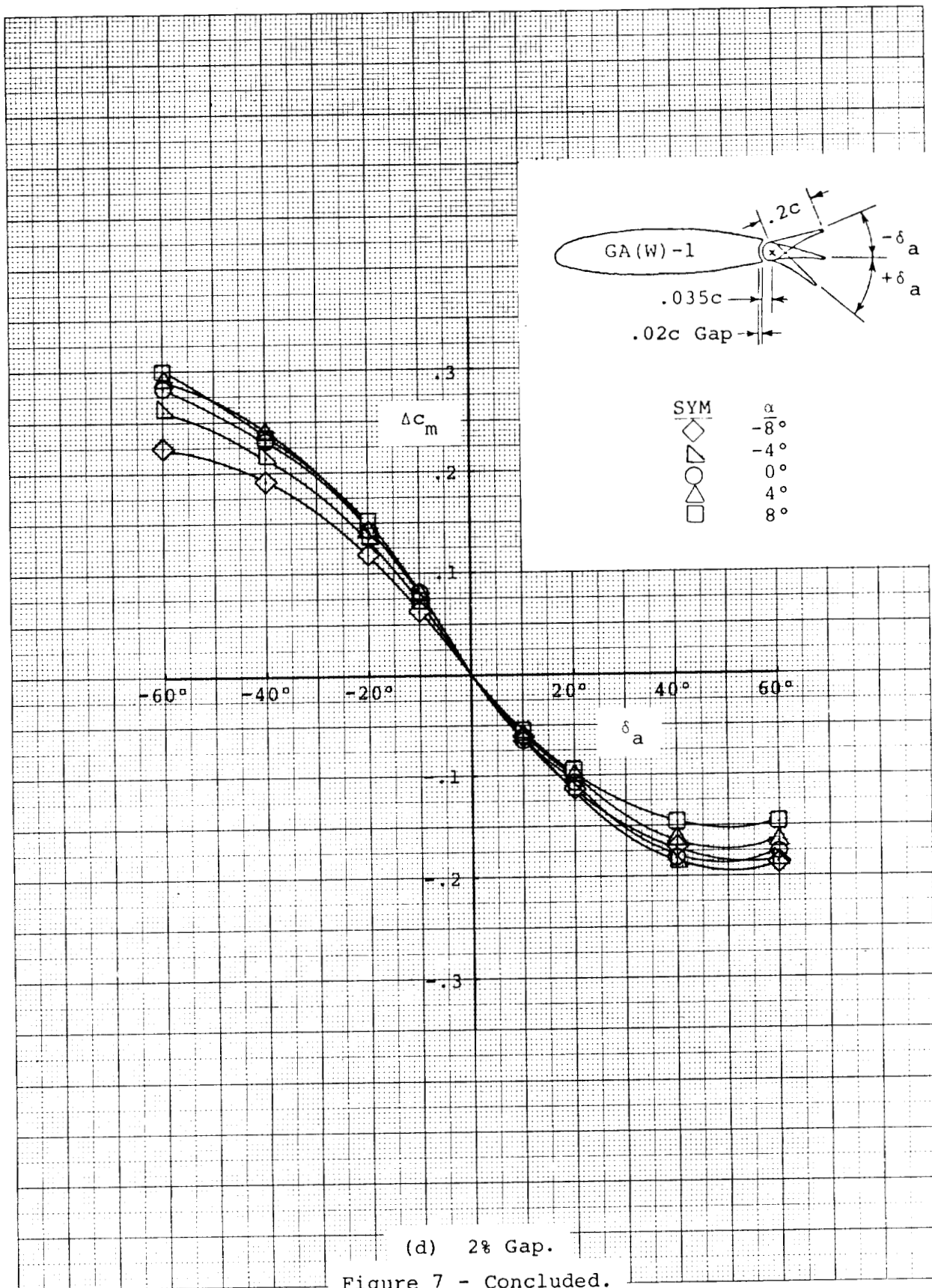
Figure 8 - Pressure Distributions with 0% Gap.

34

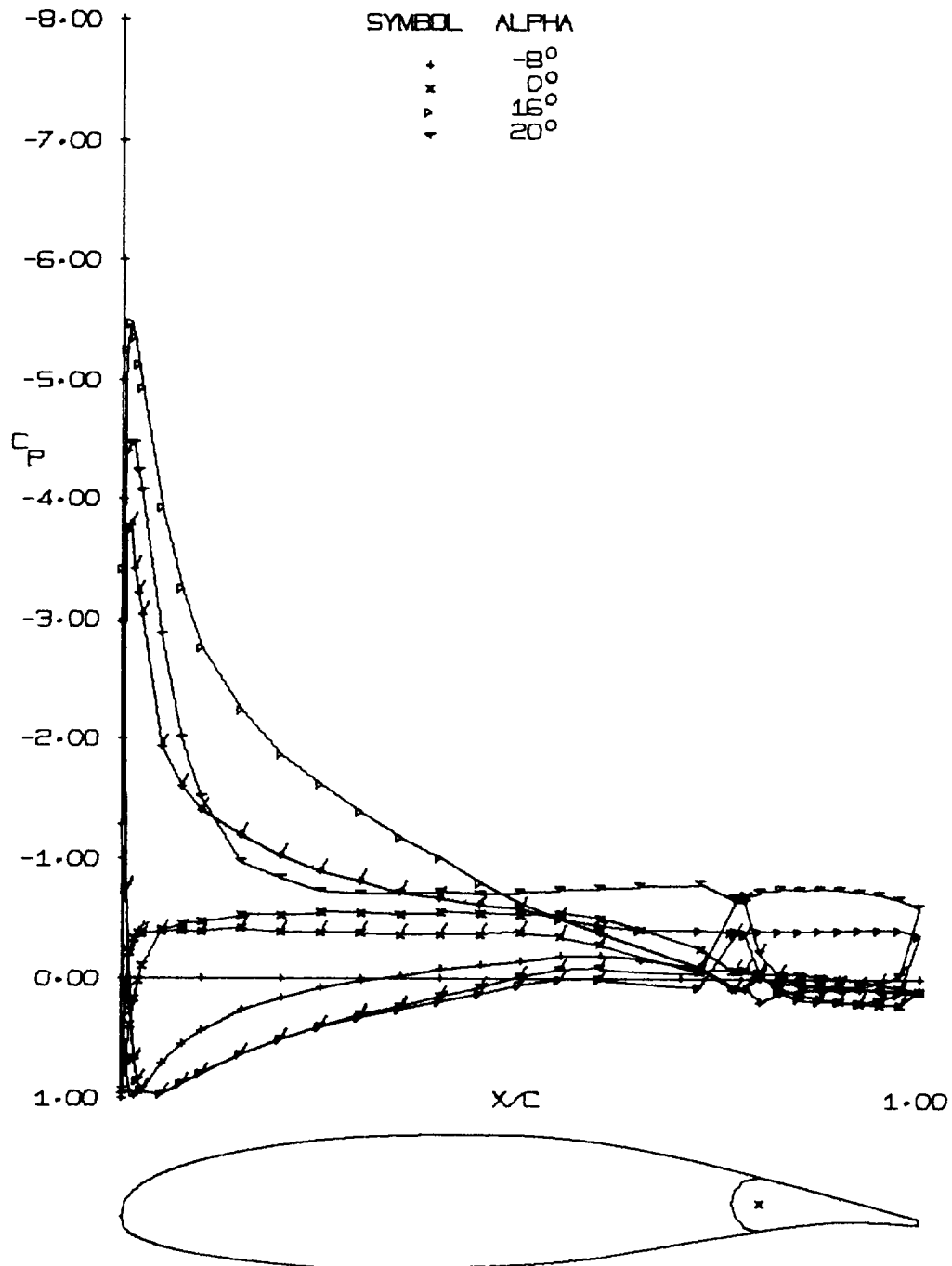AILERON DEFLECTION = -10·00 DEGREES

MACH NO· = 0·13

REYNOLDS NO· = 2·2 E 06

(b)   -10° Aileron, Moderate α's.

Figure 8 - Continued.

35

AILERON DEFLECTION = -5.00 DEGREES
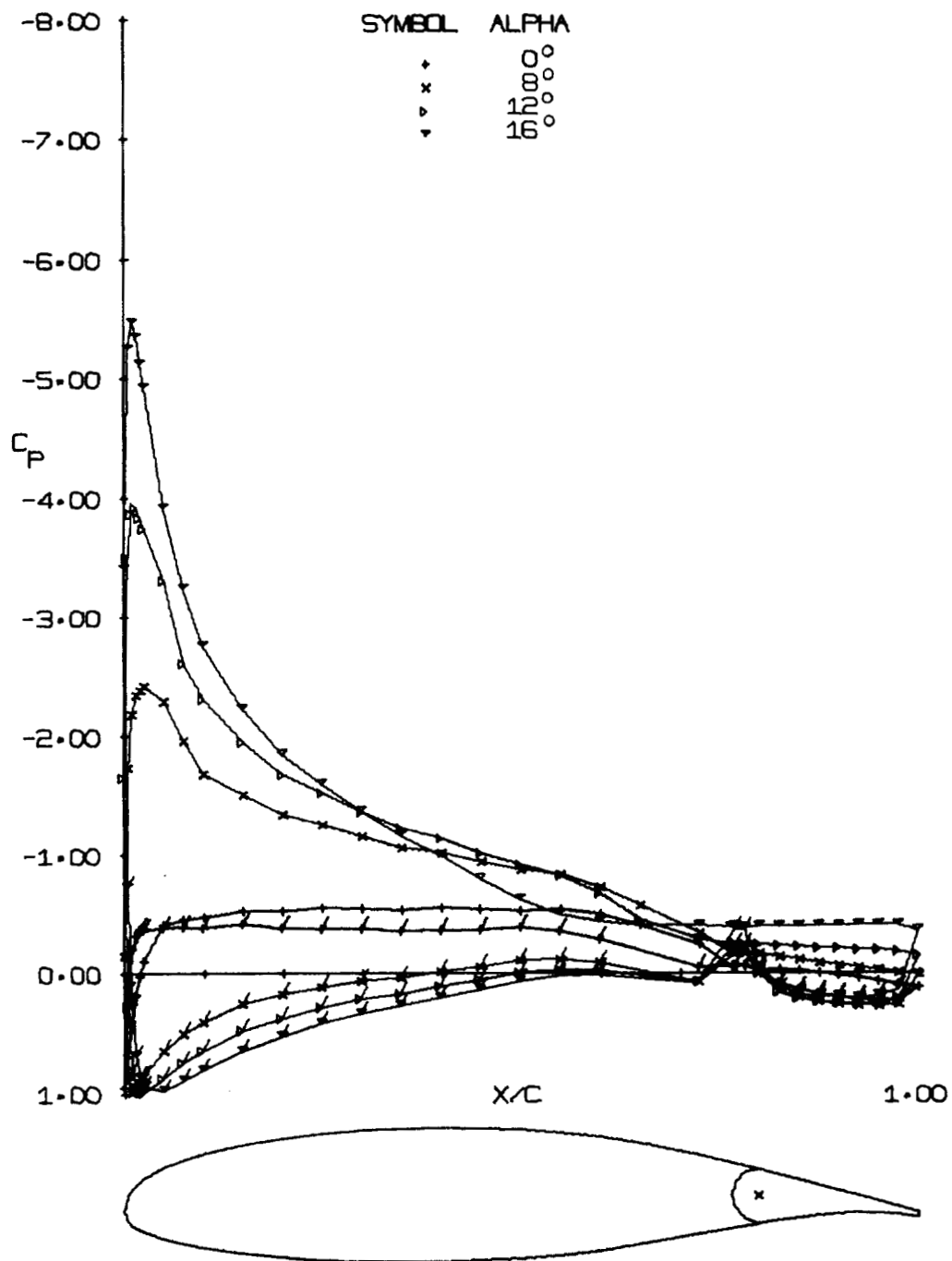
MACH NO. = 0.13

REYNOLDS NO. = 2.2 E 06

SYMBOL	ALPHA
+	$-8°$
×	$0°$
□	$16°$
▼	$20°$

C_P

X/C

(c)   -5° Aileron, Large α's.

Figure 8 - Continued.

36

AILERON DEFLECTION = -5·00 DEGREES

MACH NO· = 0·13

REYNOLDS NO· = 2·2 E 06

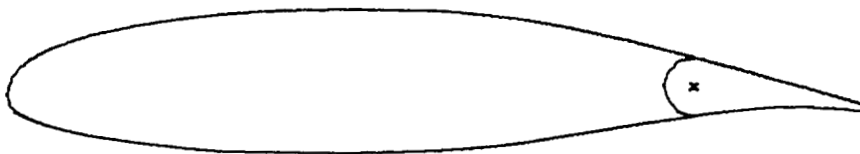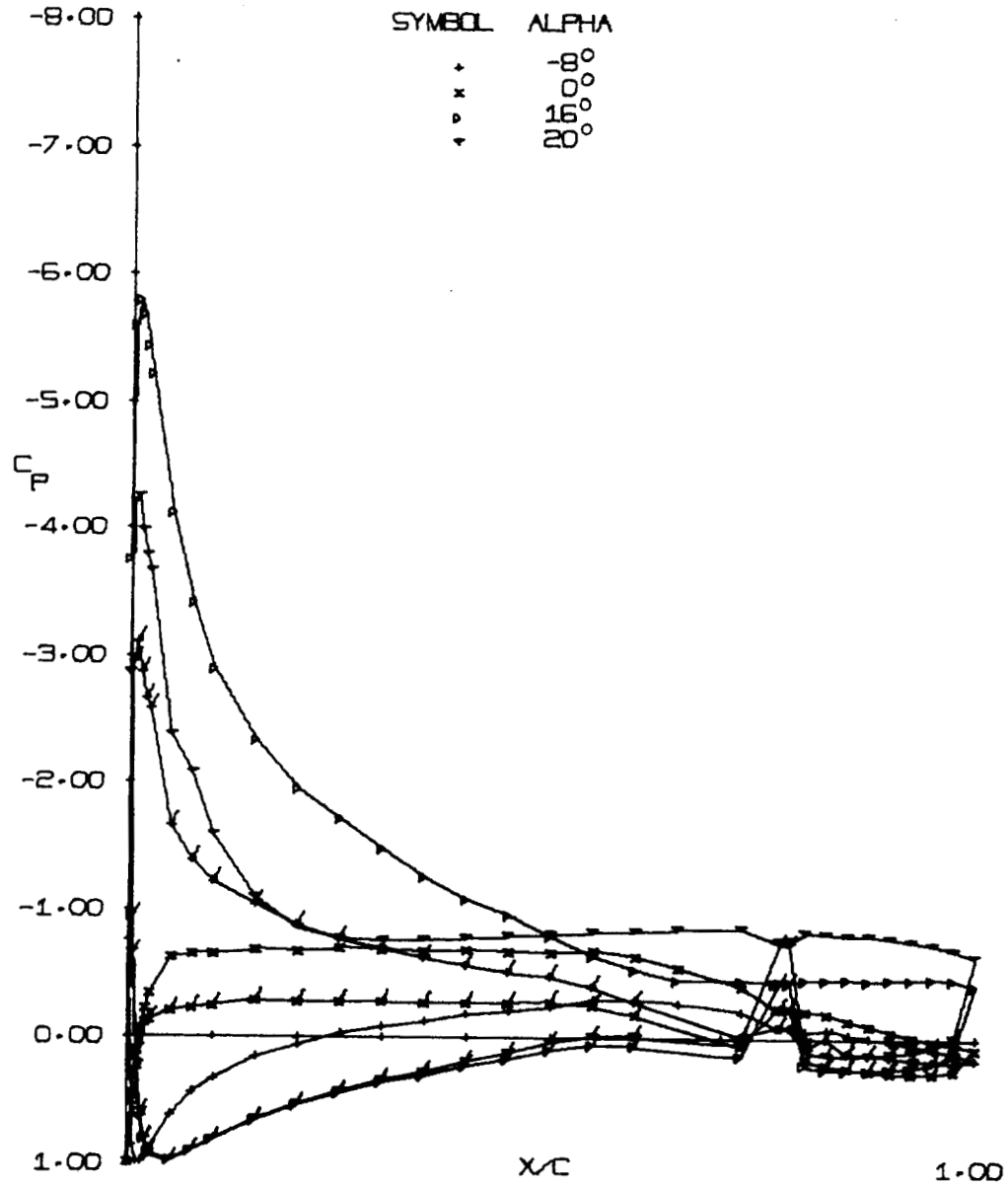SYMBOL   ALPHA
  ◆   0°
  ✕   8°
  ▷   12°
  ▼   16°

(d)   -5° Aileron, Moderate α's.

Figure 8 - Continued.

37

AILERON DEFLECTION = 0·00 DEGREES

MACH NO· = 0·13

REYNOLDS NO· = 2·2 E 06

SYMBOL   ALPHA

+	-8°
x	0°
▷	16°
▼	20°

(e)   0° Aileron, Large α's.

Figure 8 - Continued.

38

(f) 0° Aileron, Moderate α's.

Figure 8 - Continued.

39

AILERON DEFLECTION =   5.00 DEGREES
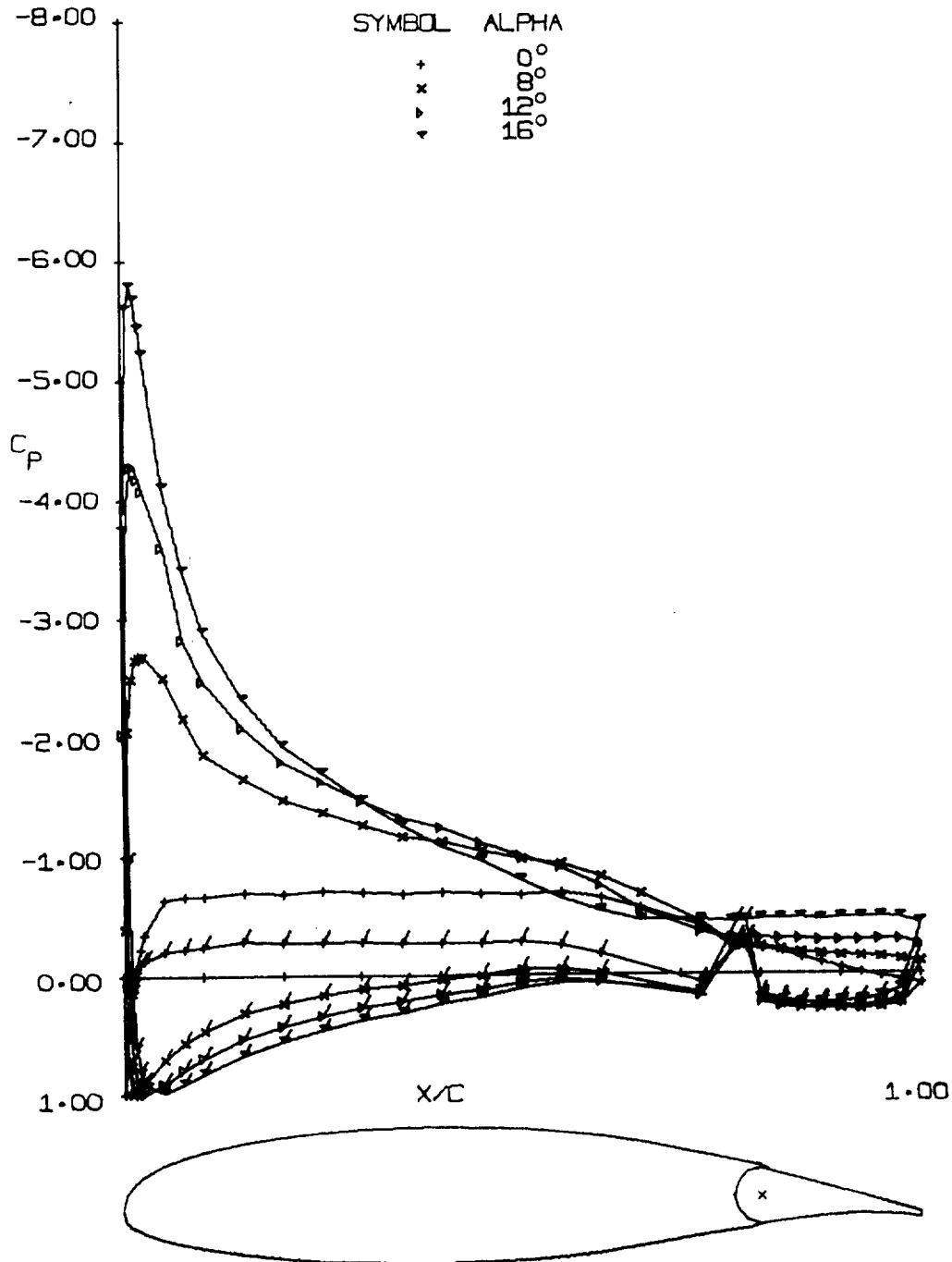
MACH NO. = 0.13

REYNOLDS NO. = 2.2 E 06

SYMBOL   ALPHA

+   -8°
×   0°
▪   16°
▾   20°

(g)   +5° Aileron, Large α's.

Figure 8 - Continued.

40

AILERON DEFLECTION = 5·00 DEGREES

MACH NO· = 0·13

REYNOLDS NO· = 2·2 E 06

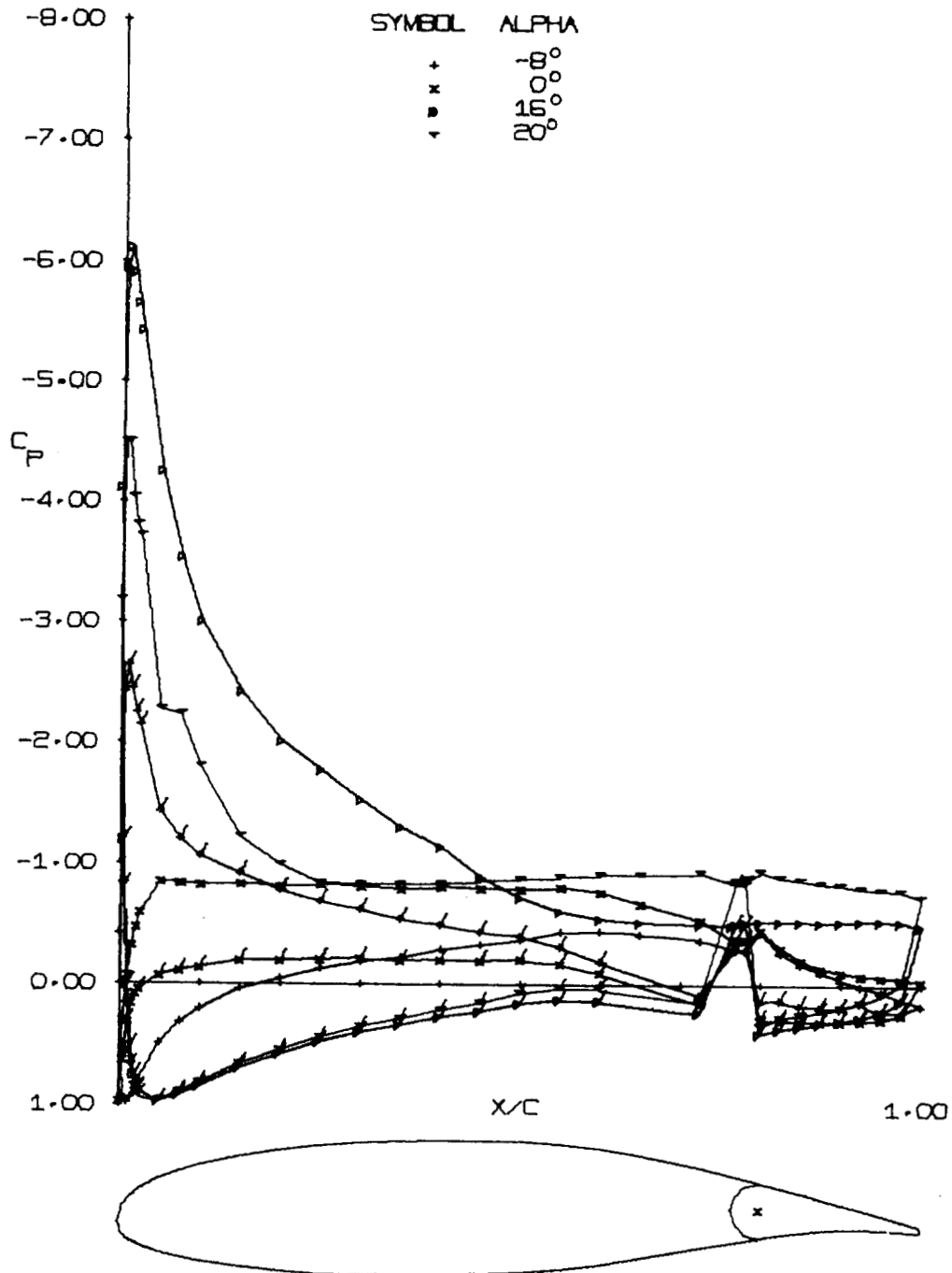SYMBOL   ALPHA
   +   0°
   x   8°
   ◊   12°
   ▼   16°

(h)   +5° Aileron, Moderate α's.

Figure 8 - Continued.

41

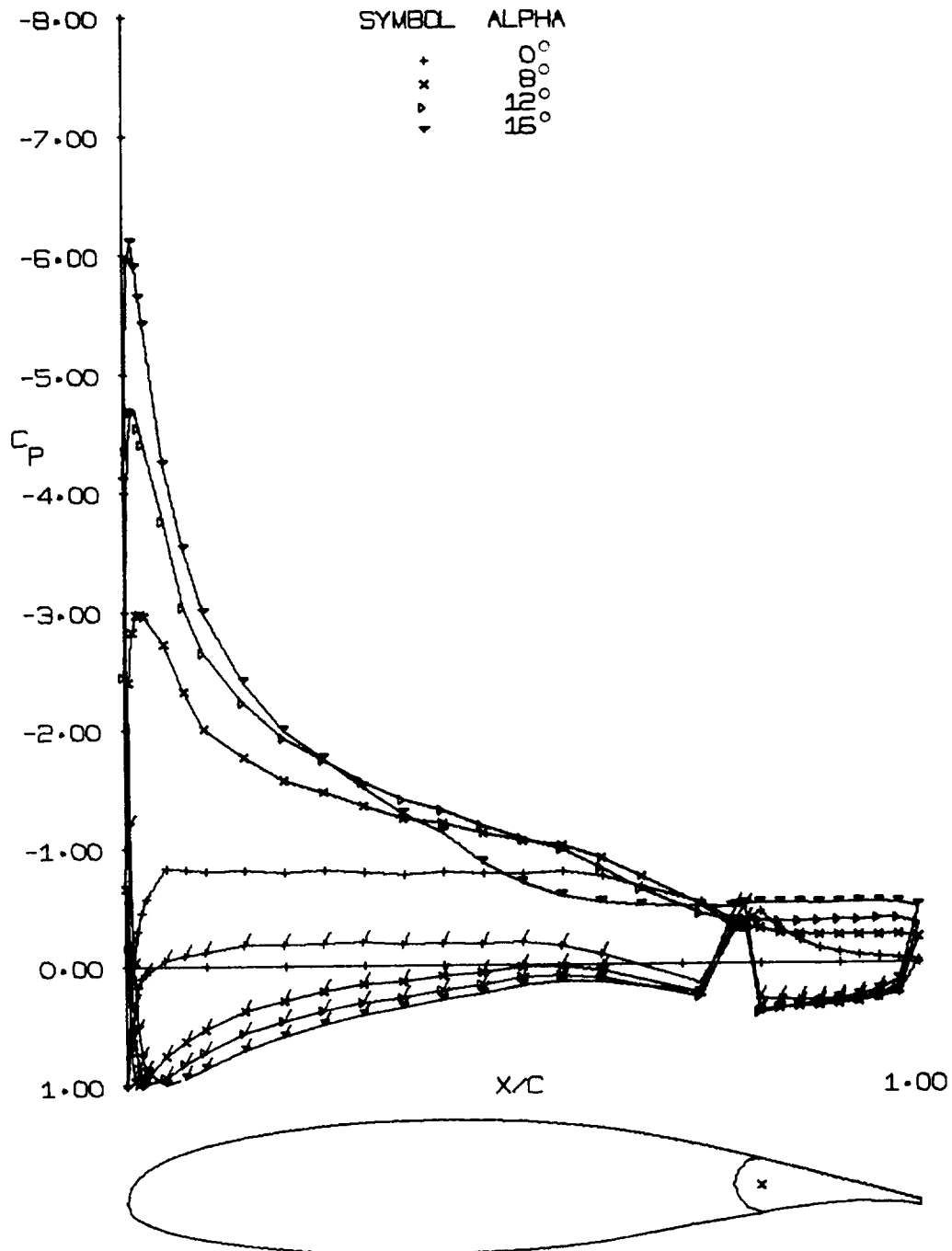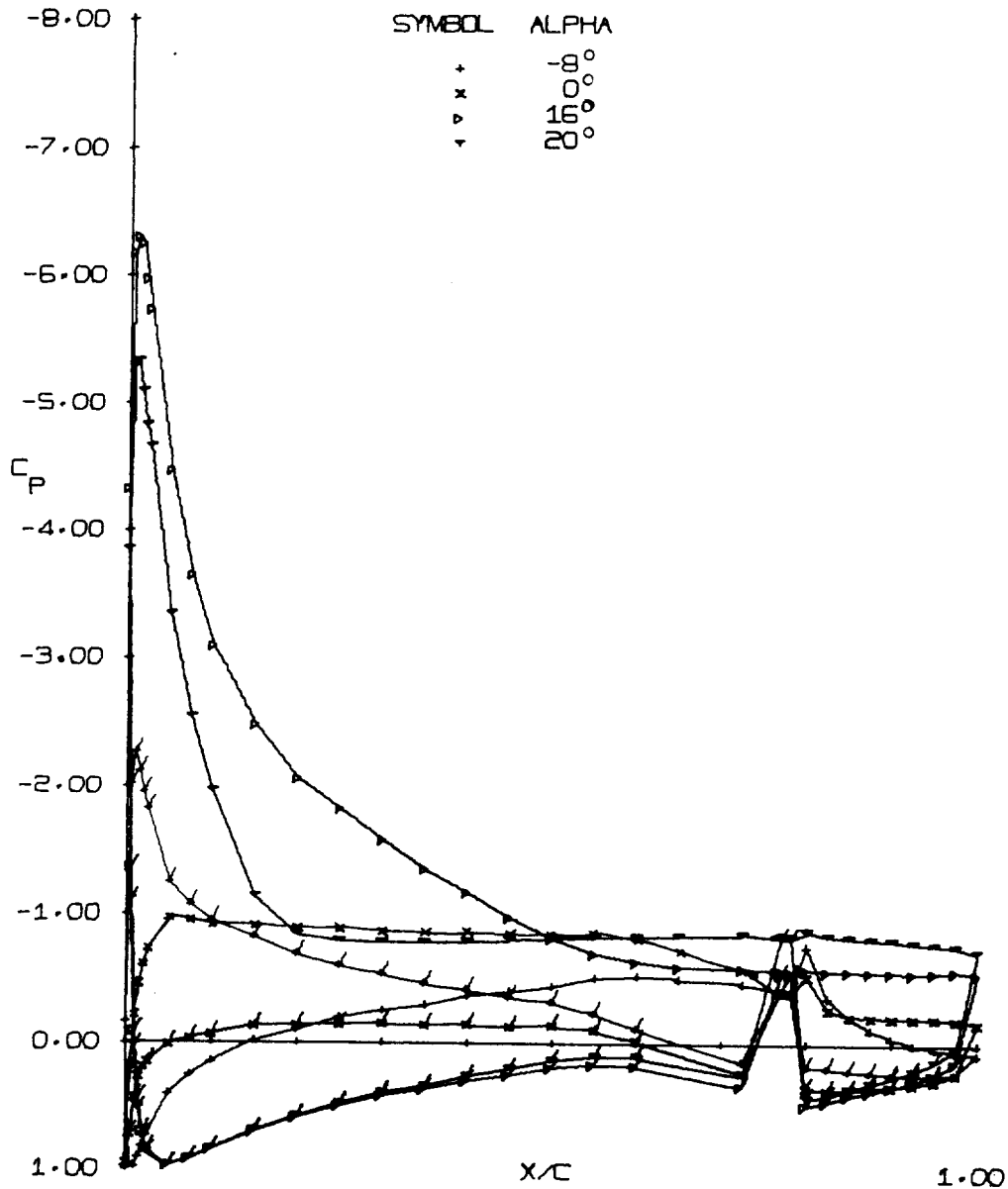AILERON DEFLECTION = 10.00 DEGREES

MACH NO. = 0.13

REYNOLDS NO. = 2.2 E 06
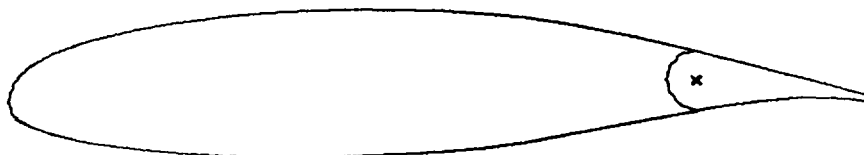
SYMBOL   ALPHA

+   -8°
x   0°
▷   16°
▼   20°

C_P

X/C

1.00   1.00

(i)   +10° Aileron, Large α's.

Figure 8 – Continued.

42

AILERON DEFLECTION = 10·00 DEGREES

MACH NO· = 0·13

REYNOLDS NO· = 2·2 E 06

SYMBOL	ALPHA
+	0°
x	8°
▷	12°
▼	16°

(j) +10° Aileron, Moderate α's.

Figure 8 - Concluded.

43

AILERON DEFLECTION =-60.00 DEG.

MACH NO. = 0.13

REYNOLDS NO. = 2.2 E 06

SYMBOL   ALPHA
+   -8°
×   0°
▷   16°
▼   20°

Flagged Symbols Denote
Lower Surface Pressures

(a)   -60° Aileron, Large α's

Figure 9 - Pressure Distributions with 0.5% Gap.

44

AILERON DEFLECTION =-60.00 DEG.

MACH NO. = 0.13

REYNOLDS NO. = 2.2 E 06

(b) -60° Aileron, Moderate α's.

Figure 9 - Continued.

45

AILERON DEFLECTION =-40·00 DEG·
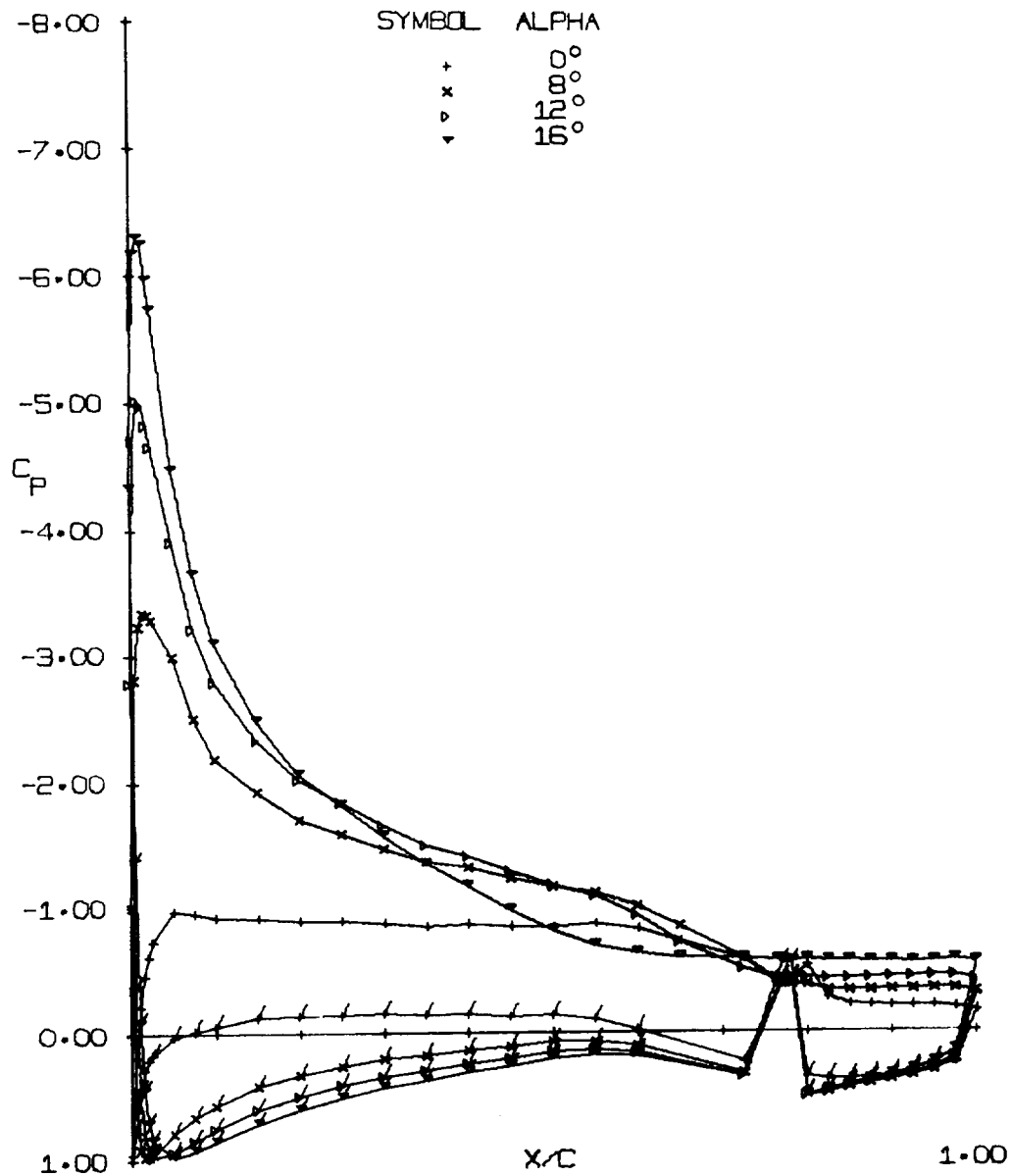
MACH NO· = 0·13

REYNOLDS NO· = 2·2 E 06

(c) -40° Aileron, Large α's.
Figure 9 - Continued.

46

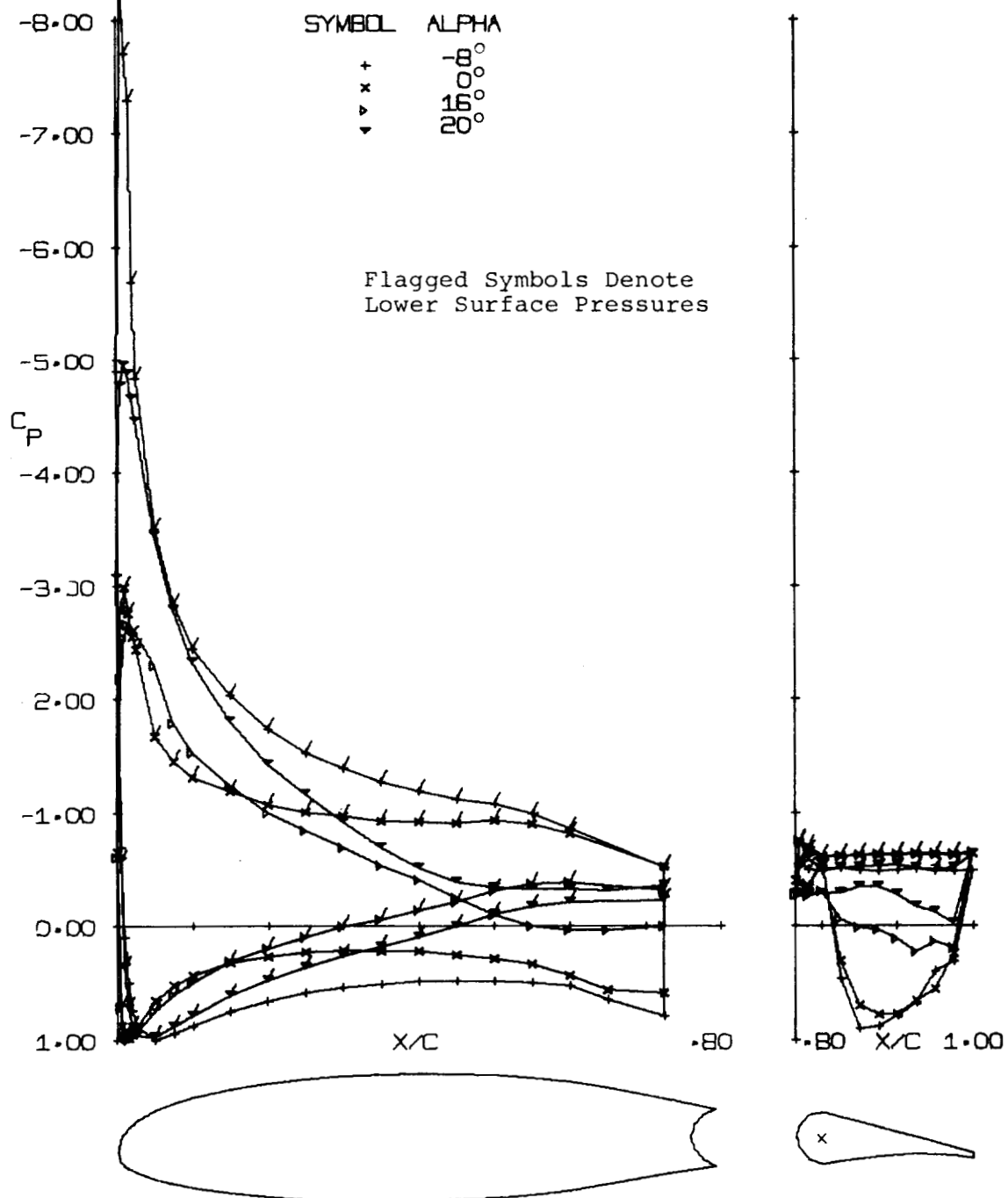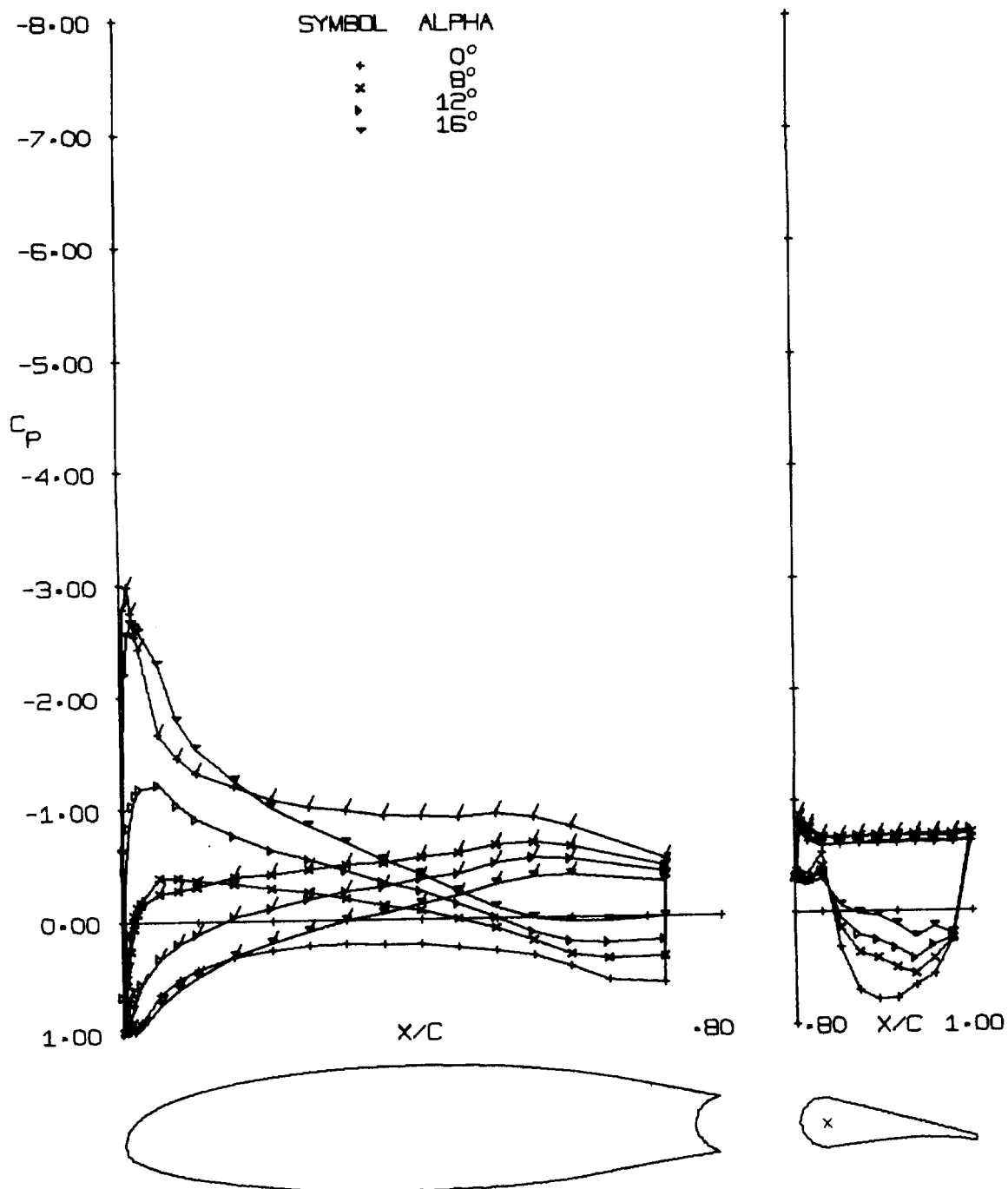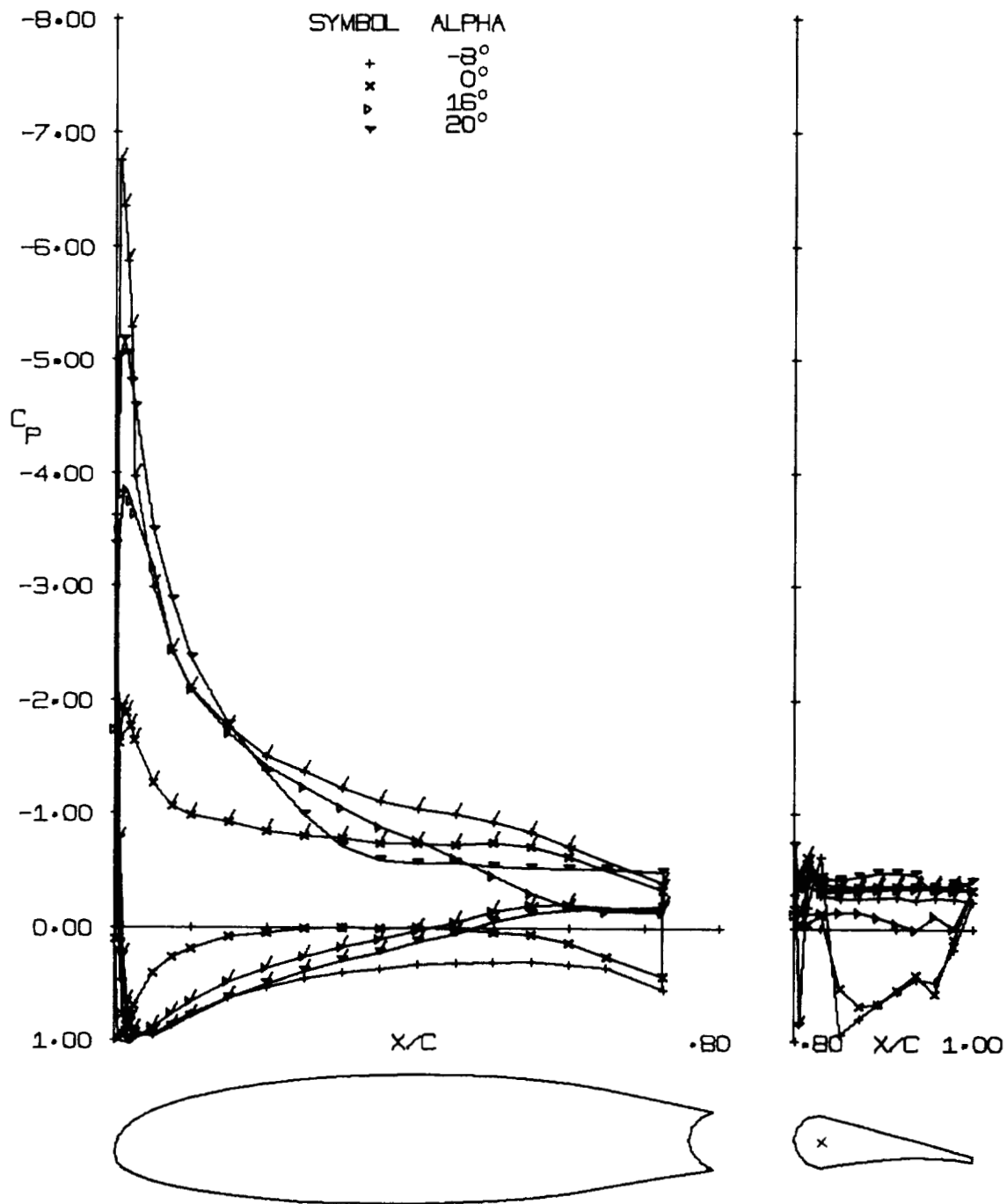AILERON DEFLECTION =-40.00 DEG.

MACH NO. = 0.13

REYNOLDS NO. = 2.2 E 06

SYMBOL   ALPHA

+   0°
x   8°
◊   12°
▼   16°

C_P

-8.00
-7.00
-6.00
-5.00
-4.00
-3.00
-2.00
-1.00
0.00
1.00

X/C   .80   .80   X/C   1.00

(d)   -40° Aileron, Moderate α's.

Figure 9 - Continued.

47

AILERON DEFLECTION =-20·00 DEG·

MACH NO· = 0·13

REYNOLDS NO· = 2·2 E 06

(e)   -20° Aileron, Large α's.
Figure 9 - Continued.

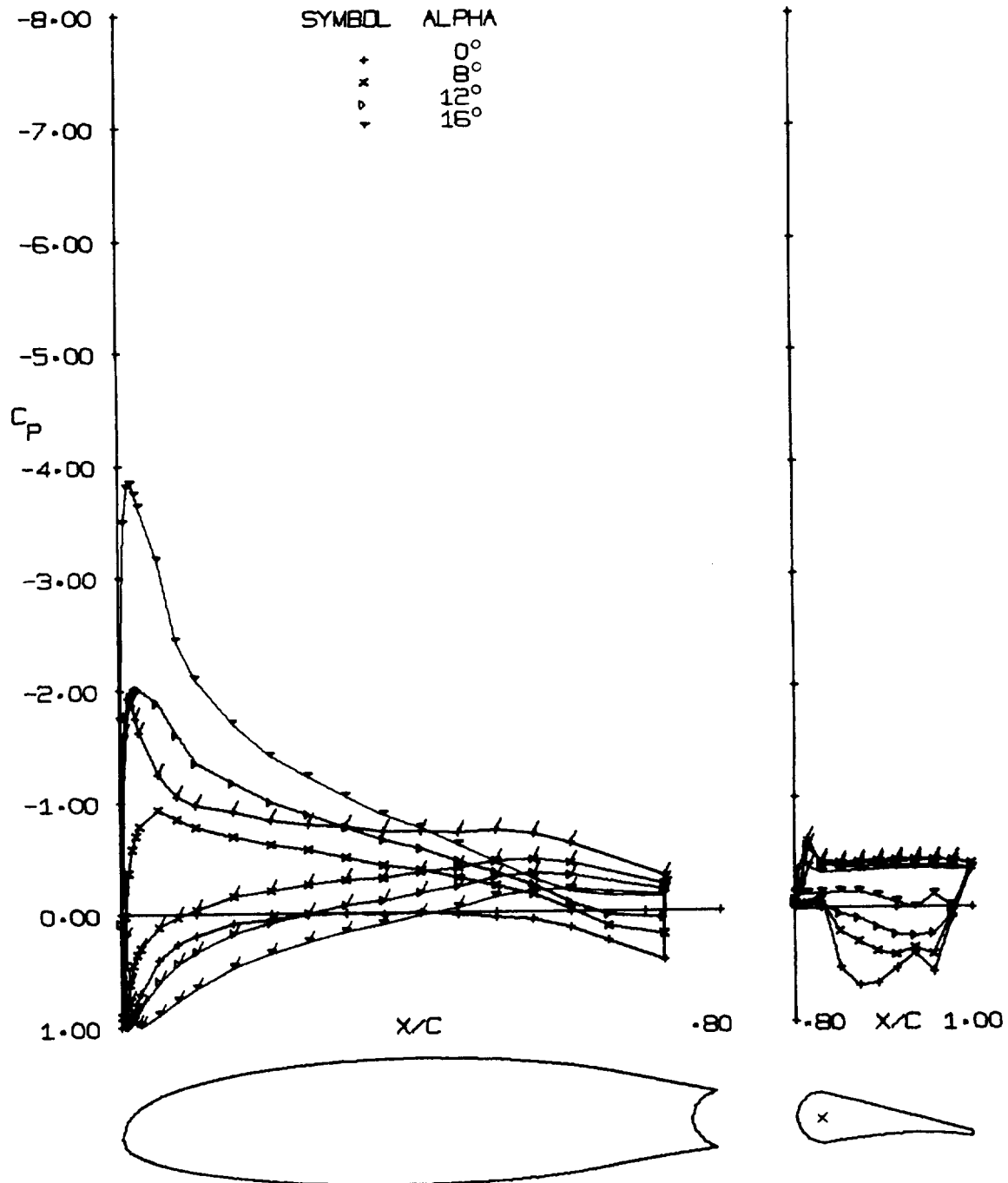AILERON DEFLECTION =-20.00 DEG.

MACH NO. = 0.13

REYNOLDS NO. = 2.2 E 06

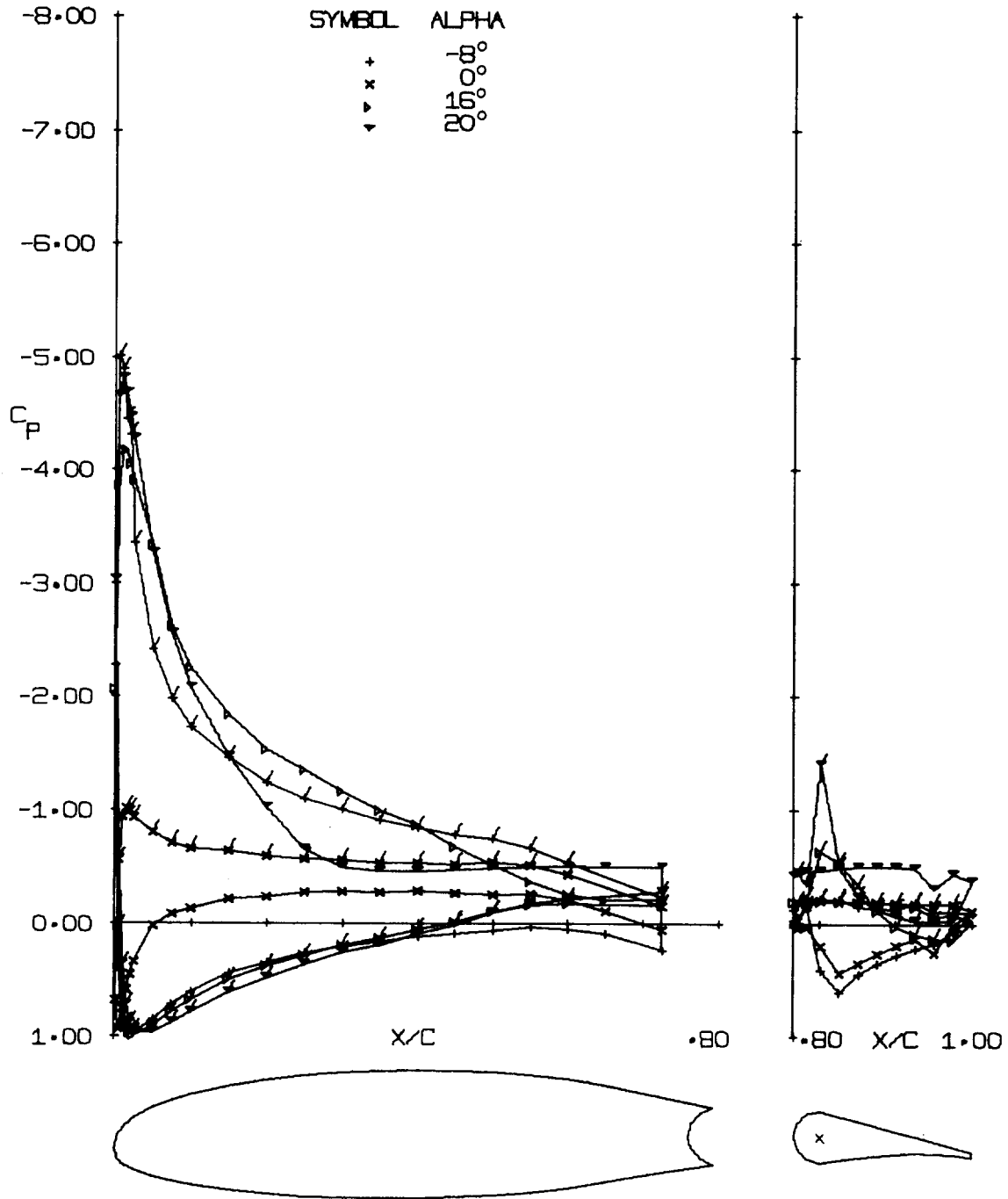| SYMBOL	ALPHA
+	0°
×	8°
▷	12°
▽	16°

C_P

X/C

.80

.80   X/C   1.00

(f)   -20° Aileron, Moderate α's.

Figure 9 - Continued.

49

AILERON DEFLECTION =-10.00 DEG.

MACH NO. = 0.13

REYNOLDS NO. = 2.2 E 06

(g) -10° Aileron, Large α's.

Figure 9 - Continued.

50

AILERON DEFLECTION =-10·00 DEG·

MACH NO· = 0·13

REYNOLDS NO· = 2·2 E 06

SYMBOL   ALPHA

+	0°
×	8°
▶	12°
▼	16°

(h)   -10° Aileron, Moderate α's.

Figure 9 - Continued.

51

AILERON DEFLECTION = -5.00 DEG.

MACH NO. = 0.13

REYNOLDS NO. = 2.2 E 06

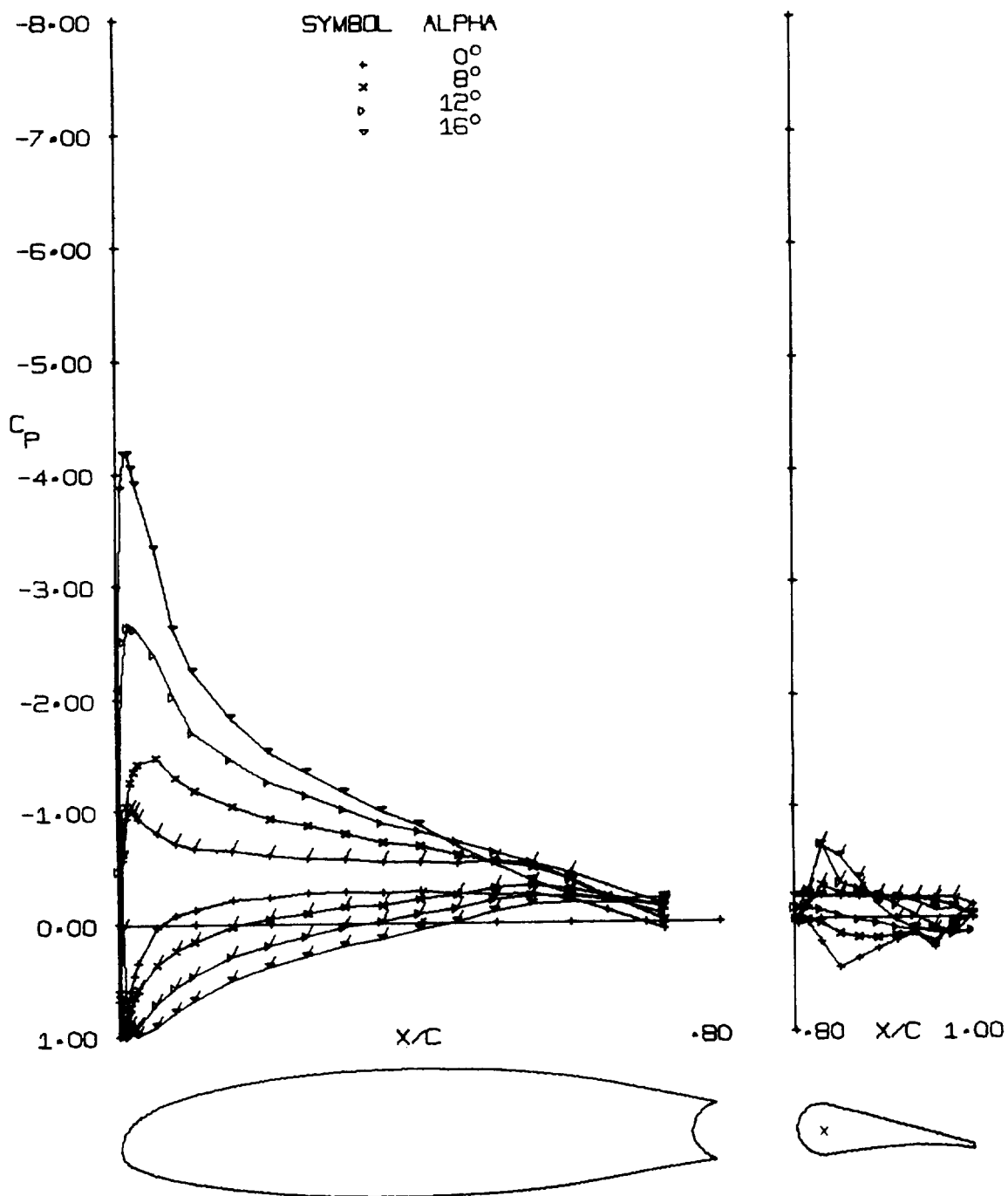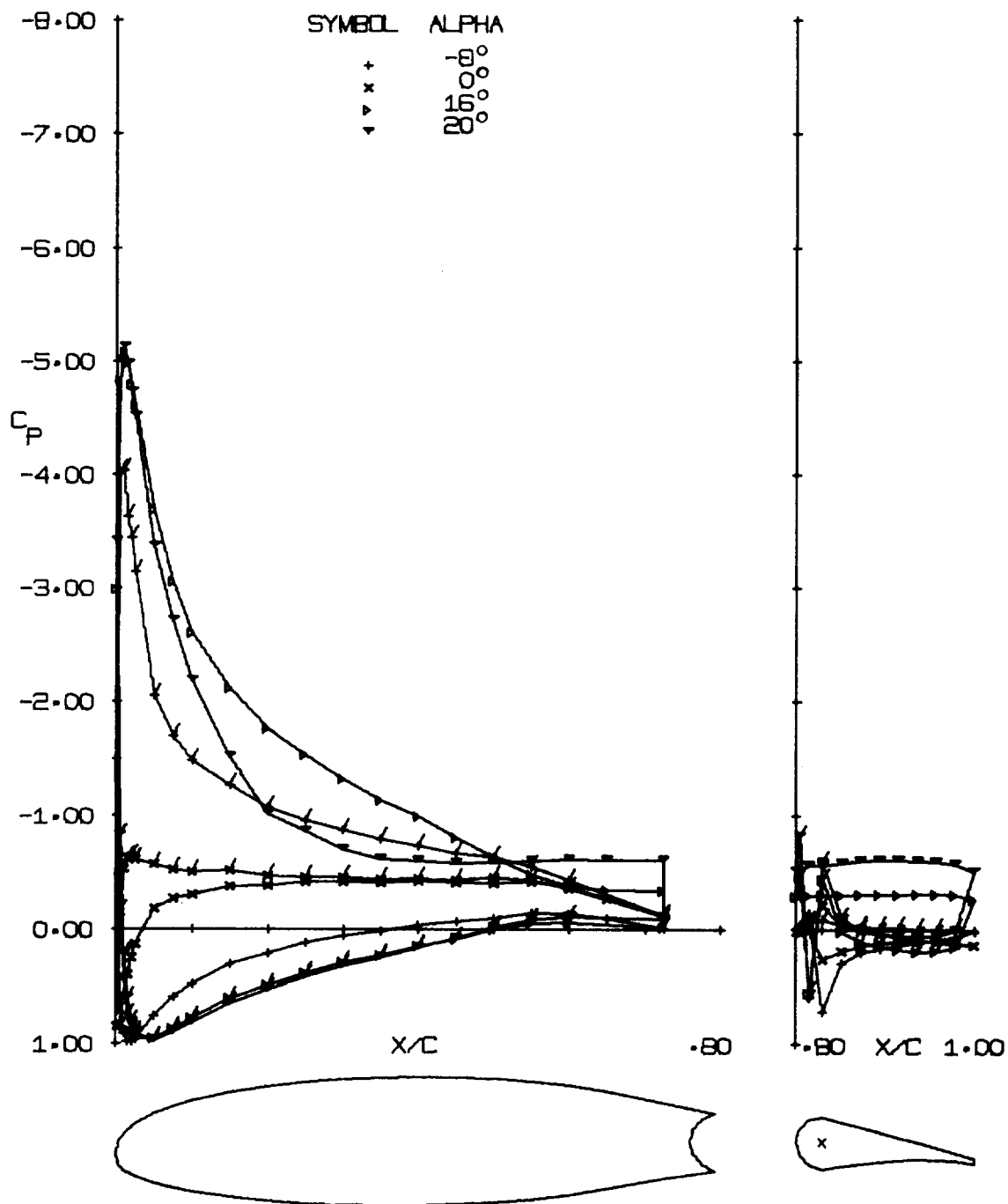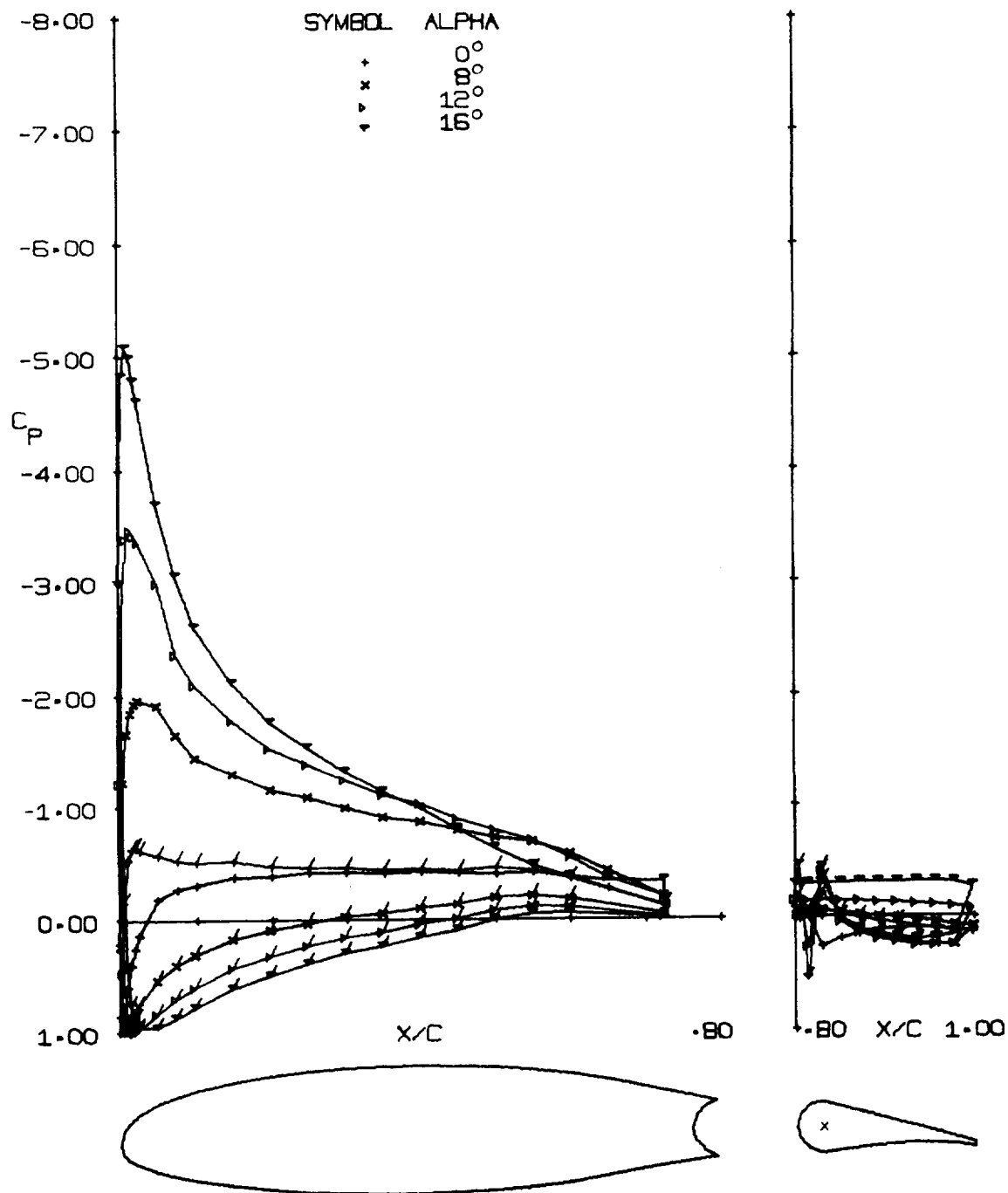| SYMBOL	ALPHA
□	-8°
+	0°
×	16°
▶	18°
▼	20°

(i) -5° Aileron, Large α's.

Figure 9 - Continued.

52

AILERON DEFLECTION = -5.00 DEG.

MACH NO. = 0.13

REYNOLDS NO. = 2.2 E 06

(j) -5° Aileron, Moderate α's.

Figure 9 - Continued.

53

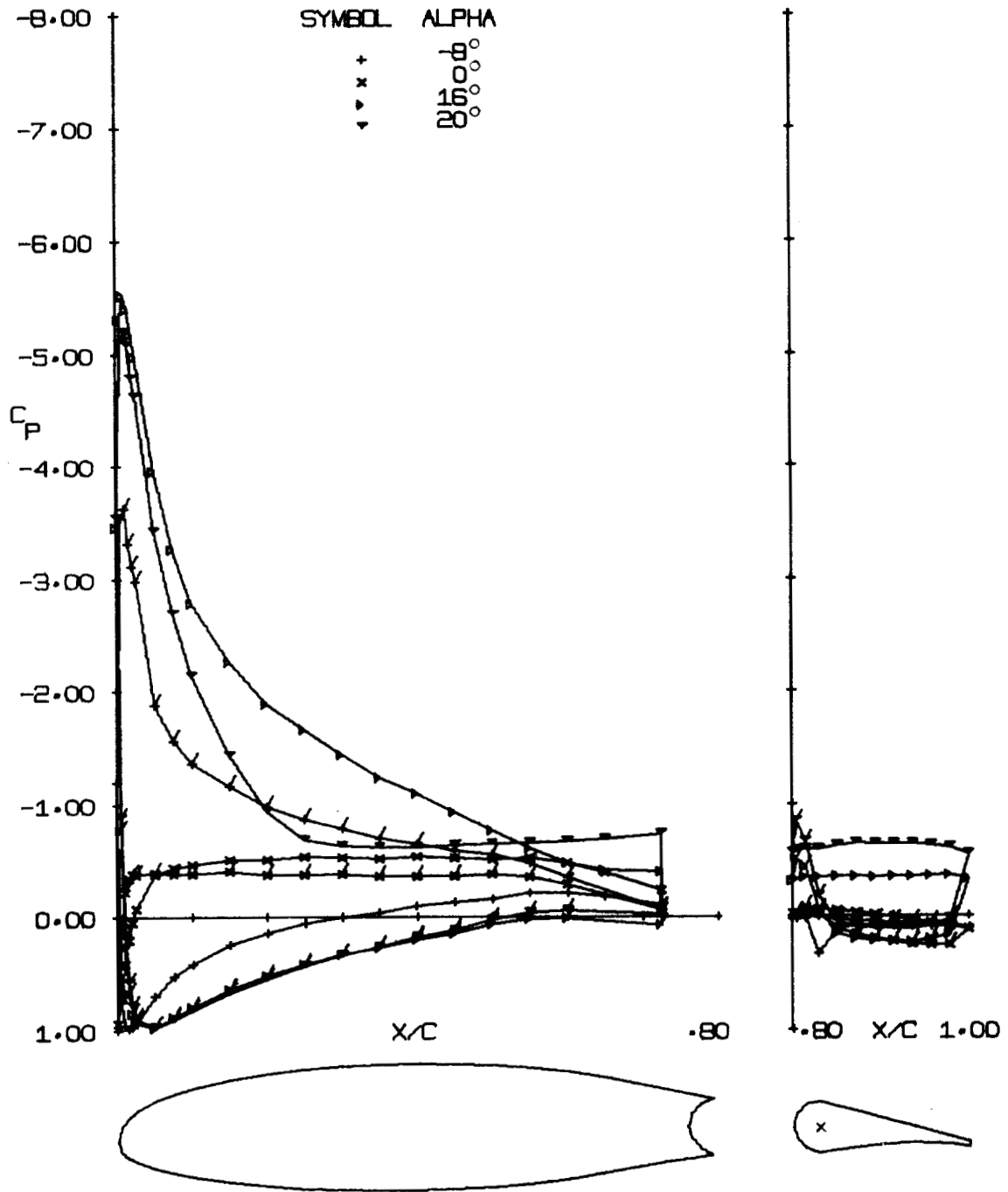AILERON DEFLECTION = 0·00 DEG·

MACH NO· = 0·13

REYNOLDS NO· = 2·2 E 06

SYMBOL	ALPHA
+	$-8°$
×	$0°$
▶	$16°$
▼	$20°$

(k) 0° Aileron, Large α's.

Figure 9 - Continued.

54

AILERON DEFLECTION = 0.00 DEG.

MACH NO. = 0.13

REYNOLDS NO. = 2.2 E 06

SYMBOL	ALPHA
+	0°
+	8°
×	12°
▷	16°

C_P

-8.00

-7.00

-6.00

-5.00

-4.00

-3.00

-2.00

-1.00

0.00

1.00

X/C   .80   .80   X/C   1.00

(1)   0° Aileron, Moderate α's.

Figure 9 - Continued.

55

AILERON DEFLECTION = +5.00 DEG.

MACH NO. = 0.13

REYNOLDS NO. = 2.2 E 06

SYMBOL	ALPHA
+	-8°
×	0°
▷	16°
▼	20°

C_P
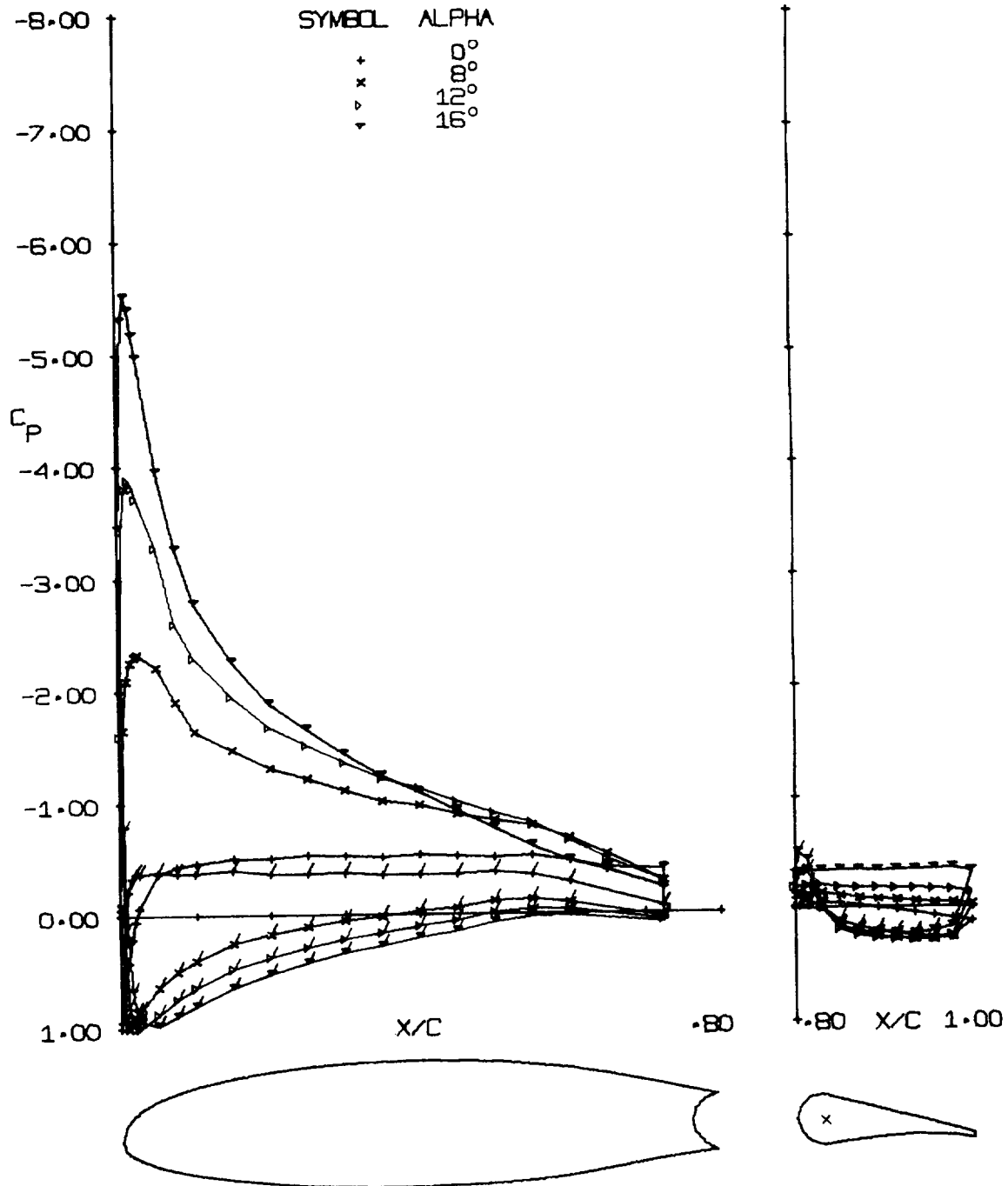
X/C

.80

.80   X/C   1.00

(m)   5° Aileron, Large α's.

Figure 9 - Continued.

56

AILERON DEFLECTION = +5.00 DEG.
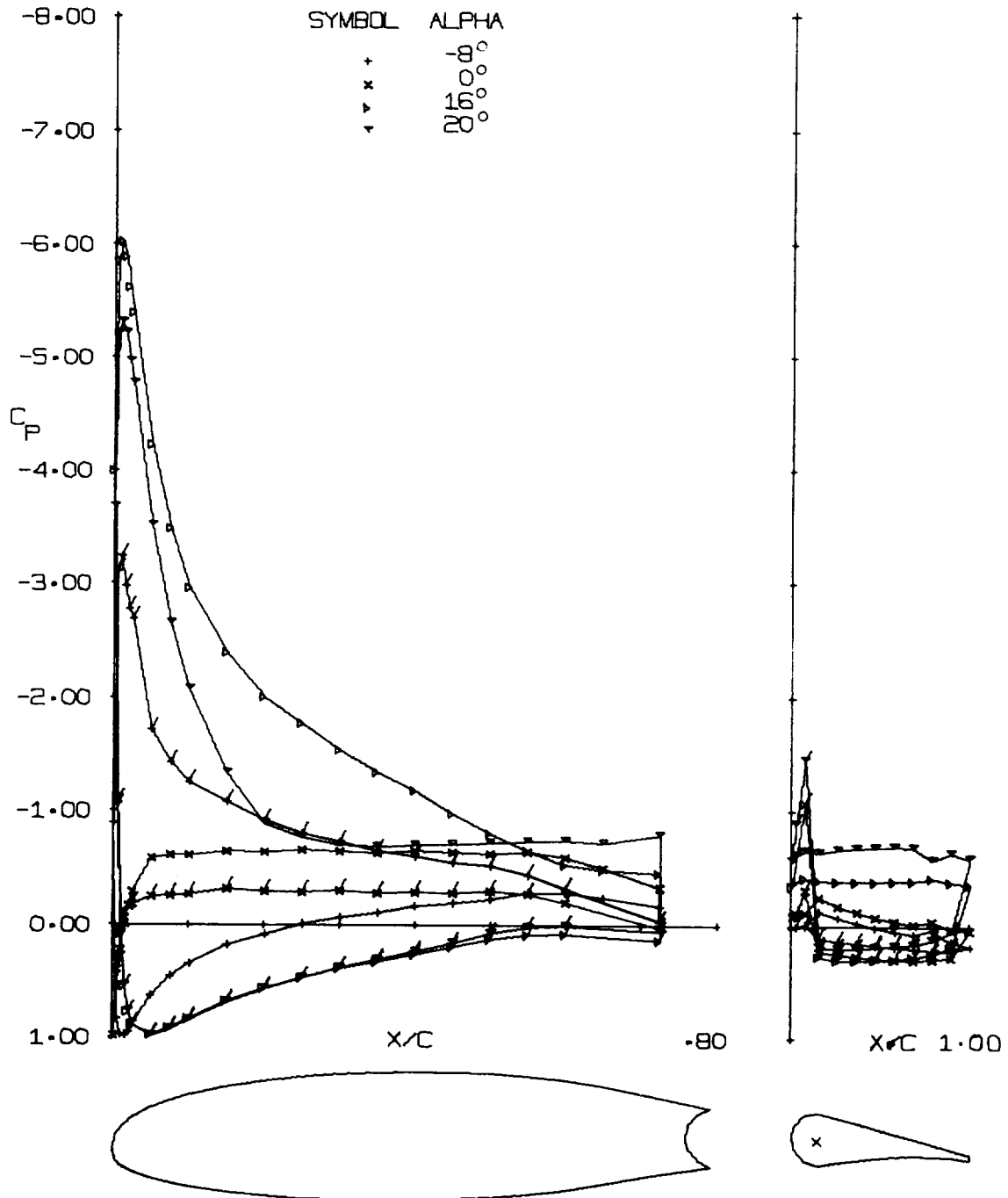
MACH NO. = 0.13

REYNOLDS NO. = 2.2 E 06

(n)   5° Aileron, Moderate α's.

Figure 9 - Continued.

57

AILERON DEFLECTION =+10.00 DEG.
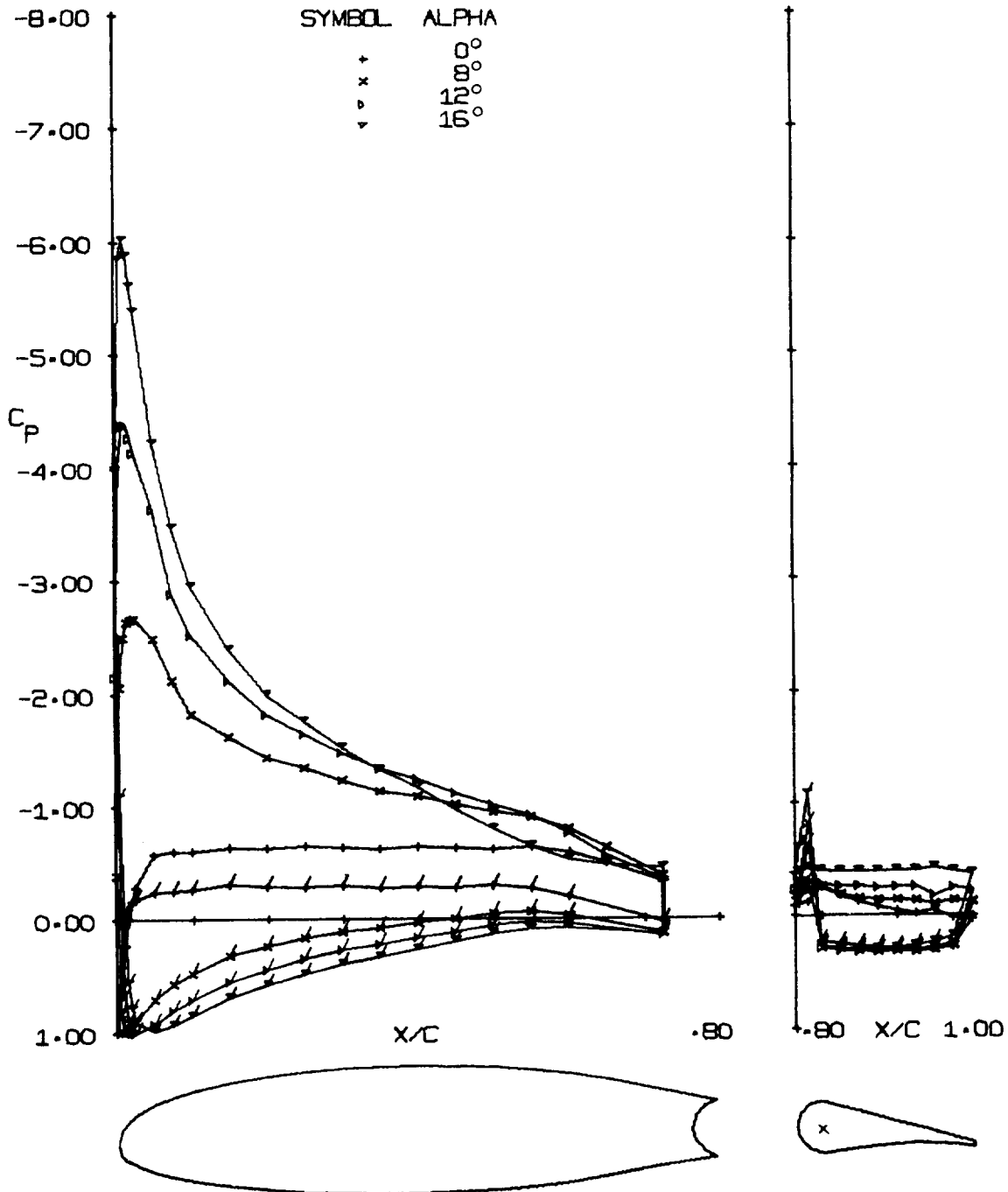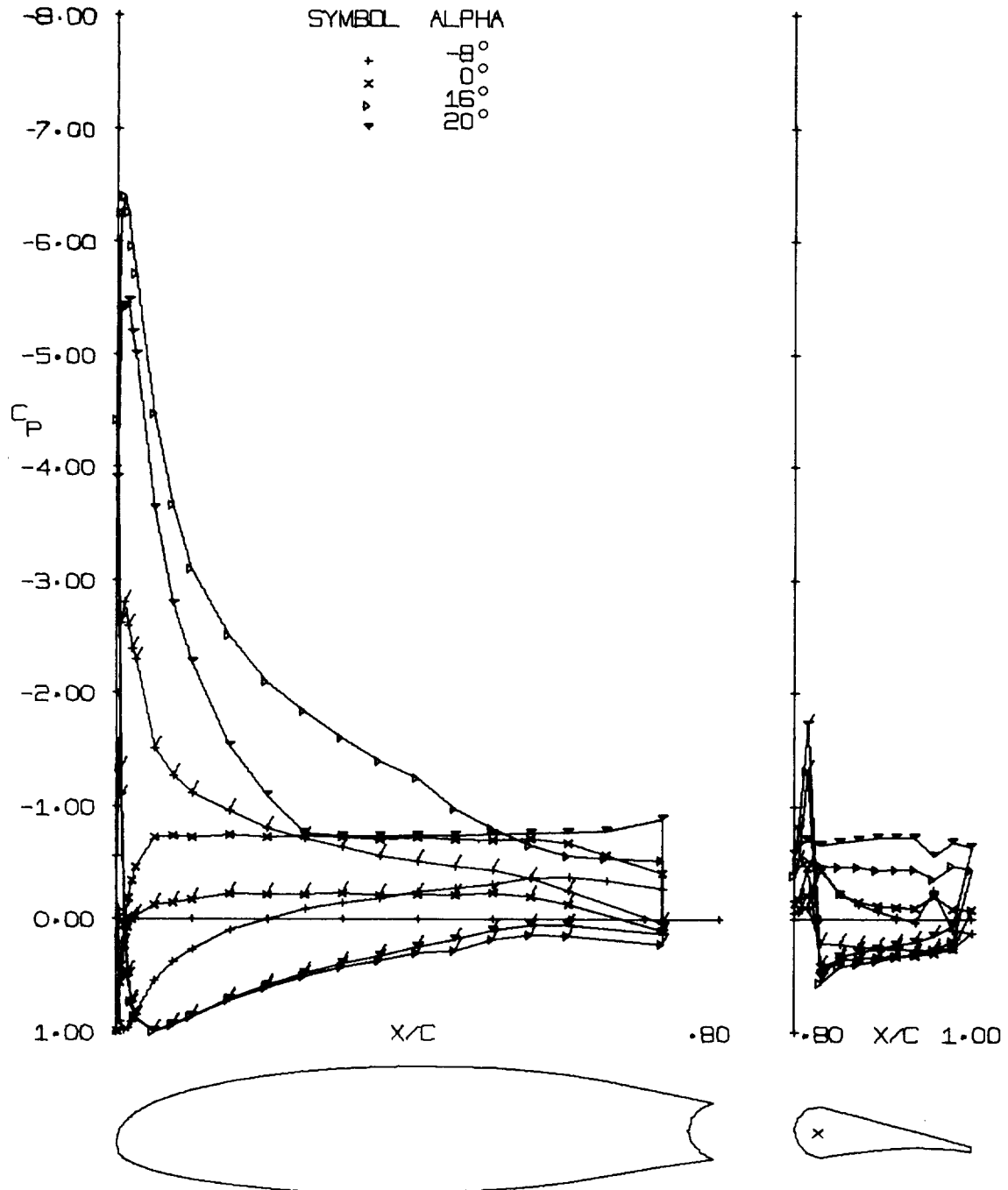
MACH NO. = 0.13

REYNOLDS NO. = 2.2 E 06

(o)   10° Aileron, Large α's.

Figure 9 - Continued.

58

AILERON DEFLECTION =+10.00 DEG.

MACH NO. = 0.13

REYNOLDS NO. = 2.2 E 06

SYMBOL   ALPHA

+   0°
+   8°
×   12°
▷   16°

(p)   10° Aileron, Moderate α's.

Figure 9 - Continued.

59

AILERON DEFLECTION =+20.00 DEG.

MACH NO. = 0.13

REYNOLDS NO. = 2.2 E 06

SYMBOL   ALPHA
   +   -8°
   ×   0°
   ▶   16°
   ▼   20°

(q)   20° Aileron, Large α's.

Figure 9 – Continued.

60

AILERON DEFLECTION =+20.00 DEG.

MACH NO. = 0.13

REYNOLDS NO. = 2.2 E 06

(r)   20° Aileron, Moderate α's.

Figure 9 - Continued.

AILERON DEFLECTION =+40.00 DEG.

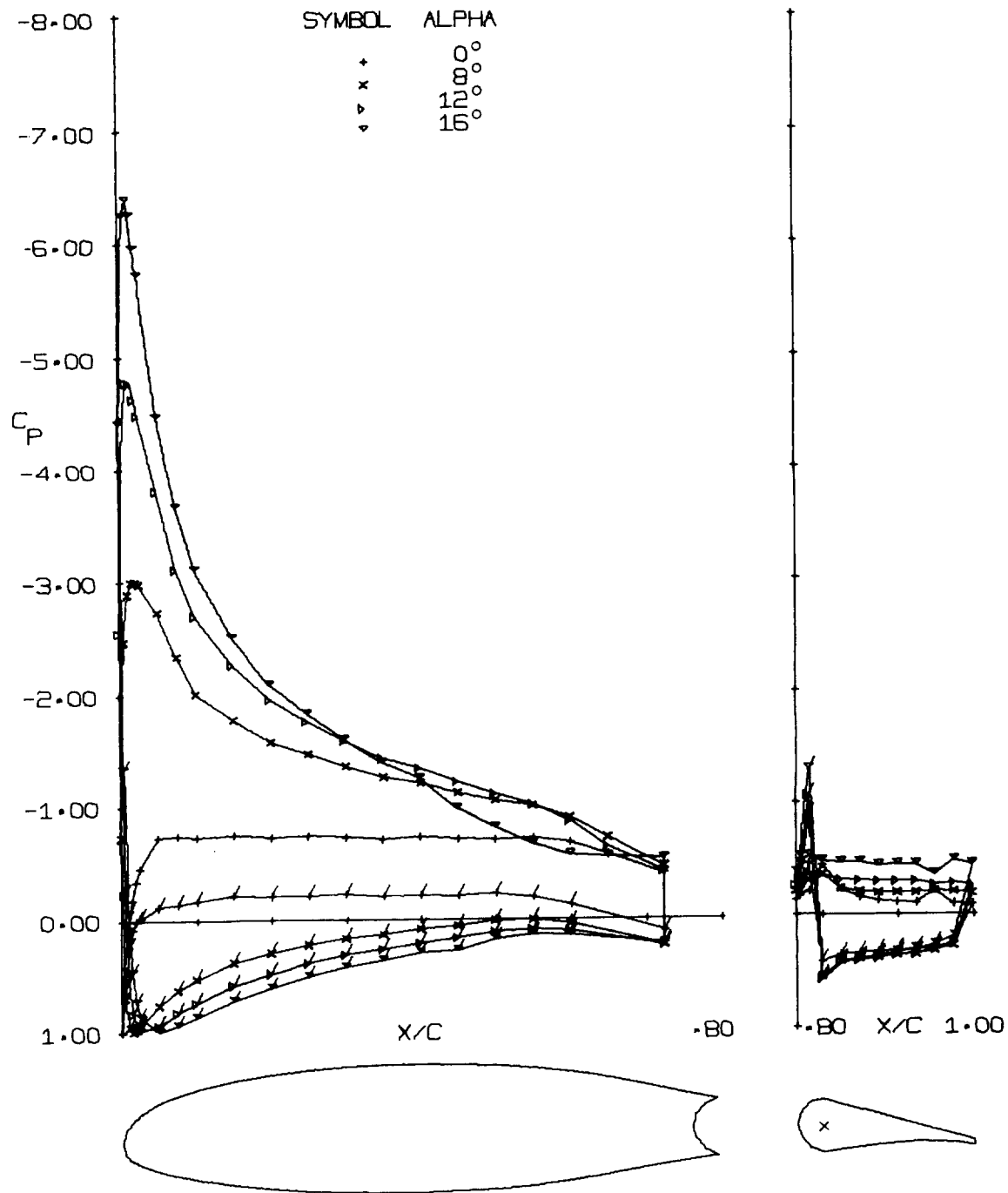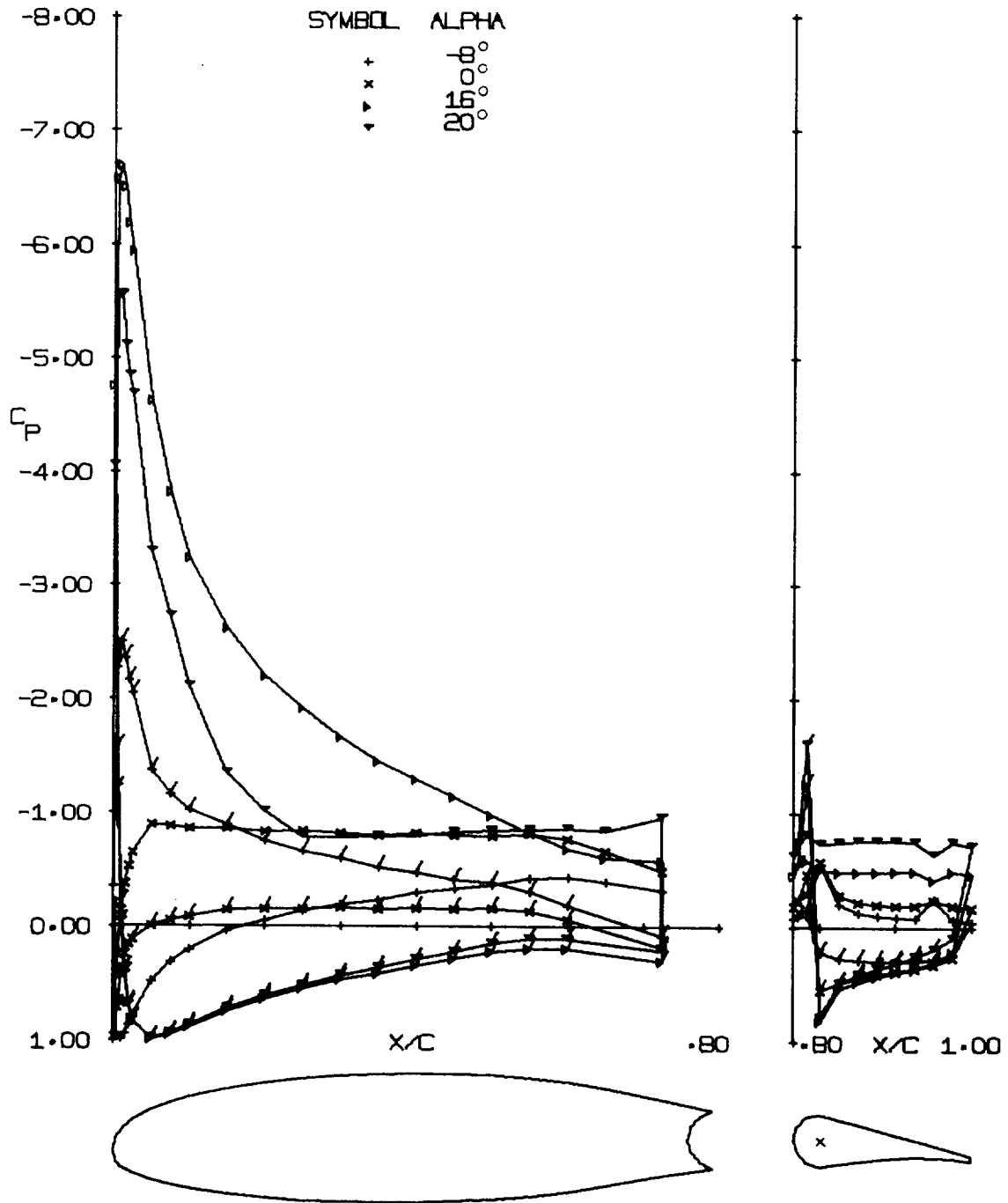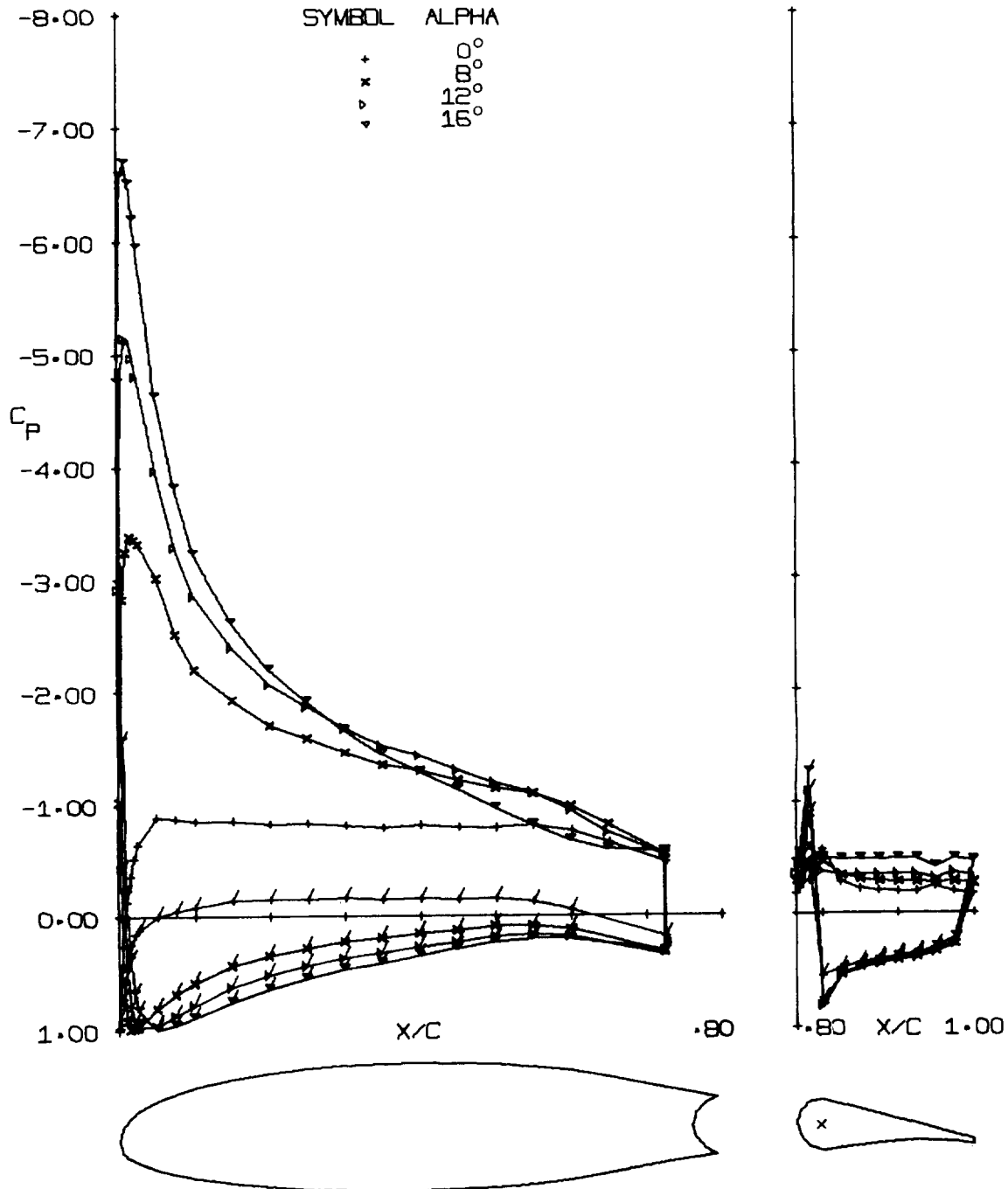MACH NO. = 0.13

REYNOLDS NO. = 2.2 E 06

SYMBOL ALPHA

+   -8°
×   0°
▷   16°
▼   20°

(s)   40° Aileron, Large α's.

Figure 9 - Continued.

AILERON DEFLECTION =+40.00 DEG.

MACH NO. = 0.13

REYNOLDS NO. = 2.2 E 06

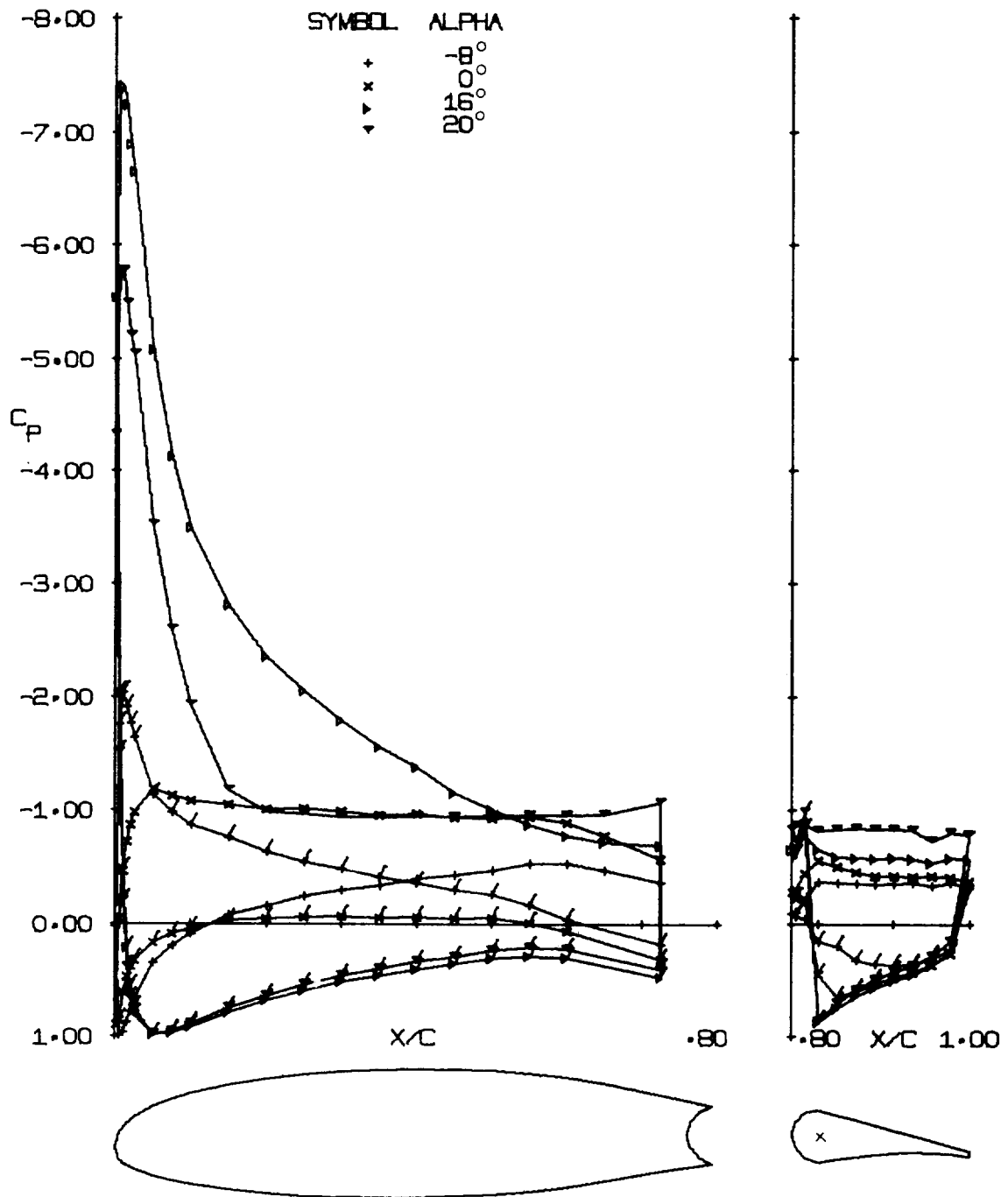| SYMBOL	ALPHA
+	$0°$
×	$8°$
▷	$12°$
▼	$16°$

(t)   40° Aileron, Moderate α's.

Figure 9 - Continued.

63

AILERON DEFLECTION =+60.00 DEG.

MACH NO. = 0.13

REYNOLDS NO. = 2.2 E 06

SYMBOL   ALPHA
+   -8°
×   0°
▶   16°
▼   20°

C_P

-8.00
-7.00
-6.00
-5.00
-4.00
-3.00
-2.00
-1.00
0.00
1.00

X/C   .80

.80   X/C   1.00

(u)   60° Aileron, Large α's.

Figure 9 - Continued.

64
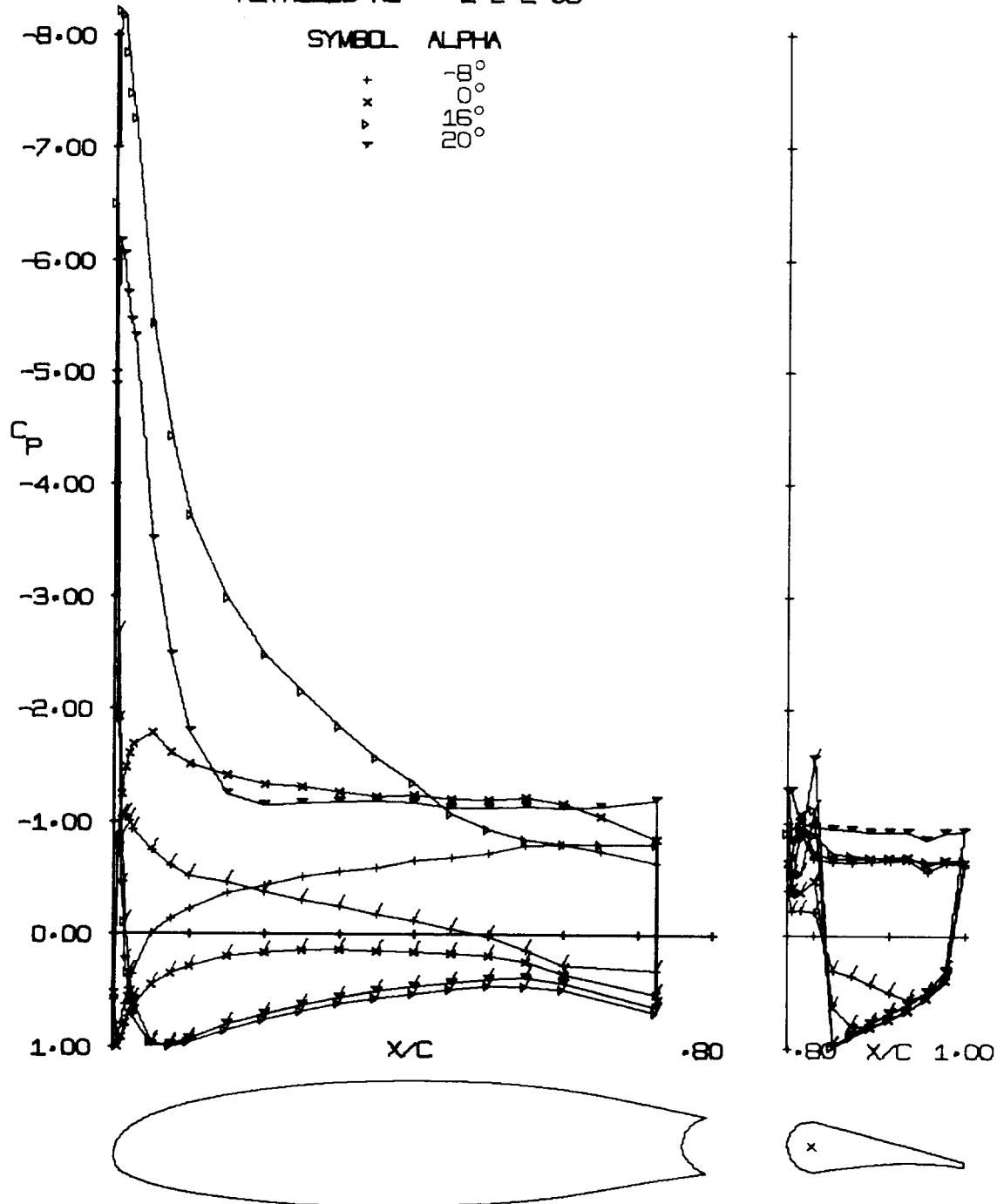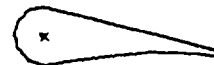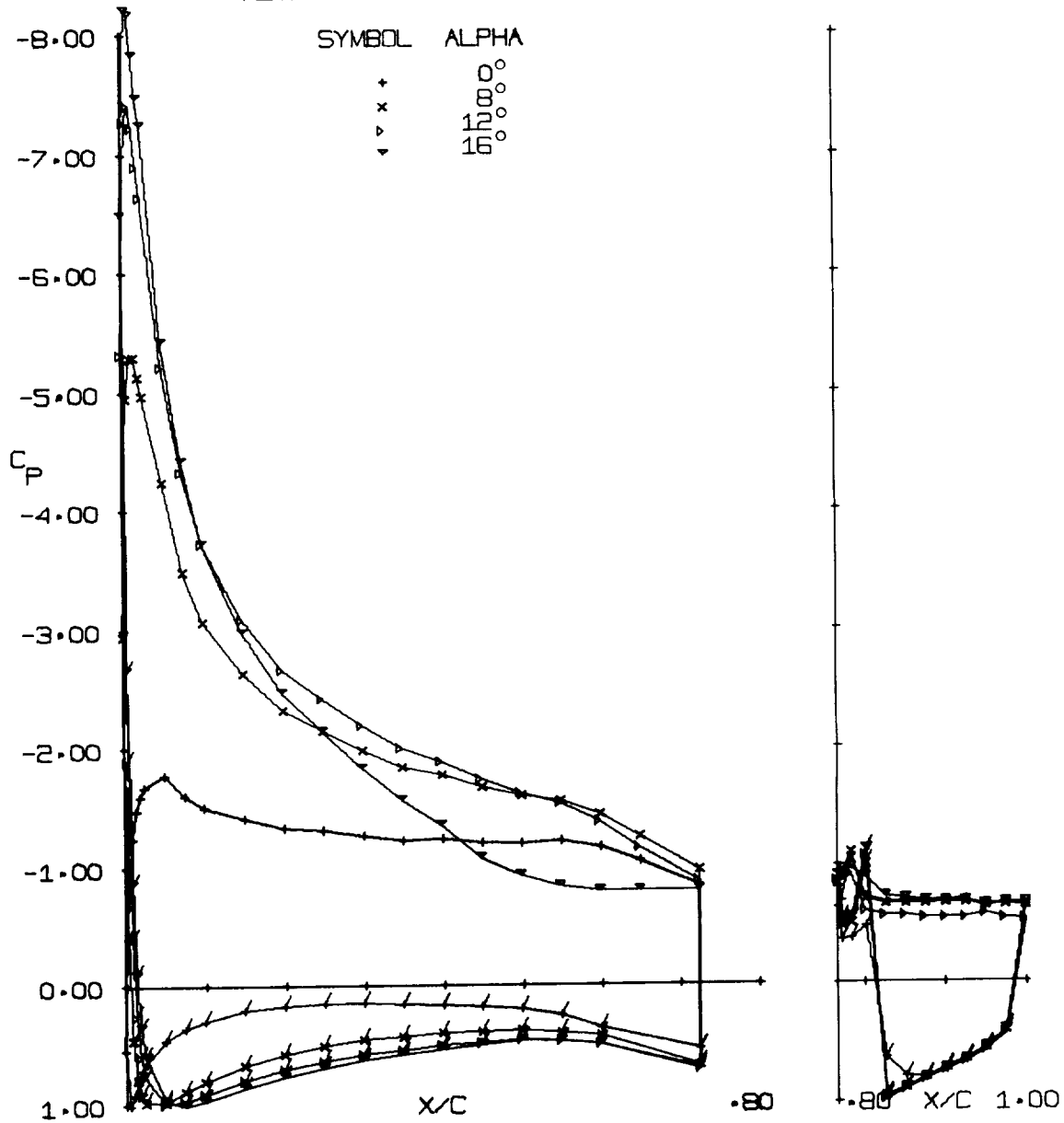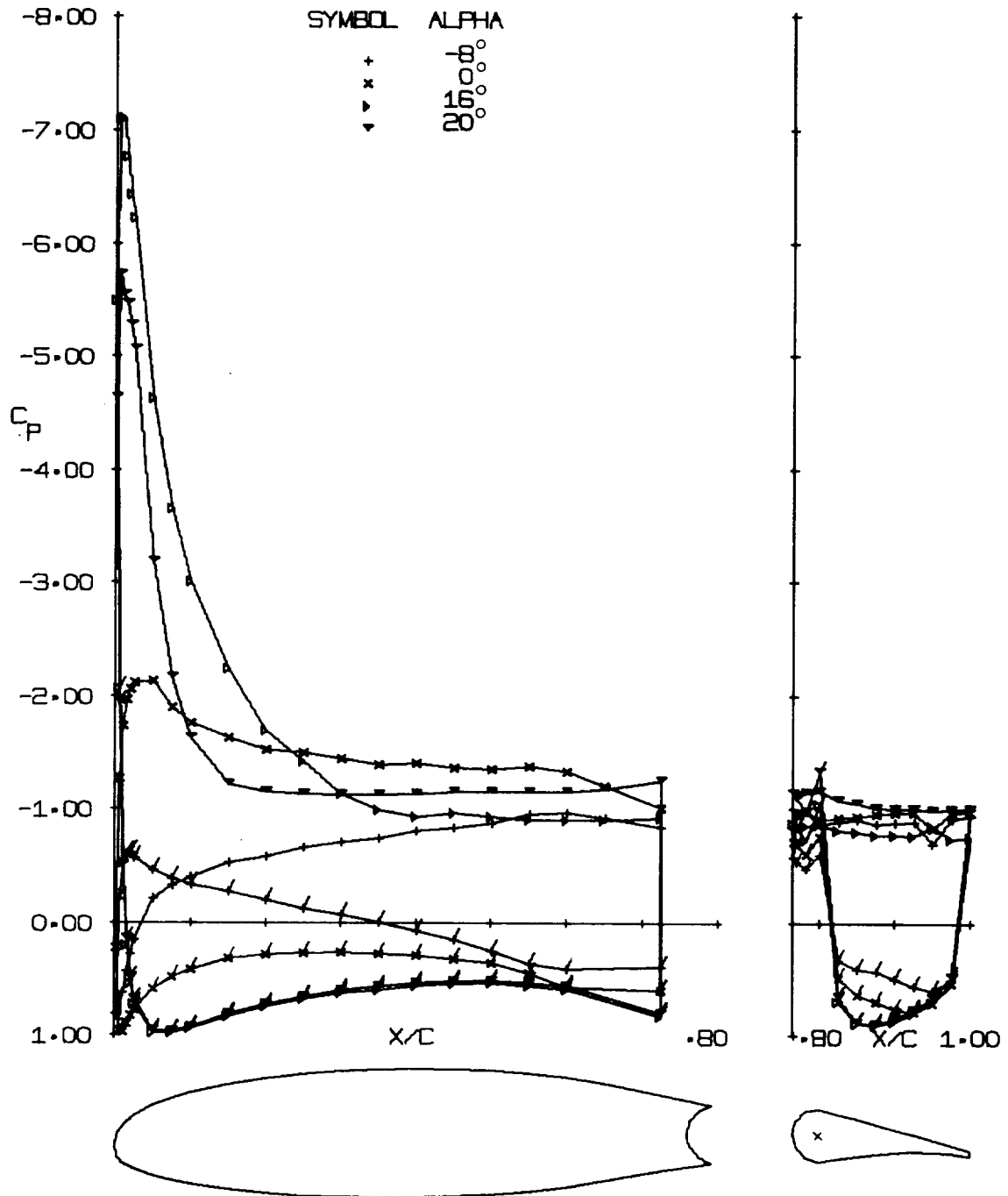
AILERON DEFLECTION =+60·00 DEG·

MACH NO· = 0·13

REYNOLDS NO· = 2·2 E 06

SYMBOL	ALPHA
+	0°
x	8°
▶	12°
▼	16°
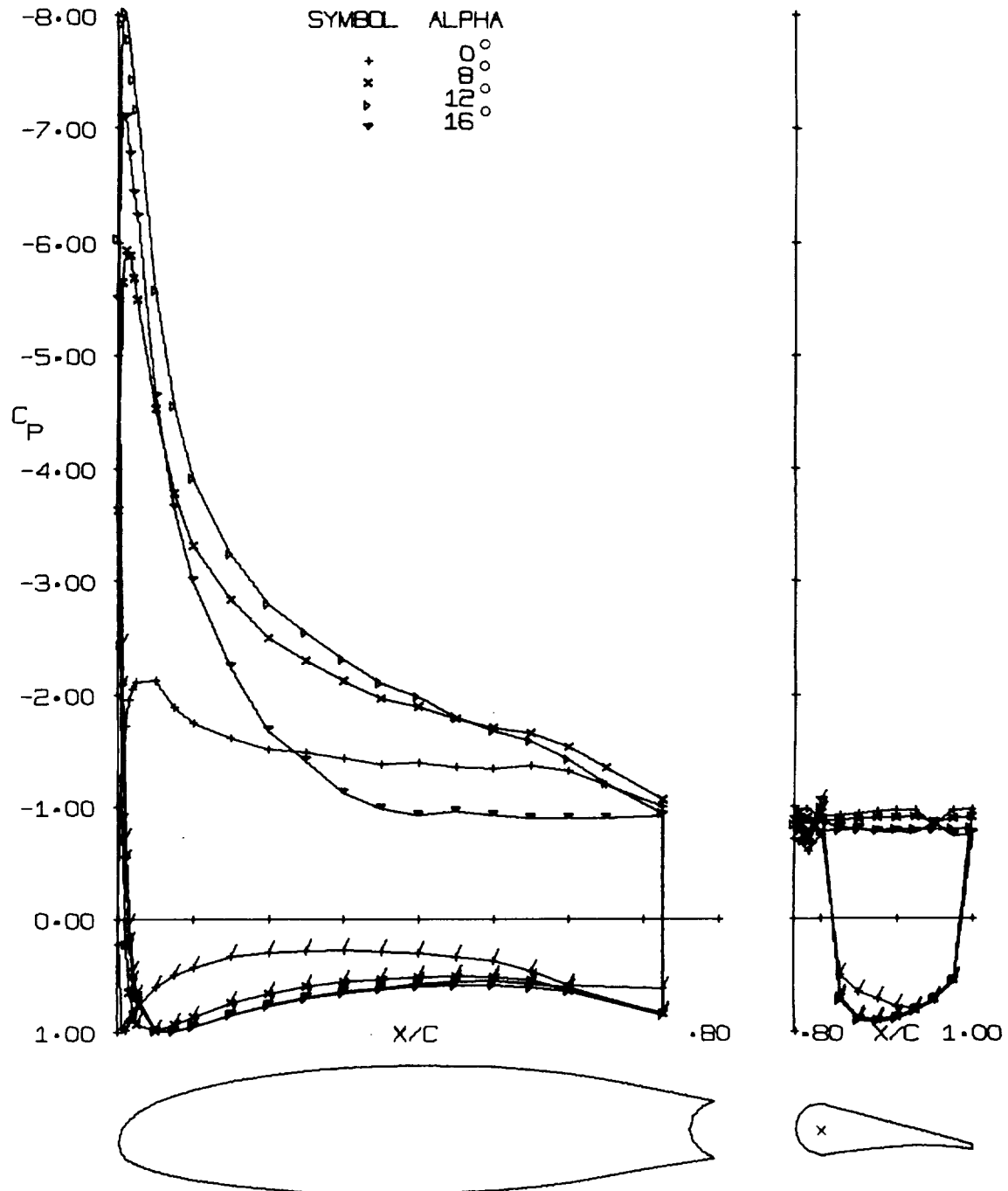
(v)   60° Aileron, Moderate α's.

Figure 9 - Concluded.

65
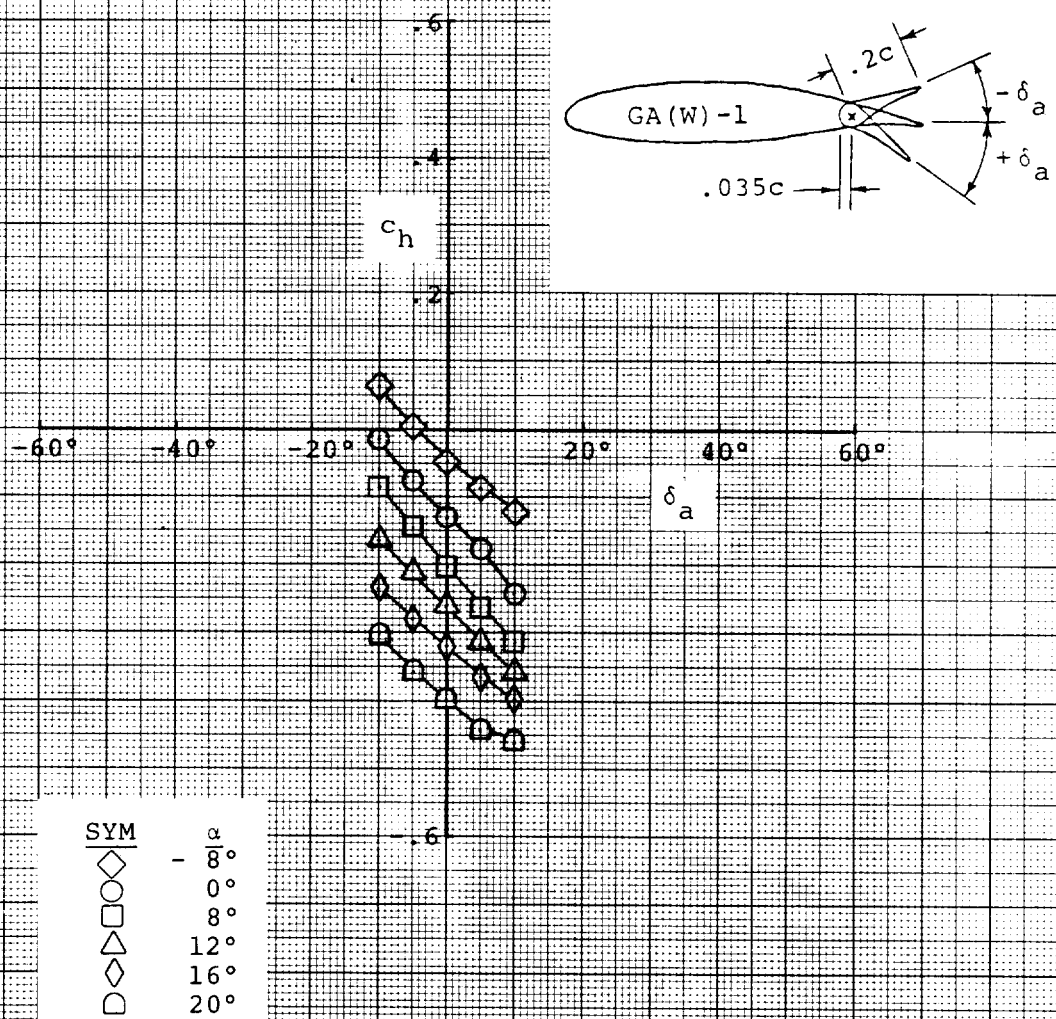
(a)   0% Gap.

Figure 10 - Aileron Hinge Moment.

66

(b) 0.5% Gap.

Figure 10 – Concluded.
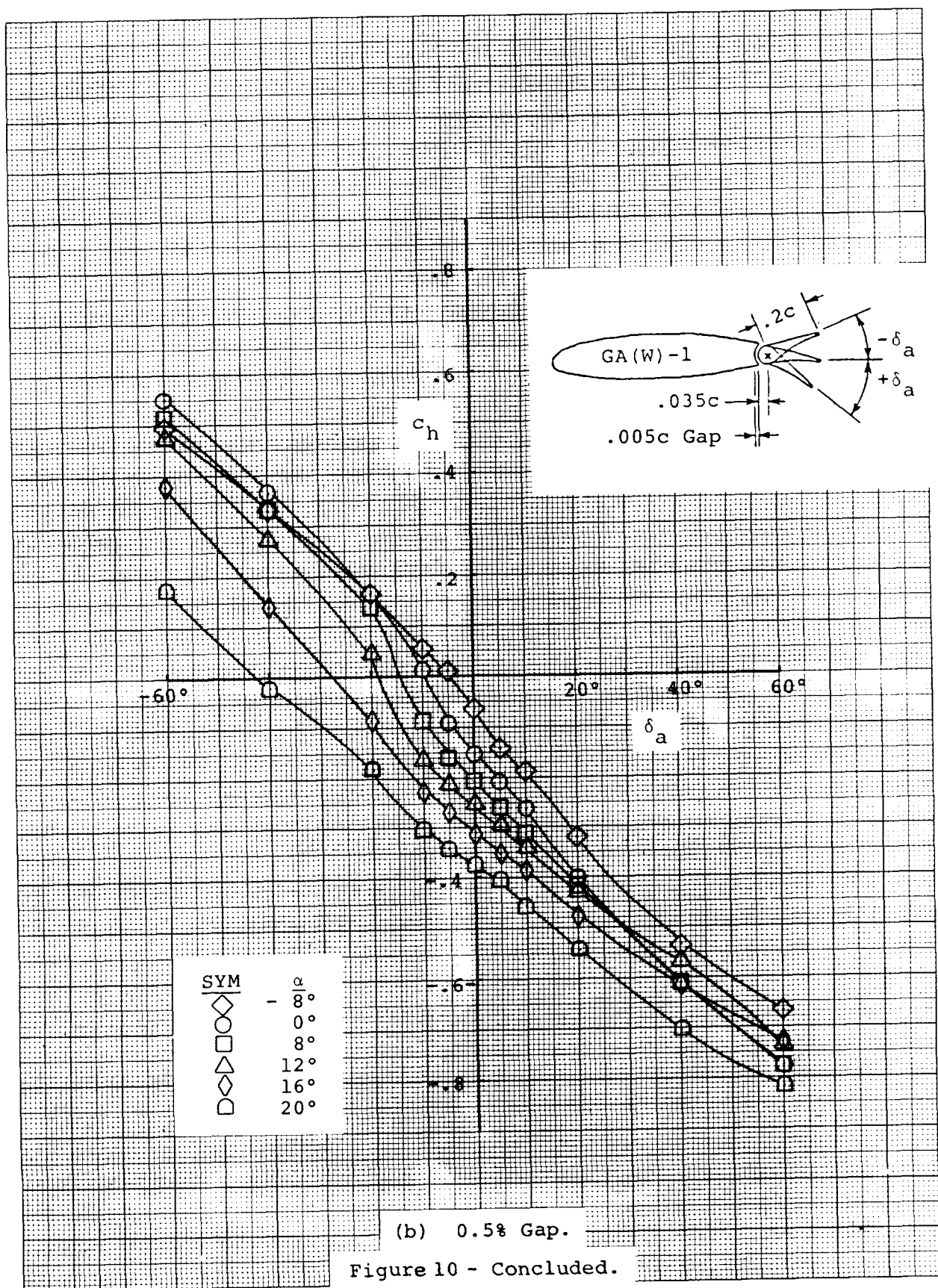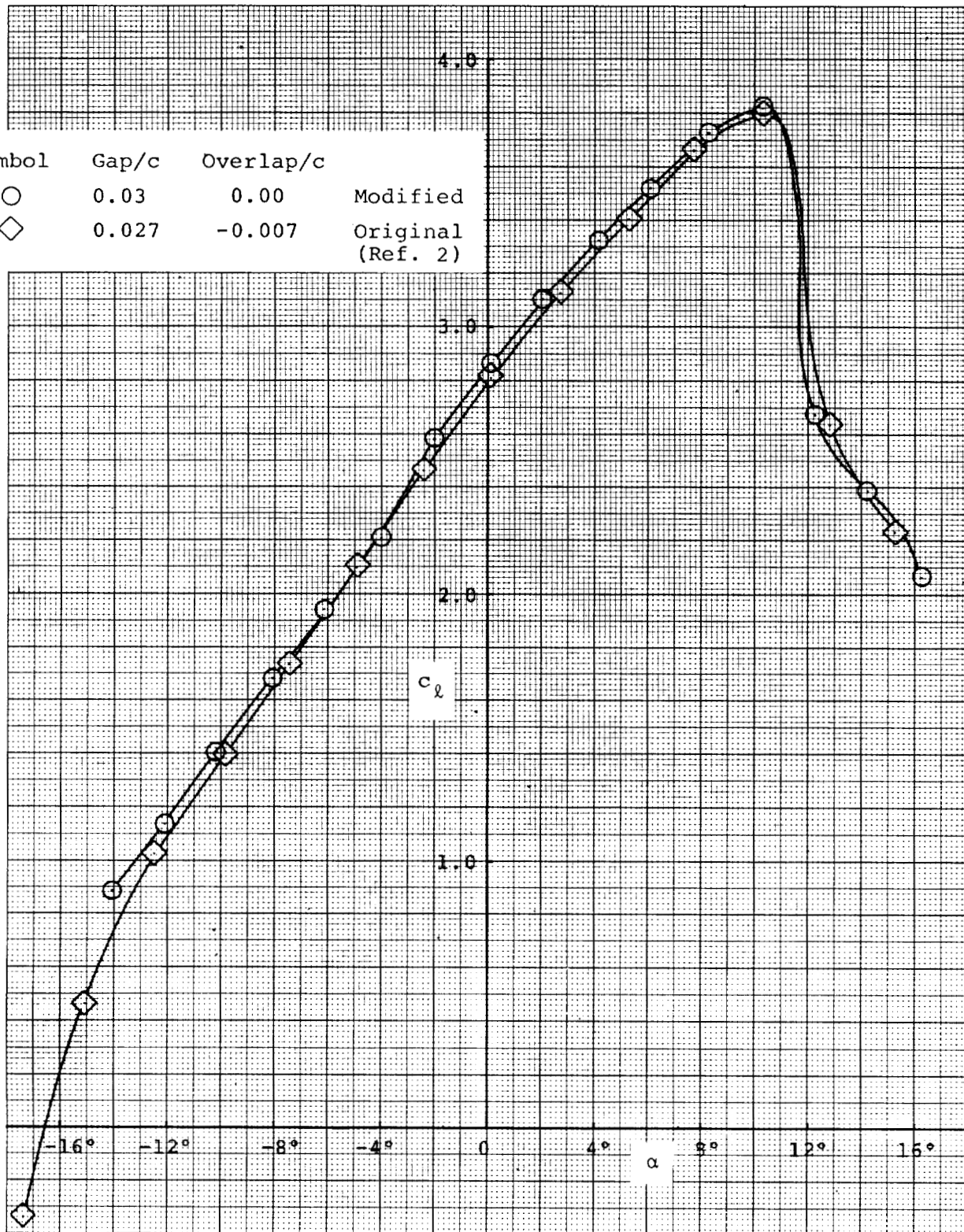
Figure 11 - Lift comparison between modified flap geometry and original flap geometry, $\delta_f = 40°$.

68

FLAP DEFLECTION = 10.0 DEGREES

MACH NO. = 0.13

REYNOLDS NO. = 2.2 E 06

SYMBOL	ALPHA
+	0.2°
x	5.2°
▷	10.3°
▼	12.8°

Flagged Symbols Denote
Lower Surface Pressures
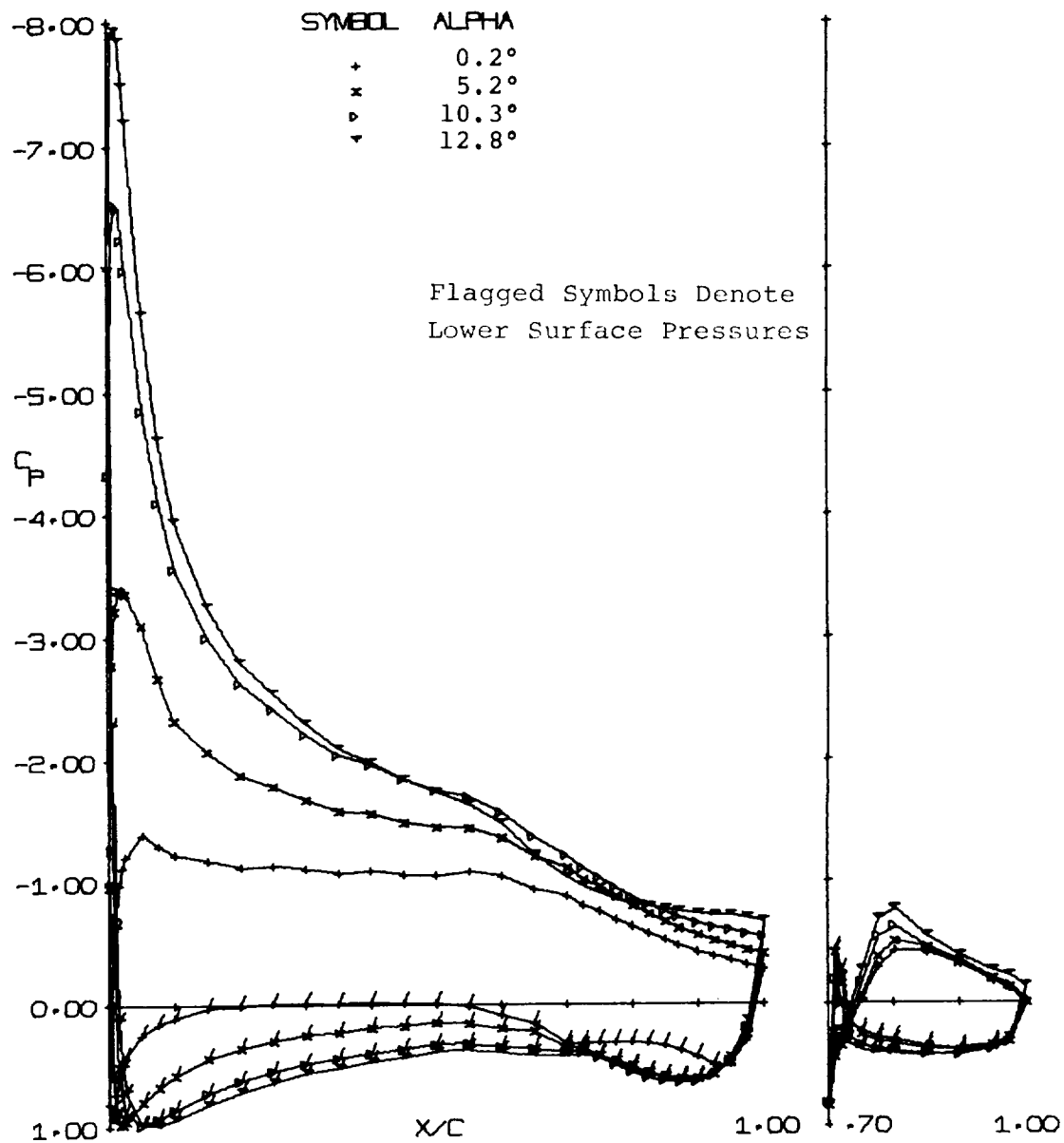
(a) 10° Flap.

Figure 12 - Experimental Pressure Distributions.

FLAP DEFLECTION = 20.0 DEGREES

MACH NO. = 0.13

REYNOLDS NO. = 2.2 E 06

(b) 20° Flap.

Figure 12 - Continued.

70
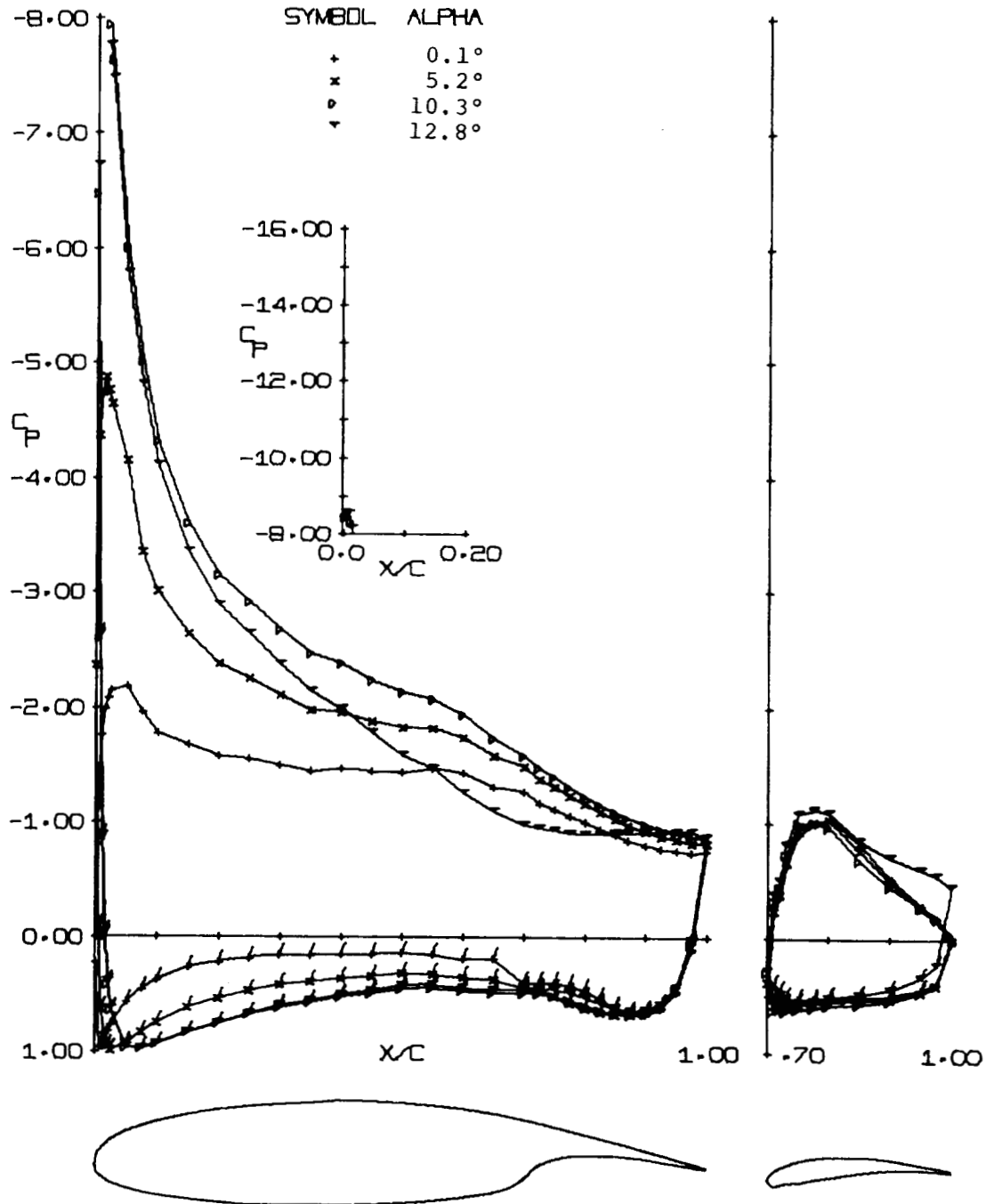
FLAP DEFLECTION = 30.0 DEGREES

MACH NO. = 0.13

REYNOLDS NO. = 2.2 E 06

SYMBOL	ALPHA
+	0.1°
×	5.2°
▷	10.3°
▼	12.7°

(c) 30° Flap.

Figure 12 - Continued.

71

FLAP DEFLECTION = 40.0 DEGREES

MACH NO. = 0.13

REYNOLDS NO. = 2.2 E 06

(d) 40° Flap.
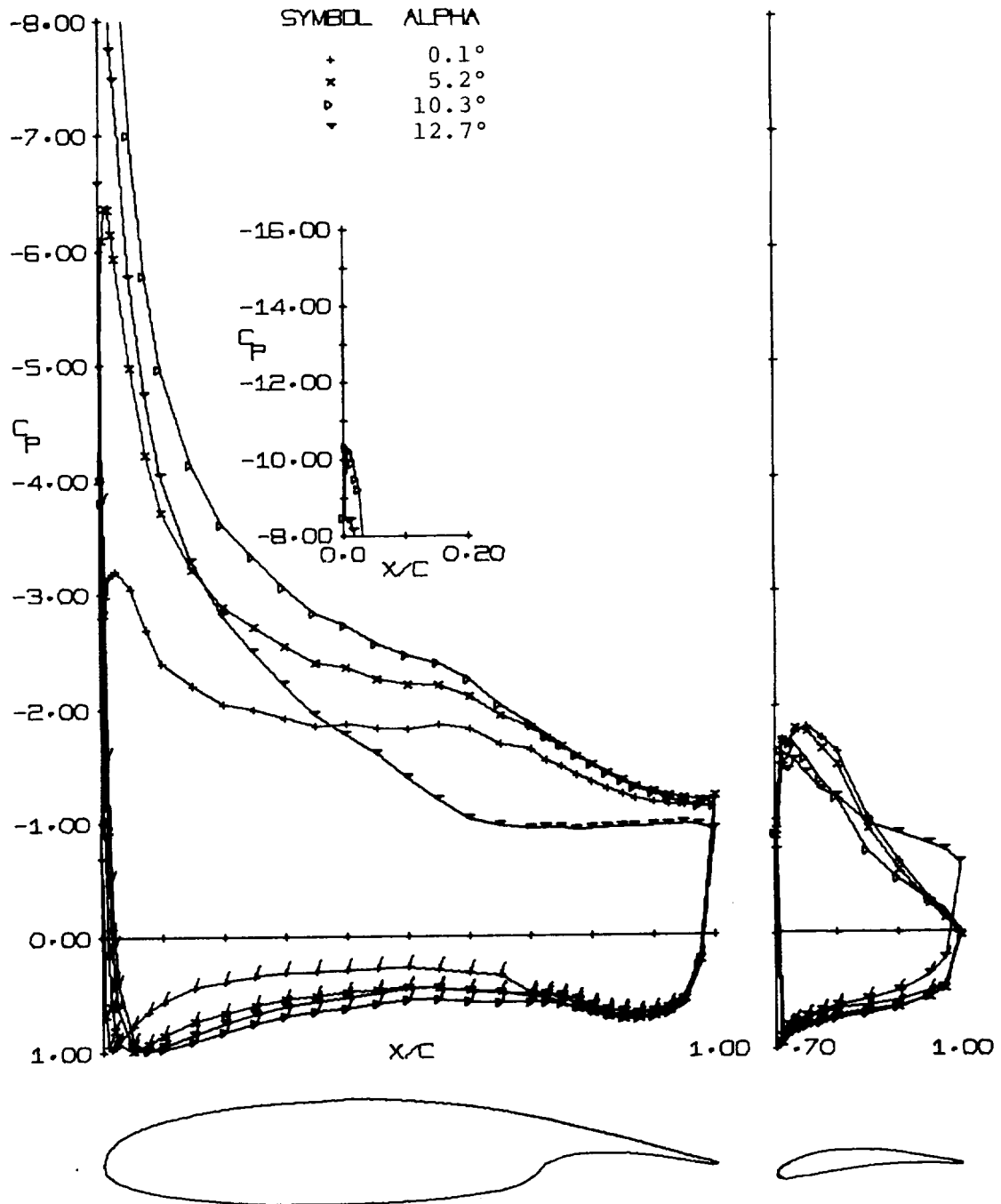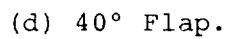
Figure 12 - Concluded.
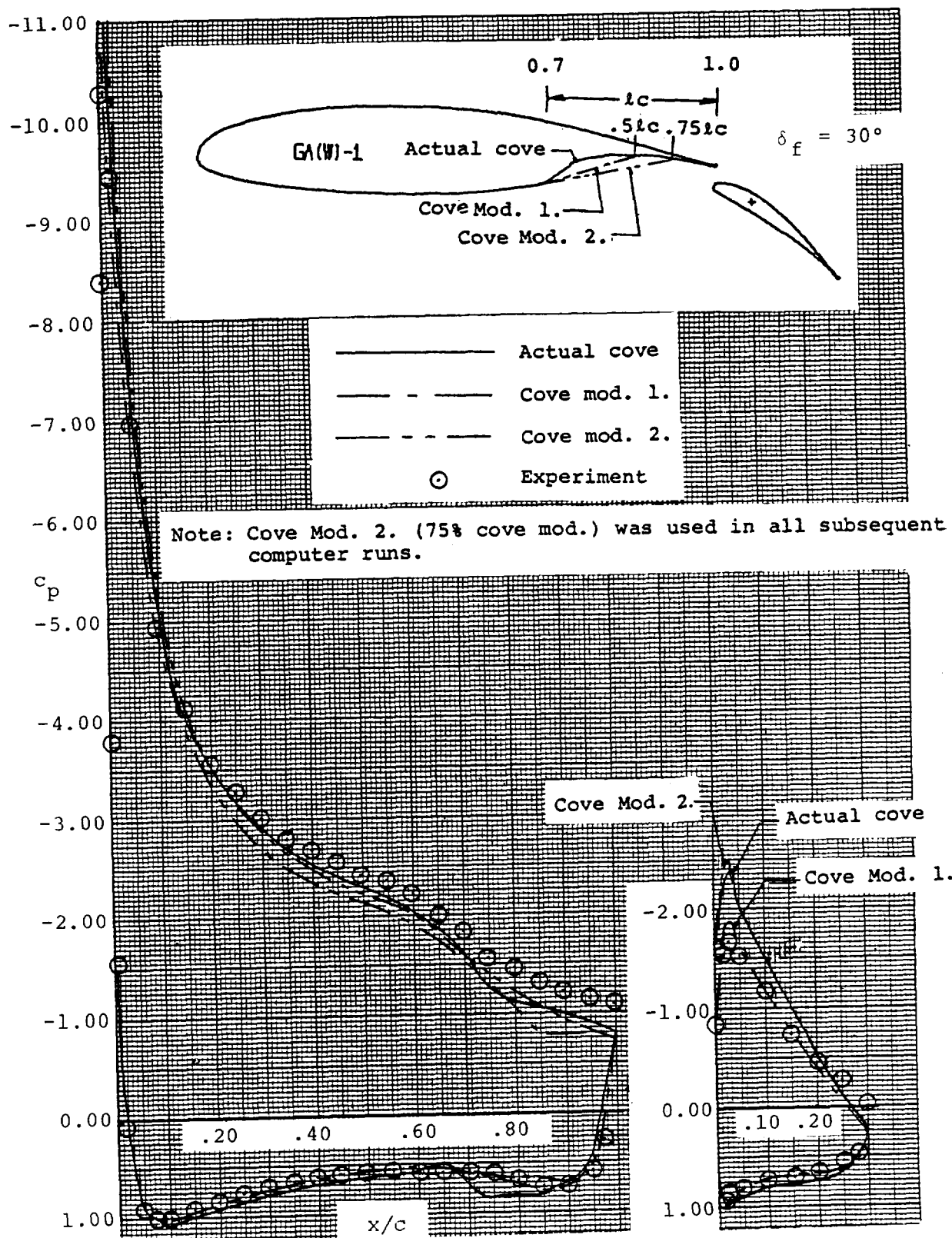
Figure 13 - Effects of cove modifications on pressure distributions, 30° flap, 10.3° angle of attack.

GA(W)-1 with 30% Flap

$\delta_f = 10°$

⊙ Experiment

– – – – Theory (Ref. 7)

Separation predicted at 0.98 c (upper surface)

Confluent boundary layer error encountered

	c_n	
	Theory	Experiment
Airfoil	0.92	1.09
Flap	0.13	0.14

(a) $\alpha = 0.2°$

Figure 14 – Experimental and Theoretical Pressures, 10° Flap

GA(W)-1 with 30% Flap

$\delta_f = 10°$

⊙   Experiment

- - - - -   Theory (Ref. 7)

Separation predicted at 0.98 c (upper surface)

Confluent boundary layer error encountered

	c_n	
	Theory	Experiment
Airfoil	1.63	1.84
Flap	0.17	0.16
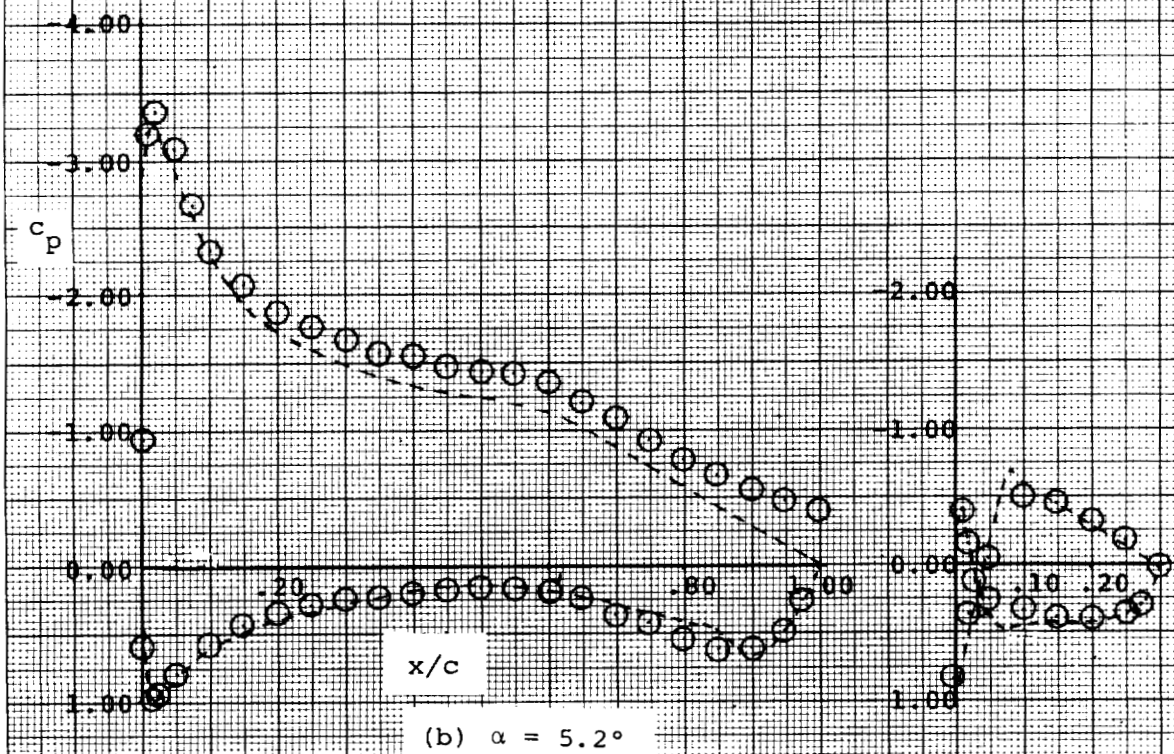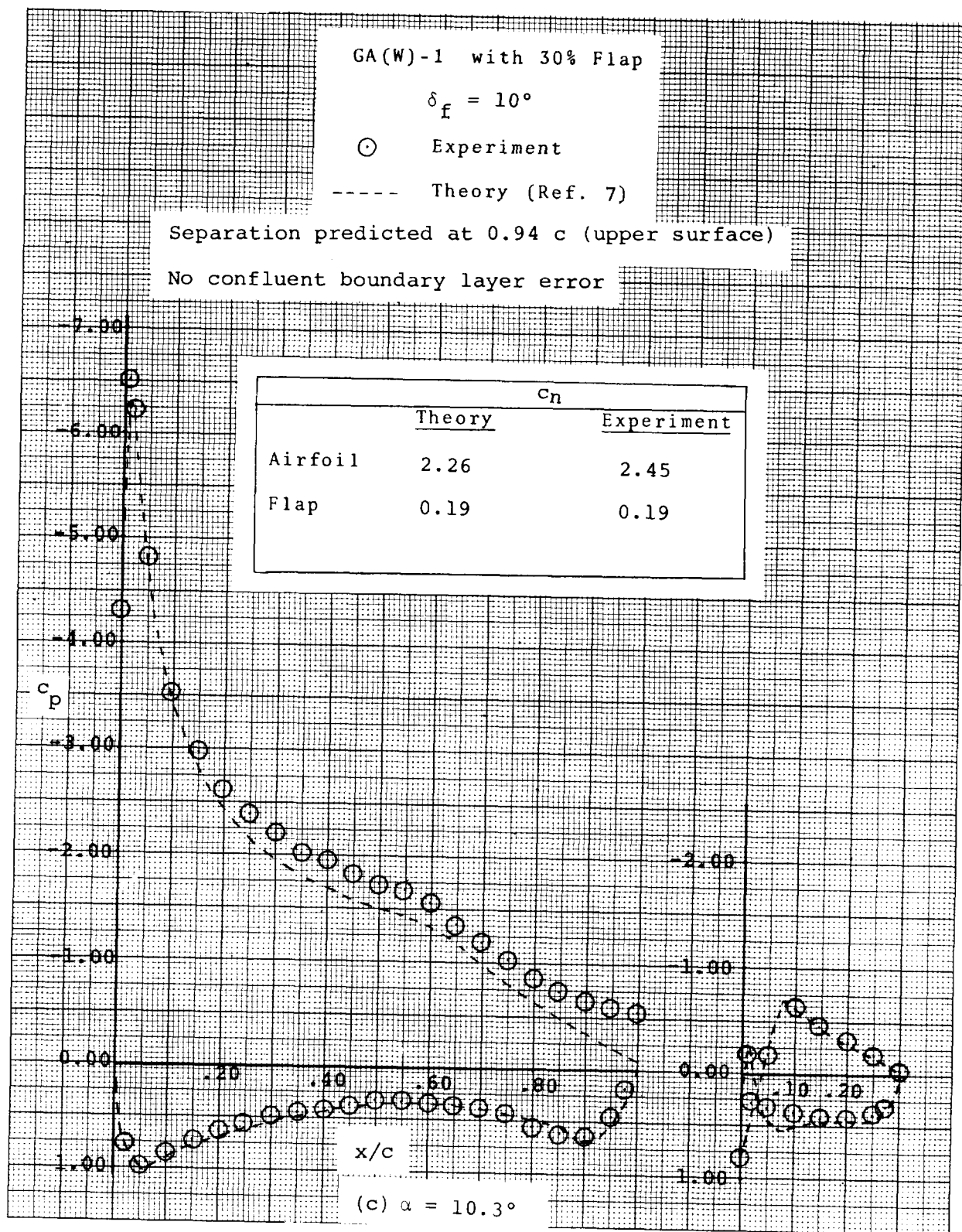
(b) $\alpha = 5.2°$

Figure 14 - continued

75

Figure 14 - continued

76

GA(W)-1 with 30% Flap

$\delta_f = 10°$

⊙ Experiment

- - - - - Theory (Ref. 7)

Separation predicted at 0.90 c (upper surface)

No confluent boundary layer error

	c_n	
	Theory	Experiment
Airfoil	2.50	2.60
Flap	0.19	0.21

(d) $\alpha = 12.8°$

Figure 14 - concluded

77
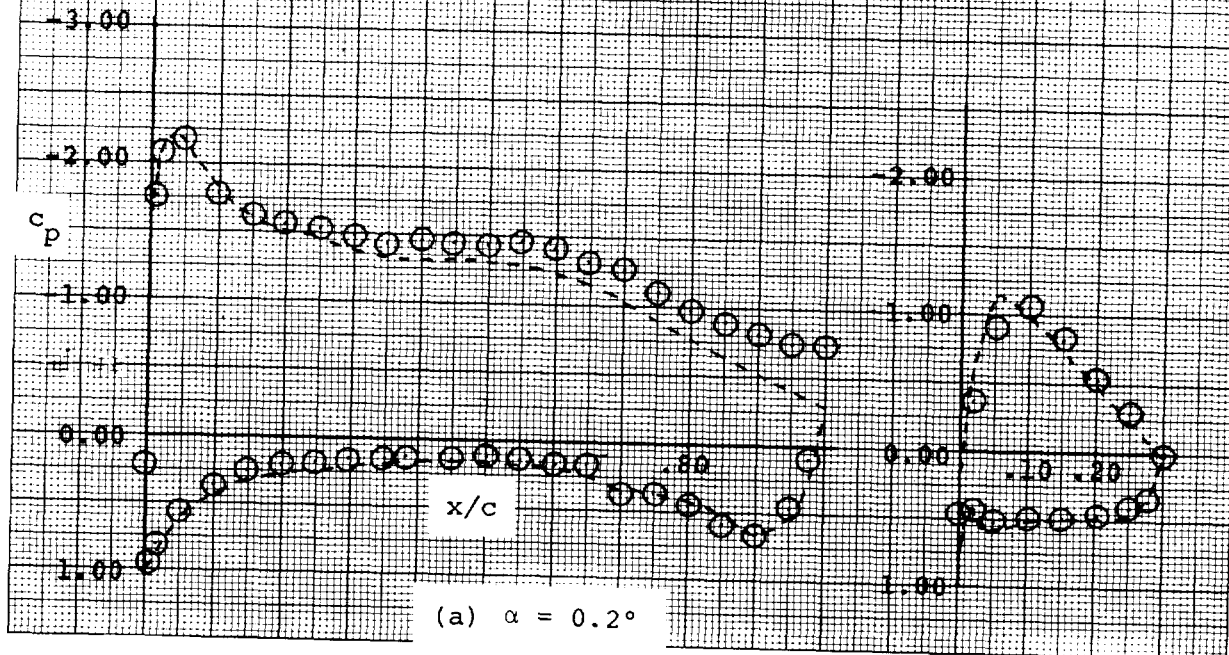
Figure 15 - Experimental and Theoretical Pressures, 20° Flap

78

GA(W)-1 with 30% Flap

$\delta_f = 20°$

⊙ Experiment

- - - - - Theory (Ref. 7)

No separation predicted (upper surface)

Confluent boundary layer error encountered

	c_n	
	Theory	Experiment
Airfoil	2.24	2.40
Flap	0.34	0.33

(b) $\alpha = 5.2°$

Figure 15 - continued

GA(W)-1 with 30% Flap

$\delta_f = 20°$

⊙   Experiment

----- Theory (Ref. 7)

Separation predicted at 0.98 c (upper surface)

Confluent boundary layer error encountered

	c_n	
	Theory	Experiment
Airfoil	2.82	3.02
Flap	0.38	0.34

(c) $\alpha = 10.3°$

Figure 15 - continued

80

(d) $\alpha = 12.8°$

Figure 15 - concluded

GA(W)-1 with 30% Flap

$\delta_f = 30°$

⊙   Experiment

- - - - -   Theory (Ref. 7)

No separation predicted (upper surface)

Confluent boundary layer error encountered

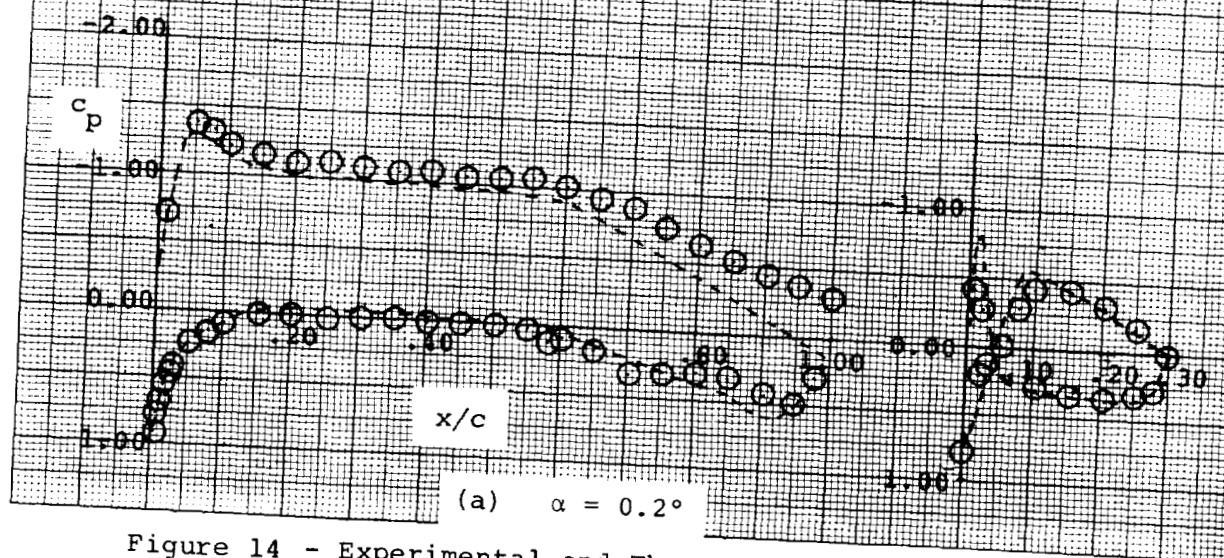|	c_n	
	Theory	Experiment
Airfoil	2.10	2.25
Flap	0.52	0.49

(a) $\alpha = 0.1°$

Figure 16 - Experimental and Theoretical Pressures, 30° Flap

82

GA(W)-1 with 30% Flap

$\delta_f = 30°$

⊙ Experiment

----- Theory (Ref. 7)

No separation predicted (upper surface)

Confluent boundary layer error encountered

	c_n	
	Theory	Experiment
Airfoil	2.76	2.96
Flap	0.53	0.48

(b) $\alpha = 5.2°$

Figure 16 - continued

83

GA(W)-1 with 30% Flap

$\delta_f = 30°$

⊙   Experiment

-----   Theory (Ref. 7)

No separation predicted (upper surface)

Confluent boundary layer error encountered

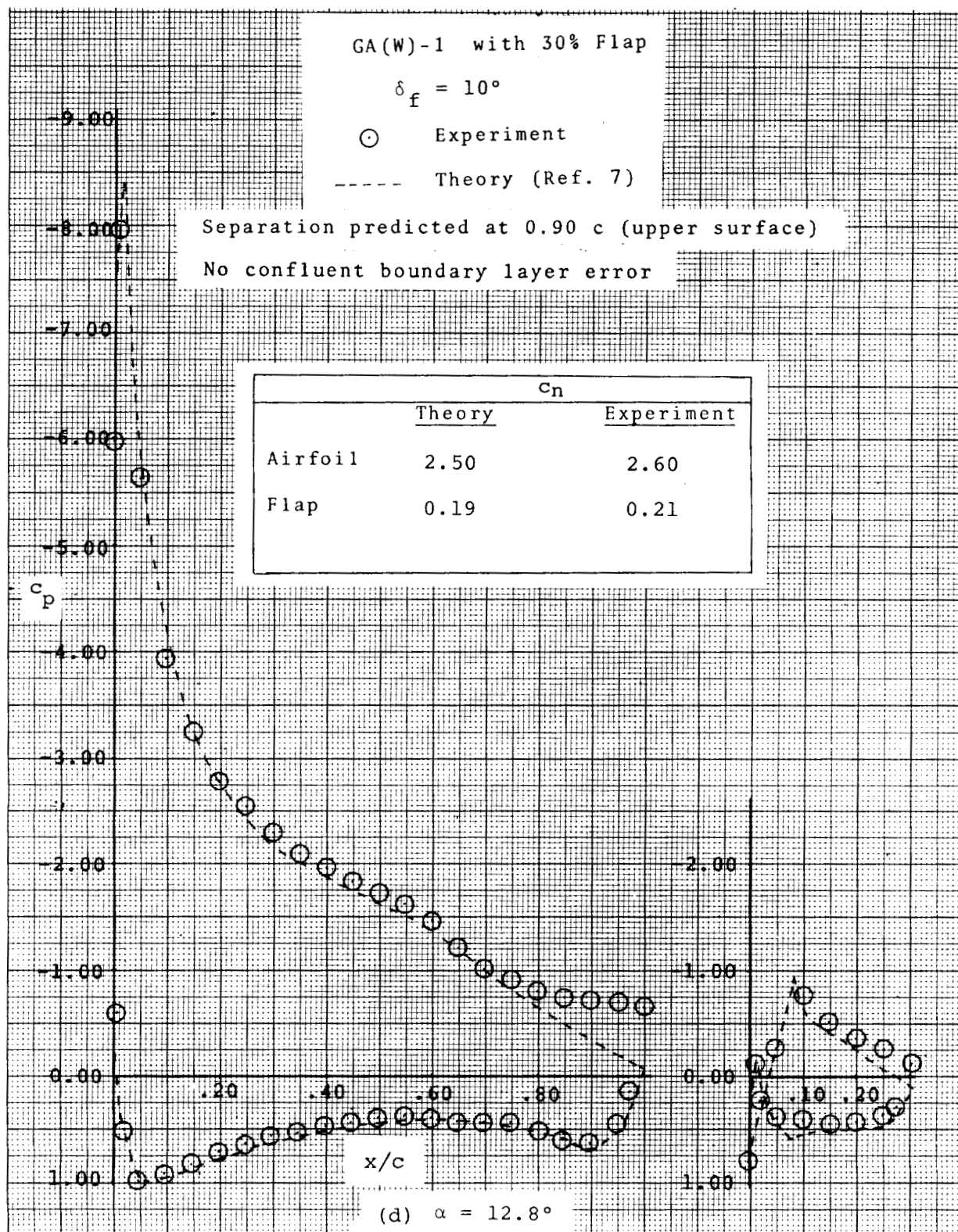|	c_n	
	Theory	Experiment
Airfoil	3.33	3.49
Flap	0.54	0.45

(c) $\alpha = 10.3°$

Figure 16 - continued

84

GA(W)-1 with 30% Flap

$\delta_f = 30°$

⊙   Experiment

- - - - - Theory (Ref. 7)

No separation predicted (upper surface)

Confluent boundary layer error encountered

	c_n	
	Theory	Experiment
Airfoil	3.61	2.60
Flap	0.55	0.47

(d) $\alpha = 12.8°$

Figure 16 - concluded

GA(W)-1 with 30% Flap

$\delta_f = 40°$

$\odot$ Experiment

- - - - - Theory (Ref. 7)

No separation predicted (upper surface)

No confluent boundary layer error

	c_n	
	Theory	Experiment
Airfoil	2.53	2.51
Flap	0.69	0.53

(a) $\alpha = 0.2°$

Figure 17 - Experimental and Theoretical Pressures, 40° Flap

GA(W)-1 with 30% Flap

$\delta_f = 40°$

⊙   Experiment

– – – – –   Theory (Ref. 7)

No separation predicted (upper surface)

	c_n	
	Theory	Experiment
Airfoil	2.85	2.85
Flap	0.69	0.52

No confluent boundary layer error

(b) $\alpha = 2.7°$

Figure 17 – continued

GA(W)-1 with 30% Flap

$\delta_f = 40°$

⊙ Experiment

- - - - - Theory (Ref. 7)

No separation predicted (upper surface)

	c_n	
	Theory	Experiment
Airfoil	3.17	3.16
Flap	0.69	0.51

No confluent boundary layer error

c_p

x/c

(c) $\alpha = 5.2°$

Figure 17 - continued

GA(W)-1 with 30% Flap

$\delta_f = 40°$

⊙ Experiment

- - - - - Theory (Ref. 7)

No separation predicted (upper surface)

	c_n	
	Theory	Experiment
Airfoil	3.48	3.49
Flap	0.70	0.51

No confluent boundary layer error

(d) $\alpha = 7.7°$

Figure 17 - continued

89

GA(W)-1 with 30% Flap

$\delta_f = 40°$

⊙   Experiment

- - - - -   Theory (Ref. 7)

No separation predicted (upper surface)

	c_n	
	Theory	Experiment
Airfoil	3.64	3.72
Flap	0.69	0.51

No confluent boundary layer error

(e) $\alpha = 10.3°$

Figure 17 - continued

GA(W)-1 with 30% Flap

$\delta_f = 40°$

⊙   Experiment

- - - - -   Theory (Ref. 7)

No separation predicted (upper surface)

	c_n	
	Theory	Experiment
Airfoil	3.94	2.58
Flap	0.69	0.55

No confluent boundary layer error

c_p

-10.00

-9.00

-8.00

-7.00

-6.00

-5.00

-4.00

-3.00

-2.00

-1.00

0.00

1.00

.20   .40   .60   .80

-6.00

-5.00

-4.00

-3.00

-2.00

-1.00

0.00

1.00

.10 .20

x/c

(f) $\alpha = 12.8°$

Figure 17 - concluded